2010

Visualizing Synaptic Specificity with GRASP

Evan H. Feinberg

VISUALIZING SYNAPTIC SPECIFICITY WITH GRASP

A Thesis Presented to the Faculty of

The Rockefeller University

In Partial Fulfillment of the Requirements for

The degree of Doctor of Philosophy

by

Evan H. Feinberg

June 2010

VISUALIZING SYNAPTIC SPECIFICITY WITH GRASP

Evan H. Feinberg, Ph.D.

The Rockefeller University 2010

A maxim of modern neuroscience holds that the structures of neural circuits dictate their function. Circuit assembly requires each neuron to exercise remarkable precision as it selects a unique ensemble of synaptic partners from a vast array of potential targets. Visualization of individual synapses in the central nervous system is difficult in some contexts and impossible in others, and the ability to rapidly monitor connectivity in living animals would greatly facilitate deeper understanding of synaptic specificity. In this thesis, I describe the development of a method, GFP reconstitution across synaptic partners (GRASP), that allows visualization of defined synapses *in vivo*, and apply this method at one set of synapses in the brain of the nematode *C. elegans*.

The principle of GRASP relies on bimolecular assembly of two GFP fragments expressed on two cells at a synapse. To this end, I appended fragments of green fluorescent protein (GFP) to the extracellular portions of transmembrane carrier proteins in apposing cells. When complementary CD4-tethered GFP fragments were brought into proximity at sites of cell contact, GFP fluorescence was observed both *in vitro* and *in vivo*. Split GFP fragments fused to the presynaptic phosphatase PTP-3A labeled synapses when expressed in connected neurons. This method detected known mutations that alter synaptic connectivity, such as *syg-1* and *syg-2*, which affect development of synapses between HSN neurons and their postsynaptic nerve and muscle partners. These observations suggest that GRASP could aid efforts to trace behavioral circuits and investigation of the mechanisms of synaptic specificity. Additional tools based on Cre recombinase were developed to confine labeling to single cells and synapses of interest.

The ability of GRASP to detect known specificity mutants prompted an investigation of synapse formation in the central nervous system of *C. elegans*. I

generated a transgenic strain, *kyIs501*, in which GRASP labels synapses formed by the ASH sensory neuron onto the AVA interneuron. A genetic screen in *kyIs501* identified one promising mutation, *ky957*, that causes loss of GRASP labeling. However, subsequent analyses revealed that *ky957* is not a *bona fide* specificity mutant, and appears instead to be associated with alterations in the integrated *kyIs501* transgene. Potential solutions to the problems raised by transgene-based approaches as well as further refinements of GRASP are discussed.

Acknowledgements

I am indebted to the many friends and colleagues whose contributions were indispensable to the completion of this work. Geoff Waldo developed split GFP fragments and provided crucial advice, Yishi Jin and Brian Ackley provided PTP-3A constructs, and Kang Shen and Miri VanHoven conducted critical NLG-1-GRASP experiments. Andres Bendesky carefully characterized GRASP labeling of synapses in the egg-laying circuit and Rick Fetter corroborated these findings with painstaking electron microscopy. Scott Dewell performed whole-genome sequencing of *ky957* and with Patrick McGrath analyzed the sequencing data. Computational methods developed by Patrick identified the *kyIs501* transgene insertion.

In the course of this research, I have had the great good fortune to work with an exceptional group of people in the Bargmann Lab. Christian Woods has been a wonderful lab manager and darts partner, while Hernan Jaramillo always provides a warm, welcoming presence. Manoush Ardzivian spoils us as she accommodates every media request and plies us with Armenian delicacies. Holly Hunnicutt refers to herself as the Lab Dragon, but this nickname belies her role as the lab's caring, supportive lifeblood. The occupants of the first two bays, Greg Lee, Evan Macosko, Sreekanth Chalasani, Makoto Tsunozaki, Nikos Chronis, Bibi Lesch, Andres Bendesky, and Andrew Gordus, create an environment where conversations run from profound to absurd and from spoken to sung--often in the same sentence.

I would like to thank Cori for the rare opportunity she granted me to pursue an ambitious, risky project and the stalwart support and encouragement she provided

throughout. Nevertheless, I am most grateful for the indelible impression she leaves as a model citizen of science. With a singular grace, Cori imbues her relentless pursuit of scientific truth with an unmatched generosity of spirit and collegiality. I will always strive to match this example.

Table of Contents

List of Figures

List of Tables

Chapter 1

Introduction

Synapses are specialized cell-cell junctions that allow information to propagate through neural circuits to generate behavior. Within the human brain, more than 100 billion neurons form more than 100 trillion synapses with remarkable precision. The ability of each neuron to identify and form synapses with a unique subset of the cells that it contacts is termed synaptic specificity. Specificity requires neurons to avoid inappropriate targets while identifying suitable subcellular regions on appropriate target cells. The synapses that form then must differentiate into excitatory or inhibitory synapses, and presynaptic neurotransmitters and postsynaptic neurotransmitter receptors must be matched.

Synaptic specificity requires the orchestration of multiple spatial processes. First, neurons must target their axons and dendrites to the appropriate anatomical regions. Within their target areas, neurons then make fine-scale decisions with regard to synapse formation. Some neurons must identify the appropriate neural laminae (layers) in which to synapse (Yamagata et al., 2002). Finally, neurons may discriminate amongst a pool of possibilities to identify their cognate synaptic partners. In *Caenorhabditis elegans*, for example, an average neuron is presynaptic to only fifteen percent of the neurons it contacts (White et al., 1986). Analyses in the fly eye and mammalian cortex suggest that

cellular and subcellular selectivity are general features of synapse formation (Clandinin and Zipursky, 2002; Yoshimura and Callaway, 2005). However, few molecules or mechanisms are known to regulate the selection of a specific target cell in the central nervous system.

A genetic blueprint specifies synaptic targeting

Neurons can undergo significant morphological changes such as axon turning and arborization and dendritic spine growth in response to both genetic cues and circuit activity. Similarly, both genetic mechanisms and circuit activity play roles in synaptic specificity. Studies in the mammalian visual system have found that a genetic blueprint specifies an initial connectivity map subject to activity-dependent refinements. Evidence for a genetic blueprint comes from many experiments showing that an approximately accurate synaptic connectivity is established in the absence of neuronal activity in salamanders, flies, mice, and zebrafish (Harris, 1980, Clandinin and Zipursky 2002, Verhage et al., 2000, Nagiel et al., 2009). However, activity does play important roles as well, both in invertebrates and vertebrates. In *C. elegans*, reduced activity at early stages of development leads to increased elaboration of presynaptic varicosities at neuromuscular junctions in SAB neurons (Zhao and Nonet, 2000). In mammals, pharmacologic inhibition of action potentials during development disrupts proper segregation of retinal ganglion cell inputs in the thalamus (Shatz and Stryker, 1988; Sretavan et al., 1988) The emerging picture from several decades of investigation is that neurons use a genetic blueprint to identify their synaptic partners during development,

while activity serves to refine these connections, changing their number, strength, and other properties to generate a functional brain.

In the introduction below, I will discuss molecular mechanisms and functional strategies implicated in synapse formation. As a result of this parallel structure, some molecules will be discussed more than once.

Combinatorial coding in synaptic specificity

The notion that synaptic selection stems from a genetic template poses an intriguing problem: the number of synapses in the human brain exceeds the number of genes in the human genome by many orders of magnitude. Generation of a vast yet precise synaptic map with a comparatively small repertoire of molecules is likely to require the integration of several cues. Therefore, it is likely that synapses are specified combinatorially. Several candidate recognition molecules have been implicated in synapse formation, including adhesion molecules, secreted attractants and repellents, and guidepost molecules. The combinatorial code for synaptogenesis is likely to involve the integration of positive and negative inputs, as observed in *Drosophila melanogaster* neuromuscular junction formation, where neurons select target muscles by integrating attractive cues such as Fasciclin II and Capricious, negative cues such as Semaphorin II, and molecules that attract some neurons and repel others, such as Netrin B (Winberg et al., 1998; Shishido et al., 1998). Moreover, synaptogenic molecules may be arrayed in gradients in pre-and post-synaptic cells. Gradients of Ephrin/Eph molecules are used to generate topographic maps in the retinotectal projection on a tissue-wide scale, while intracellular gradients of neurofascin in cerebellar Purkinje cells regulate subcellular

synaptic targeting (Lemke and Reber, 2005; Ango et al., 2004). Within the central nervous system, any or all of these mechanisms working in concert may enable a few molecules to specify many synapses.

Synaptic specificity is likely to involve transsynaptic adhesive interactions between pre- and postsynaptic recognition molecules. *Drosophila* Capricious, a member of a family of leucine-rich repeat (LRR) proteins, is coordinately expressed on at least two sets of synaptic pairs: body wall muscle 12 and the motor neurons that innervate it, and the R8 photoreceptor and its synaptic target lamina (Shishido et al., 1998; Shinza-Kameda et a., 2006). Other LRR proteins are expressed on other *Drosophila* body wall muscles, and recent analyses suggest that some of these LRR proteins are also required for innervation of muscle 12 (Kurusu et al., 2008). Vertebrate LRR proteins such as LRRTM1 can induce synaptogenesis in cultured neurons, and LRRTM knockout mice display altered distribution of the synaptic vesicular glutamate transporter VGLUT1, suggesting that LRR proteins have a conserved synaptogenic role (Linhoff et al., 2009).

Specific cadherins have also been localized to synapses in many contexts. In the *Drosophila* eye, loss of N-cadherin causes R7 photoreceptors to target the synaptic layer normally innervated by R8 cells, while R1-6 cells fail to extend their axons to the appropriate target cartridges (Lee et al., 2001). Vertebrate N-cadherin is concentrated at the synaptic sites in retinorecpient laminae of the chick optic tectum, and its intracellular tail can interact with alpha-catenin to recruit the cytoskeletal machinery (Yamagata et al., 1995). A related family of molecules, the protocadherins, display a striking genomic organization, with various splice isoforms arrayed tandemly on the same chromosome. Their expression pattern, with distinct subsets of neurons expressing individual

molecules, suggests a potential adhesive code (Sano et al., 1993; Wu and Maniatis, 1999). Mice lacking protocadherins appear to have normal synaptic targeting but abnormal synaptic function and increased neuronal apoptosis (Wang et al., 2002).

The immunoglobulin superfamily (IgSF) includes many proteins that have been suggested to be synaptogenic. Sidekicks and DSCAMs appear to specify laminar targeting in the chick retina, while DSCAMs in other contexts appear to regulate self-avoidance (Yamagata et al., 2002; Yamagata and Sanes 2008; Wang et al., 2002). The IgSF family members synCAMs, with intracellular PDZ domains, can promote synapse formation *in vitro* through homotypic interactions (Biederer et al., 2002). An important challenge in studying these molecules will be to understand how a symmetric adhesive interaction results in asymmetric pre- and postsynaptic differentiation.

A number of heterotypic adhesive interactions have been observed at synapses as well. Presynaptic neurexins paired with postsynaptic neuroligins are sufficient to induce synapse formation *in vitro*, although *in vivo* Neurexins and Neuroligins are mainly required for synapse differentiation (Scheiffele et al., 2000; Graf et al., 2004; Varoqueax et al., 2006). Ephrins and Eph receptors are also localized to synapses, where they play largely regulatory roles (Torres et al., 1998; Dalva et al., 2000). Other heterotypic adhesion molecules promote synaptogenesis without directly interacting with the postsynaptic cell. The IgSF molecule SYG-1, expressed in the HSNL neuron, and interactions with its ligand SYG-2, expressed in the vulval epithelial cells, promote synapse formation between HSN and the adjacent VC neurons and vulval muscle (Shen and Bargmann, 2003; Shen et al., 2004). Other unknown factors likely direct HSNL to innervate the VC neurons and vulval muscle within this region. Adhesive interactions

through molecules such as Semaphorins and Integrins have also been documented at synapses (Godenschwege et al., 2002; Yamagata et al., 1995), and additional receptors are likely to be identified.

In addition to adhesive interactions, numerous secreted proteins can induce synaptogenesis. A classical example is Agrin, a protein secreted by motor neurons that binds to a receptor complex containing MuSK and LRP4 on muscle cells to induce postsynaptic localization of acetycholine receptors at neuromuscular junctions (Smith et al., 1987, Zhang et al., 2008). Wnt-7a and FGF22 both promote synaptogenesis in the cerebellum, with Wnt-7a signaling through an unknown mechanism and FGF22 binding its receptor FGFR2 on mossy fiber neurons (Hall et al., 2000, Umemori et al., 2004). WNTs can also inhibit synapse formation by motor neurons in *Drosophila* and *C. elegans* (Inaki et al., 2007; Klassen and Shen, 2007). In addition, members of the BMP family and Netrins can promote or inhibit synaptogenesis (McCabe et al., 2003, Colon-Ramos et al., 2007, Poon et al., 2008). The identification of these and other secreted factors and adhesion molecules has begun to elucidate the components of the combinatorial synaptic code, but the syntax of the code remains elusive.

Recycling and flexibility of cues

One source of diversity in the synaptic code is the ability of individual molecules to generate diverse responses. *unc-6*/Netrin was first identified in genetic and biochemical screens for its role in promoting circumferential axon guidance (Hedgecock et al., 1990; Serafini et al., 1994) UNC-6/Netrin binding to UNC-40/DCC receptors

elicits attraction (Chan et al., 1996, Keino-Masu et al., 1996), while UNC-6/Netrin binding to UNC-5 receptors elicits repulsion (Hamelin et al., 1993, Leonardo et al., 1997.) Recently, Netrin signaling through these receptors has been shown to play a role in specifying synaptic regions of axons. UNC-6 signaling through UNC-40 stimulates synaptogenesis in a segment of the AIY axon in the *C. elegans* nerve ring, and UNC-6 signaling through UNC-5 excludes presynaptic sites from the dendrite of DA9 motor neurons (Colon-Ramos et al., 2007; Poon et al., 2008). In general, receptor expression appears to dictate whether a response to Netrin is attractive or repulsive, but whether this signaling affects cell migration, guidance, or synaptogenesis likely depends on the expression of additional coreceptors and intracellular signaling components.

Another well-studied family of secreted molecules, WNTs, provide positive and negative regulation of axon polarity, axon guidance, and synaptogenesis in different contexts. In *C. elegans*, LIN-44/WNT signaling through the LIN-17/Frizzled receptor determines axodendritic polarity in the PLM neuron (Hilliard et al., 2006). WNT4 directs anterior growth of vertebrate commissural axons through the canonical WNT receptor Frizzled3 (Lyuksyutova et al., 2003), and *Drosophila* Wnt5 signals through the atypical receptor tyrosine kinase Derailed, a non-canonical WNT receptor, to repel anterior commissure neurons from the posterior commissure (Yoshikawa et al., 2003). WNTs can similarly promote or inhibit synaptogenesis. In the cerebellum, WNT7a promotes the formation of mossy fiber synapses in a manner believed to required canonical WNT signaling (Hall et al., 2000). In *C. elegans*, LIN-17/WNT signaling through LIN-44/Frizzled inhibits synaptogenesis in a portion of the axon of DA9 motor neurons

(Klassen and Shen, 2007). Overall, these data suggest that WNTs, like Netrin, act at multiple steps in circuit formation through multiple signaling pathways.

Perhaps one of the most striking examples of the diverse responses that can be generated by a single molecule have been observed with the DSCAM family of molecules. Dscam molecules have been well characterized in *Drosophila*, where alternative splicing of Dscam gives rise to 38,016 distinct isoforms (Schmucker et al., 2000). Each isoform undergoes homotypic binding that elicits repulsion, and each cell is believed to express between 15 and 50 distinct splice isoforms, such that every cell expresses a unique complement of Dscam isoforms to ensure specific self-repulsion and proper axon and dendrite patterning (Wojtowicz et al., 2004, Wang et al., 2002). DSCAM may also serve as an attractant receptor for Netrin during commissural axon growth at the midline in flies and mice (Ly et al., 2008, Andrews et al., 2008). DSCAM paralogs in other organisms, as well as other *Drosophila* Dscam homologs, do not undergo extensive alternative splicing, but the theme of homophilic repulsion is conserved. *Drosophila* Dscam2 mediates tiling of L1 neuron axons in the eye (Millard et al., 2008), and mouse DSCAM and DSCAML1 mediate self-repulsion to promote proper cell placement and process arborization in ganglion cells, rod bipolar cells, and AII amacrine cells in the retina (Fuerst et al., 2009). Remarkably, synapse-localized DSCAM and its homologs, Sidekicks, appear to promote laminar targeting of chick amacrine, bipolar, and and retinal ganglion cells via adhesive homophilic interactions (Yamagata and Sanes 2008). R-cadherin-positive ganglion cells express DSCAM and synapse in sublamina 5 (S5) of the inner plexiform layer, and depletion of DSCAM led to mistargeting of their processes but not the processes of other neurons. Ectopic expression

of DSCAM in other ganglion cells types diverted their processes to S5, suggesting that DSCAM is necessary and sufficient for targeting S5. Moreover, DSCAM expression in a cultured human neuroblastoma line promoted cell adhesion and synaptogenesis. These data are in contrast to the results observed in mouse DSCAM knockouts, in which laminar targeting was believed to be largely normal, but these analyses may have focused on different cell types. (Fuerst et al., 2009, Yamagata and Sanes, 2008). Echoing the effects observed with Netrins and WNTs, DSCAM appears to serve attractive and repulsive roles at multiple steps in circuit formation.

In light of the diversity of responses a single molecule can elicit, it is clear that individual cells must rely on expression of appropriate receptors and intracellular signaling pathways to generate the appropriate responses. In particular, the ability of DSCAM to serve as a putative attractant along one axis and a repellant along orthogonal axes in the developing vertebrate retina suggests the complexity of this regulatory problem, as responses to each cue may be dynamic in both space and time in a single cell. The regulatory logic that governs receptor expression, localization, and coupling to intracellular signaling components is likely to be highly complex.

Cell identity and transcriptional control of synaptic specificity

As described above, neurons are able to generate a diverse array of responses to single guidance factors. To do so, neurons must express the appropriate complement of receptors, ligands, and intracellular signaling molecules at the appropriate time and place to ensure that they reach and synapse with the correct targets. Connectivity is an integral feature of a cell's function, and studies in numerous systems have explored this

phenomenon. In *C. elegans*, the *unc-4* and *unc-37* transcription factors promote proper innervation in the VA neurons by repressing the factors that specify the synaptic connectivity of VB neurons (Von Stetina et al., 2007). Similarly, in the fly eye sensory receptor choice and synaptic laminar targeting are controlled by the same transcription factors, ensuring proper matching of cellular function to cellular connectivity (Morey et al., 2008). In the vertebrate spinal cord, a transcription factor code of Hox genes, LIM homeodomain proteins, and other factors dictate cell identity and motor neuron target innervation through regulation of guidance cues such as EphA4 (Dasen et al., 2005, Kania and Jessell, 2003). Interestingly, in some instances innervation of muscle targets appears to reinforce motor neuron identity and expression of ETS transcription factors (Arber et al., 2000, Livet et al., 2002), suggesting that synaptic connectivity can also feed back onto cell identity. As with adhesion molecules, there are many fewer transcription factors than synapses, and how transcriptional control is orchestrated remains unknown.

Studies in *Drosophila* have identified a few candidate means by which a single transcription factor can specify different connectivity in different cells. In the *Drosophila* olfactory system, each projection neuron (PN) has a unique projection pattern determined through lineage-dependent and age-dependent mechanisms. Early-born PNs express high levels of the transcription factor Chinmo, while later-born PNs express lower levels of Chinmo (Zhu et al., 2006). Loss of Chinmo causes early-born cells to acquire the glomerular projection patterns of late-born neurons, suggesting that graded Chinmo expression specifies multiple distinct projection patterns, although the molecular mechanism is unclear. PNs innervate these glomeruli prior to arrival of olfactory neurons through the activity of Chinmo and additional transcription factors (Komiyama et al.,

2003), which may provide a combinatorial code. N-cadherin and Dscam are required for glomerular targeting and elaboration of dendrites, respectively, but appear to do so permissively (Zhu and Luo, 2004, Zhu et al., 2006). A spatial gradient of Semaphorin-1a appears to provide additional targeting information, as loss of Semaphorin-1a partially disrupts glomerular targeting, particularly for later arriving axons (Komiyama et al., 2007). In this way, small numbers of adhesion molecules and transcription factors can define the complex glomerular map.

An intriguing study in the fly eye documented another form of temporal control by transcription. Both the R7 and R8 photoreceptors target distinct synaptic laminae in an N-cadherin-dependent manner, and how a single adhesion molecule could direct formation of adjacent specific synapses is unclear. A potential solution involves sequential expression of the transcription factor Sequoia, which dictates N-cadherin responsiveness, in R8 and R7 to promote orderly innervation of the appropriate synaptic layers (Petrovic and Hummel, 2008). This mechanism allows a single transcription factor and adhesion molecule to direct multiple distinct recognition events. These phenomena offer a glimpse into the logic of synaptic specificity, although numerous additional mechanisms are likely to be involved as well.

Guidepost cells promote or inhibit synaptogenesis

Transsynaptic interactions through adhesion molecules such as cadherins, Sidekicks, synCAM, neurexins and neuroligins facilitate direct interactions between pre- and postsynaptic cells. Third-party cells other than the pre- and postsynaptic cells also play significant roles at several steps in synapse development. Guidepost interactions

with glia and other non-neuronal cells can facilitate and reinforce targeting decisions by narrowing the search for synaptic partners. In the mouse brain, immature astrocytes secrete Thrombospondins 1 and 2 to promote synaptogenesis, and mice lacking Thrombospondins 1 and 2 show a 40% reduction in synapses (Christopherson et al., 2005). Interestingly, astrocyte-conditioned medium can induce formation of functional synapses *in vitro*, but the synapses induced by purified Thrombospondins 1 and 2 are silent due to a failure to recruit post-synaptic AMPA receptors. This result suggests that astrocytes secrete factors in addition to Thrombospondins to stimulate synapse maturation. Astrocytes play similar roles in eliminating synapses, inducing postnatal neurons to secrete complement factor C1q, which is used to eliminate synapses (Stevens et al., 2007). Mice lacking C1q or the downstream effector C3 show defects in refinement of retinogeniculate projections, suggesting that these factors may be molecular mediators of remodeling in this system. C1q and C3 are synapse localized, suggesting that they may tag individual synapses for elimination. In *C. elegans*, the axon guidance and synaptic guidepost molecule UNC-6/Netrin is secreted by the glial sheath cell in the nerve ring where it promotes synaptogenesis, supporting a conserved role for glial cells in promoting synaptic interactions. Moreover, in the *C. elegans* egg-laying circuit, receptor-ligand guidepost interactions between SYG-1 expressed on the HSNL neuron and SYG-2 expressed on vulval epithelial cells target HSNL synapses to the adjacent VC neurons and vulval muscle (Shen and Bargmann, 2003, Shen et al., 2004). These results support a conserved role for permissive and instructive guidepost signals from glia and other non-neuronal cells.

While orchestrating their own guidance decisions, neurons can assist their neighbors. In a classical example, vertebrate subplate neurons provide guidepost signals for thalamocortical afferents in the visual system (Ghosh et al., 1990). Cajal-Retzius cells secrete reelin to promote entorhinal innervation of hippocampal pyramidal cells (Del Rio et al., 1997). Interactions between neurons in the same function class are also observed in many cases. Vertebrate olfactory neurons expressing the same olfactory receptor coalesce into glomeruli in the olfactory bulb (Mombaerts et al., 1996), and pre-target sorting of axons is believed to aid in the establishment of the proper topographic map in the olfactory bulb (Imai et al., 2009). These results indicate that target identification often involves the collaborative efforts of many cells, a strategy that may provide a form of proofreading to increase the fidelity of target recognition.

Subcellular targeting of synapses

Guidepost molecules such as SYG-1 and SYG-2 couple specification of synaptic partners to identification of appropriate subcellular regions. In the cerebellum, the adhesion molecule Neurofascin 186 localizes pinceau synapses from basket cells to the axon-initial segment (AIS) of Purkinje cells (Ango et al., 2004). Neurofascin is localized to the AIS through intracellular interaction with Ankyrin G. Mislocalized Neurofascin 186 can direct basket cells to innervate other regions of the Purkinje cell. This mechanism couples target selection to subcellular position. Similarly, Cajal-Retzius-secreted reelin ensures proper subcellular positioning of entorhinal inputs onto hippocampal pyramidal neurons (Del Rio et al., 1997). In other instances, a negative guidepost signal is used to prevent synapse formation in inappropriate regions. In *C*.

elegans, LIN-44/WNT signals through LIN-17/Frizzled to excludes synapses from a portion of the axon of the DA9 neuron (Klassen and Shen, 2007), and UNC-6/Netrin signaling through UNC-5 excludes presynapses from dendrites of DA9 neurons (Poon et al., 2008). These data suggest that target identification and subcellular targeting are often, but not always, coupled processes.

Hierarchical targeting of synapses

Some insight into how neurons interpret the combinatorial synaptic code can be garnered from studies of mutants with altered synaptic specificity. In *C. elegans* lacking *syg-1* or *syg-2*, the HSNL neuron fails to synapse with appropriate targets and forms ectopic synapses with inappropriate targets such as body wall muscle (Shen et al., 2004). SYG-1 promotes formation of presynapses in the correct region of the HSNL axon by locally inhibiting an E3 ubiquitin ligase to prevent synapse elimination, stabilizing the deposition of synaptic machinery at appropriate presynaptic sites (Ding et al., 2007). Loss of localized SYG-1 leads to synapse elimination at this site and the appearance of ectopic synapses at other sites (Ding et al., 2007). Similarly, loss of the correct target cells in the *Drosophila* ommatidium causes R1-6 cells to synapse with available secondary synaptic targets (Hiesinger et al., 2006). These data suggest that the combinatorial code of synaptic specificity may not be all-or-none, and that neurons may compare options to identify the best available. This would be consistent with the explorations performed by neuronal growth cones at *Drosophila* neuromuscular junctions and retinal ganglion cell axons within laminae of the mouse tectum (Shishido et al., 1998, Huberman et al., 2009), suggesting that neurons sample their environments to identify

suitable partners. By contrast with HSNL and R1-6 photoreceptors, loss of the proper synaptic targets causes GABAergic interneurons in the mouse spinal cord to retract their axons, indicating that these neurons may demand a minimum suitability from their targets (Betley et al., 2009). These results offer some insight into different strategies for combinatorial coding, suggesting that cells do not always identify their targets through a cognate, all-or-none recognition event, and that neurons may differ in the reliance on classes of positive and negative cues.

Synapse differentiation

Once two partners have identified each other, they must recruit the appropriate machinery for synaptic transmission. For example, a presynaptic neuron could release excitatory transmitters such as glutamate or inhibitory transmitters such as GABA, and for the synapse to be functional the postsynaptic cell should express the appropriate receptor type. The full details of this process are not clear, but it appears that some of the factors implicated in target recognition can serve parallel or independent roles in synapse differentiation and maturation. The transynaptic adhesion molecules Neurexins were identified as the target for the spider venom alpha-Latrotoxin, and were found to localize to presynaptic sites (Ushkaryov et al., 1992). Beta-Neurexins were subsequently shown to interact with postsynaptic Neuroligins (Ichtchenko et al., 1995). Neuroligin expressed in non-neuronal cells can induce the formation of presynaptic structures in co-cultured neurons (Scheiffele et al., 2000), while Neurexin expressed in non-neuronal cells can induce the formation of post-synaptic structures in co-cultured neurons (Graf et al., 2004). These synaptogenic abilities and the existence of multiple genes and splice

isofoms for Neurexins and Neuroligins suggested the possibility of a Neurexin-Neuroligin code for synapse formation. However, mice lacking the three brain-expressed Neuroligins were analyzed and found to have normal synaptic number and ultrastructure but impaired synaptic function, suggesting that Neurexin-Neuroligin interactions are required for functional maturation and differentiation of synapses (Varoqueax et al., 2006). Biochemical studies have identified signaling components downstream of both molecules. Neurexins bind presynaptic components such as CASK to recruit presynaptic machinery (Hata et al., 1996). Interestingly, the cytosolic tails of Neuroligins bind the third PDZ domain of the post-synaptic scafolding protein PSD-95 and may thereby recruit NMDA-type glutamate receptors to postsynaptic sites (Irie et al., 1997), while Neuroligin 2 selectively localizes to inhibitory synapses where it binds Gephyrin, which activates Collybistin to recruit an inhibitory postsynaptic scaffold and GABA and possibly glycine receptors (Graf et al., 2004, Poulopoulos et al., 2009). In this way, neurexins and neuroligins can link transsynaptic adhesion to synapse differentiation and maturation.

Several secreted molecules can also promote synapse formation. WNT7a promotes synapse maturation and growth in cerebellar mossy fibers (Hall et al., 2000), and Wg and the bone morphogenetic protein homolog Gbb signaling at *Drosophila* neuromuscular junctions promote synaptic maturation (Packard et al., 2002; McCabe et al., 2003). The abilities of synaptic adhesion molecules and synaptogenic factors to function in synapse maturation and differentiation suggest that target selection and acquisition of function are often coordinated processes.

Figure 1.1. Molecular regulators of synaptic specificity. This schematic illustrates the diversity and cellular sources of extracellular signaling molecules that guide synaptic target selection.

Figure 1.1

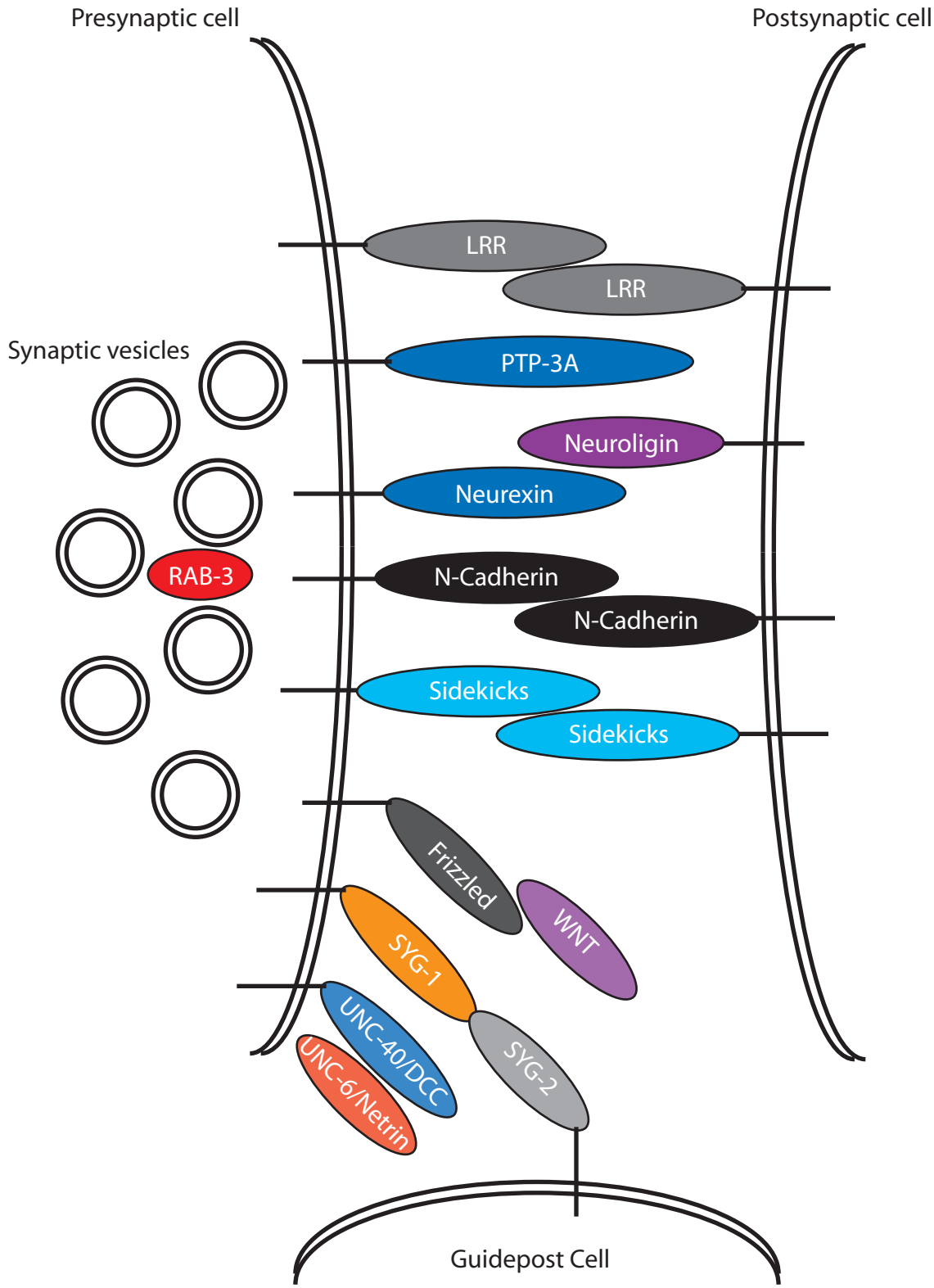
Presynaptic cell
Postsynaptic cell
Synaptic vesicles
LRR
LRR
PTP-3A
Neuroligin
Neurexin
RAB-3
N-Cadherin
N-Cadherin
Sidekicks
Sidekicks
Frizzled
WNT
SYG-1
UNC-40/DCC
UNC-6/Netrin
SYG-2
Guidepost Cell

Chapter 2

GFP reconstitution across synaptic partners (GRASP) defines cell contacts and synapses in living nervous systems

Summary:

The identification of synaptic partners is challenging in dense nerve bundles, where many processes occupy regions beneath the resolution of conventional light microscopy. To address this difficulty, I have developed GRASP, a system to label membrane contacts and synapses between two cells in living animals. Two complementary fragments of GFP are expressed on different cells, tethered to extracellular domains of transmembrane carrier proteins. When the complementary GFP fragments are fused to ubiquitous transmembrane proteins, GFP fluorescence appears uniformly along membrane contacts between the two cells. When one or both GFP fragments are fused to synaptic transmembrane proteins, GFP fluorescence is tightly localized to synapses. GRASP marks known synaptic contacts in *C. elegans,* correctly identifies changes in mutants with altered synaptic specificity, and can uncover new information about synaptic locations as confirmed by electron microscopy. GRASP may prove particularly useful for defining connectivity in complex nervous systems.

Introduction:

After axons have been guided to their targets by long-range and short-range cues, they choose a subset of the available cells as synaptic partners. This process involves identification of appropriate partners, avoidance of incorrect partners, and selection of subcellular regions for synapse formation (Shen, 2004). Current knowledge of synaptic connectivity has been obtained largely by powerful but labor-intensive methods: electrophysiology of coupled cells, or electron microscopy and ultrastructural identification of connected cell types (White et al., 1986; Katz and Dalva, 1994; Reid and Alonso, 1995; Briggman and Denk, 2006). Because of the skill and time required for these experiments, the overall connectivity of most nervous systems remains a mystery. A near-complete ultrastructural analysis has been performed only on the nematode *Caenorhabditis elegans,* where reconstructions of serial-section electron micrographs defined the ~7000 synapses in the entire nervous system in a project spanning two decades (White et al., 1986). Perhaps the next best-understood circuit described by physiology and anatomy is the vertebrate retina, where ~50 cells types are interconnected in complex patterns that are still not fully mapped (Wassle and Boycott, 1991; Vaney and Taylor, 2002). A faster method for analyzing synaptic circuitry would be a great asset for establishing synaptic maps – the anatomical framework for nervous system function.

In recent years, the analysis of synaptic specificity has been accelerated by the use of light microscopy and synaptic labels (Ahmari and Smith, 2002). A synapse is a stable cell junction with vesicles and active zone proteins localized to the presynaptic site, receptors and a scaffolding matrix localized to the postsynaptic site, and adhesion proteins such as cadherins that can bridge both cells. Double-labeling with antibodies to

presynaptic and postsynaptic proteins can define their sites of colocalization at synapses (Ahmari and Smith, 2002). Genetically encoded fluorescent synaptic proteins such as VAMP::GFP can improve resolution by labeling synaptic structures in a subset of cells or a single cell type (Nonet, 1999). However, these approaches lose resolution in locations like the mammalian cortex that contain 100,000 synapses or more per cubic millimeter (Binzegger et al., 2004), a density at which the nearest neighbor of a synaptic marker is ambiguous. Thus in regions where many synapses coexist in a small area, light microscopy fails to provide the resolution needed to identify exact synaptic partners. Other markers that cross synapses such as lectins or rabies or pseudorabies viruses are useful for long-range pathway mapping, but some trans-cellular tracers are toxic, many have some degree of cell type-specificity, and most cross to multiple cells in a region, not just synaptic partners (Schwab and Thoenen, 1976; Card et al., 1990; Peschanski and Ralston, 1985; Cabot et al., 1991; Yoshihara et al., 1999; Maskos et al., 2002; Wickersham et al., 2007).

Here I describe GRASP, a generalizable method to label a synapse based on the proximity of the presynaptic and the postsynaptic plasma membranes. In CNS synapses, the membranes of two synaptic partners are typically separated by less than 100 nm of extracellular space, a distance that can be spanned by transmembrane proteins expressed by the two cells. I detect proximity by the stable, extracellular assembly of the green fluorescent protein from two complementary fragments expressed on different cells, in the context of transmembrane protein carriers that are either broadly distributed on the plasma membrane or narrowly localized to synaptic regions. Using these different carriers, GRASP can be used to assess nearest neighbors across the cell membrane, or the nearest neighbor at a synapse. I confirm the effectiveness of GRASP *in vivo* using the

defined connectivity of the *Caenorhabditis elegans* nervous system as a guide, and demonstrate that GRASP can identify synaptic defects in mutants as well as previously uncharacterized details of synaptic locations.

Results

Development of Cre-loxP intersectional gene expression methods in *C. elegans*

The ability to restrict transgene expression to a few or single cells is essential for any approach to labeling specific synapses *in vivo*, but many well-studied cells lack unique promoters. However, many cells could be uniquely identified by their expression of two overlapping promoters. An intersectional method that exploits this promoter overlap might be of use in restricting transgene expression to single cells. A widely validated system for intersectional gene expression exploits the bacteriophage P1 site-specific recombinase Cre, which catalyzes recombination between two repeats of a 34 base-pair loxP sequence (Abremski and Hoess, 1984). When two such sequences are arranged in tandem on a single piece of DNA, Cre-mediated recombination leads to excision of the intervening sequence (Figure 3.1A). This approach is best known for its applications in conditional knockouts (Gu et al., 1994), but the ability to conditionally excise a DNA sequence can also be exploited to generate intersectional transgene expression. In this approach, a transgene is created in which a cDNA of interest is located 3' of a transcriptional and translational stop sequence that is flanked by loxP sites (Srinivas et al., 2001). In the absence of Cre, these stop sequences preclude expression of that transgene. When a Cre recombinase is expressed, the stop sequence is excised and

Figure 2.1 Cre-mediated recombination allows intersectional control of transgene expression. (A) Schematic of loxP-LacZ-stop-loxP constructs. Black triangles indicate loxP sites. In the absence of Cre, this transgene should express LacZ but not GFP. (B) Detection of LacZ expression in 3 pairs of dopaminergic neurons in the head of a *dat-1*::loxP-LacZ-stop-loxP::GFP animal. (C) No GFP is detected in the *dat-1*::loxP-stop-loxP::GFP animal. (D) Double transgenic strain carrying *dat-1*::nCre and *tag-168*:: loxP-stop-loxP::GFP strain displays GFP expression in the dopaminergic cells only. No GFP was observed in either single strain. Scale bars, 10 μm.

Figure 2.1

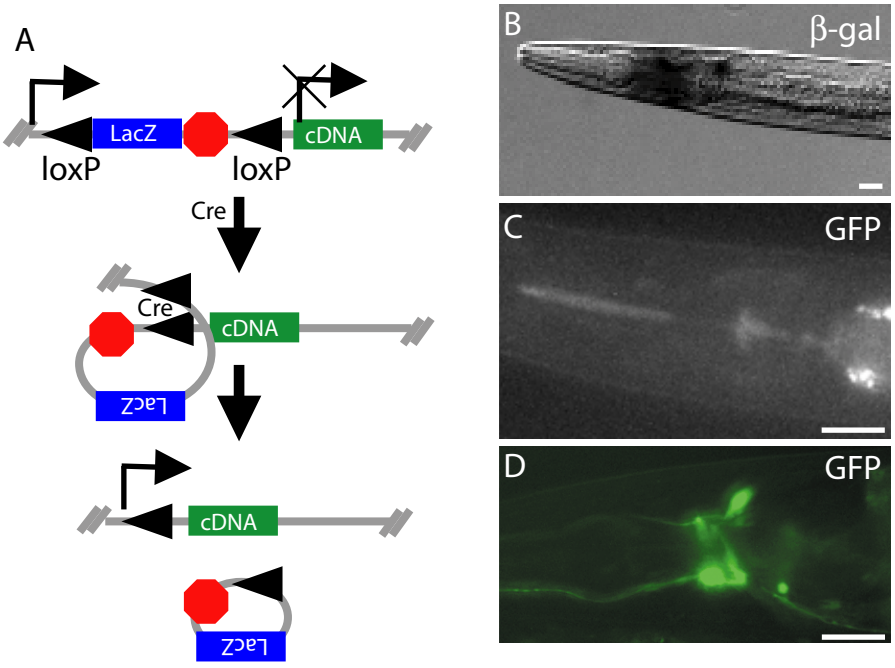
A
LacZ
cDNA
loxP
loxP
Cre
Cre
cDNA
LacZ
cDNA
LacZ
B
β-gal
C
GFP
D
GFP

the transgene is expressed. By controlling the site of Cre expression, this system provides conditional control of transgene activity.

I reasoned that this approach could be used to confine promoter expression to a single cell or group of cells. To apply this method to *C. elegans*, I generated a loxP-stop-loxP cassette with two loxP sites flanking the bacterial lacZ gene followed by a stop sequence. The loxP sites were placed in the antisense orientations to avoid spurious translational initiation from an internal ATG site on the sense strand. The lacZ sequence was included as a spacer to allow DNA bending during recombination. The stop sequence consists of two stop codons following the lacZ gene, three repeats of an AATAAA translational stop sequence (Srinivas et al., 2001), and two repeats of an mRNA cleavage and polyadenylation site (Kuersten et al., 1997). This construct was inserted downstream of the dat-1 promoter, which drives expression in four pairs of dopaminergic neurons (Carvelli et al., 2004), and upstream of GFP. Animals carrying this transgene showed detectable beta-galactosidase activity in the 4 pairs of dopaminergic neurons, but GFP expression was undetectable (Figure 2.1B-C). These data confirm that the transgene was present in these animals and that the synthetic stop sequence prevents expression of the downstream GFP protein.

I next asked whether Cre was able to excise the stop sequence to yield GFP expression. Although Cre has been shown to be active in a variety of heterologous systems, its activity at the C. elegans cultivation temperature (15-25 degrees Celsius, as compared to 37 degrees Celsius for E. coli and most vertebrates) was unknown. Cre activity in worms was tested with two transgenic strains. In the first strain, a pan-neuronal promoter was used to drive expression of the loxP-stop-loxP::GFP construct. In the second strain, the *dat-1* promoter was used to drive expression of nuclear-localized Cre (nCre), which is more active in many contexts than wild-type Cre (Sato et al., 2000),

in dopaminergic cells. GFP expression was not detected in either strain. The two strains were crossed, and GFP expression was observed exclusively in the dopaminergic neurons, indicating that Cre recombinase can be active in somatic cells in C. elegans, and that its activity can be restricted to cells of interest with suitable promoters. Taken together, these data indicate that Cre-lox technology can be used for intersectional control of gene expression in *C. elegans*.

Subsequent experiments have demonstrated limitations of this tool. First, GFP expression in the RMG neuron following Cre-mediated recombination is much dimmer than expected from a multi-copy array (E. Macosko, personal communication). This may reflect successive recombination events between loxP sites within the multicopy array that reduce transgene copy number. Second, many *C. elegans* researchers use polycistronic transgenes with cDNAs separated by SL2 splice acceptor sites, which allow splicing of a single pre-mRNA to separate mRNAs. When a polycistronic transgene containing an SL2 followed by GFP is placed downstream of the loxP-stop-loxP sequence, weak GFP expression was observed in the absence of Cre (E. Macosko, personal communication). These data suggest that the transcriptional stop sequence permits some readthrough transription, and that the lack of GFP expression observed in earlier experiments is due to the translational stop sequence. Future conditional expression of SL2 vectors or RNAi transgenes may require development of improved transcriptional stop sequences may be needed.

Split GFP reconstitutes in the extracellular space

To label synapses, or more generally to label adjacent cells, I used complementary fragments of GFP tethered to plasma membrane carrier proteins to detect the proximity of two cell membranes (Figure 2.2A). The individually non-fluorescent split GFP

Figure 2.2. GRASP strategy and demonstration of extracellular GFP reconstitution *in vitro* and *in vivo*.

(A) Schematic diagram of GRASP with (left) delocalized CD4 tethers, (center) presynaptically localized PTP-3A and a delocalized CD4 tether, and (right) pre- and post-synaptically localized NLG-1 tethers. Asterisk symbolizes presynaptic site; arrowhead, postsynaptic site.

(B-G) Extracellular GFP reconstitution in culture. Three cells express mCherry and CD4::spGFP11 and one cell expresses nuclear CFP and CD4::spGFP1-10. (B) Schematic diagram. (C) Differential interference contrast microscop.y (D) mCherr.y (E) nuclear CFP. (F) GRASP GFP signal. (G) Merge. Body wall muscle cells were labeled using the *myo-3* promoter.

(H-L) Extracellular GFP reconstitution *in vivo.* (H) Schematic drawing of two rows of dorsal body wall muscles. Medial muscle cells express mCherry and CD4::spGFP11, and lateral muscle cells express nuclear CFP and CD4::spGFP1-10. (I) mCherry. (J) nuclear CFP. (K) GRASP GFP signal; yellow arrowhead marks CFP bleed-through. (L) Merge. Medial dorsal body wall muscle cells were labeled using the *ace-4* promoter, and lateral body wall muscle cells using the *him-4* promoter. Scale bars are 5 μm in C-G, 10 μm in I-L.

Figure 2.2

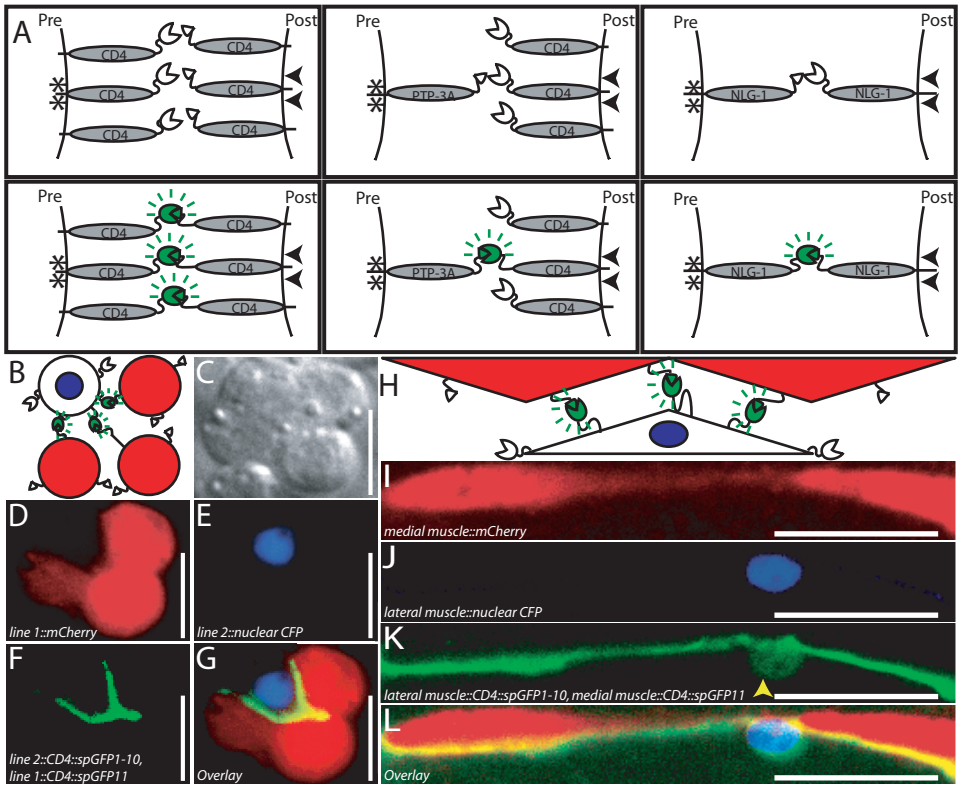
A
Pre
Post
CD4
PTP-3A
NLG-1
B
C
D
E
F
G
H
I
J
K
L
line 1::mCherry
line 2::nuclear CFP
line 2::CD4::spGFP1-10,
line 1::CD4::spGFP11
Overlay
medial muscle::mCherry
lateral muscle::nuclear CFP
lateral muscle::CD4::spGFP1-10, medial muscle::CD4::spGFP11
Overlay

fragments assemble into a fluorescent form only when the membranes are sufficiently close to permit carrier proteins to bridge the intercellular gap. This approach is conceptually similar to split-GFP methods for determining intracellular protein-protein interactions in living cells (Zhang et al., 2004), but modifications were necessary for extracellular GFP assembly. Most split GFP proteins used for intracellular assembly require exogenous dimerization domains to fold, and indeed that is the basis of their usefulness as protein interaction monitors (Zhang et al., 2004). In membrane proteins, however, unfolded protein domains activate quality-control pathways in the endoplasmic reticulum and therefore destabilize the protein before it reaches the cell surface. A split-GFP system that addresses this concern has been developed and applied in cells and cell lysates (Cabantous et al., 2005). One fragment of the split GFP contains the first 214 residues of the exceptionally stable, fast-folding "superfolder" GFP protein (Pedelacq et al., 2006), further evolved to be stable as a protein fragment. This fragment includes ten of the eleven strands of the beta-barrel structure of GFP and will be called spGFP1-10. The second split-GFP fragment consists of just 16 residues, 215-230, which make up the 11^{th} strand of the GFP beta-barrel. This second fragment, spGFP11, acts as a small protein tag that can be inserted into many different proteins without affecting their solubility (Cabantous et al., 2005). Thus each of these fragments should be soluble, nonfluorescent, and relatively inert in the absence of its complementary fragment. Moreover, superfolder GFP crystallizes as a monomer, suggesting that it should not serve as a nucleation site for further protein aggregation (Pedelacq et al., 2006).

For GRASP to act as a transmembrane proximity detector, both fragments should be tethered to the plasma membranes of the test cells. As a potentially inert tether

protein, I began with the human T cell protein CD4, a structurally characterized protein whose natural extracellular ligand, the MHC class II protein, is not present in *C. elegans.* To minimize intracellular interactions, cytosolic domains of CD4 that interact with signaling molecules were deleted, leaving a seven amino acid cytosolic tail; the extracellular domain was also truncated to include only one or two of its four immunoglobulin domains. spGFP1-10 and spGFP11 were separately inserted into extracellular loop regions defined by the crystal structure of CD4 (Ryu et al., 1990), with GFP11 followed by a glycine-serine linker (Figure 2.2A). Neither of these CD4::spGFP fragments resulted in detectable GFP fluorescence when individually expressed in *C. elegans* neurons or muscle (Figure 2.2).

As a stringent test for the extracellular assembly of the tethered split-GFP proteins, cultured cells expressing complementary CD4::spGFP fragments were mixed *in vitro.* Two different transgenic *C. elegans* strains were generated; one strain expressed CD4::spGFP1-10 and a nuclear CFP protein under the muscle-specific *myo-3* promoter, and the second strain expressed CD4::spGFP11 and a soluble mCherry protein under the *myo-3* promoter. Primary myocytes and neurons from both strains were isolated after dissociation of embryos, mixed together, and cultivated overnight (Christensen et al., 2002). GFP fluorescence was undetectable in myocytes from either transgenic strain, although the mCherry and nuclear CFP were readily detectable, but strong GFP fluorescence was observed at the interface of myocytes that expressed mCherry and myocytes that expressed nuclear CFP (Figure 2.2B-G). This experiment established that the CD4-tethered spGFP fragments were able to associate, fold, and fluoresce in the extracellular space.

To determine whether tethered CD4::spGFP molecules could assemble at extracellular sites *in vivo*, complementing fragments were expressed in nonoverlapping but adjacent sets of body wall muscle cells. In all CD4::spGFP *in vivo* GRASP experiments, the two spGFP fragments were individually injected into different strains, along with mCherry or nuclear CFP markers for the cells of interest, and the single strains were examined to ensure that they did not produce detectable GFP fluorescence. The transgenic strains were then crossed together to generate strains bearing both spGFP transgenes, which were examined for GFP fluorescence. This double-transgenic approach was used because the DNA fragments in a single transgenic array sometimes recombine with each other (Mello and Fire, 1995), and recombination or interactions between promoters in a single transgenic array had the potential to generate spurious GFP fluorescence. *C. elegans* body wall muscle is arranged in four quadrants, with each quadrant consisting of two interdigitated rows of medial and lateral myocytes. The *him-4* promoter is expressed only in lateral myocytes, while the *ace-4* promoter is expressed only in dorsal medial myocytes (Combes et al., 2003; Vogel and Hedgecock, 2001). Differential expression of CD4::spGFP fragments from the *him-4* or *ace-4* promoters would be predicted to allow GFP assembly only in the dorsal quadrants, at the contacts between the lateral and medial muscle cells. Indeed, in animals expressing both *ace-4::CD4::spGFP1-10* and *him-4::CD4::spGFP11,* GFP fluorescence appeared at the junctions of dorsal medial and lateral muscle cells (Figure 2.2H-L). As observed in culture, the GRASP GFP signal *in vivo* was restricted to sites of cell contact, suggesting that the membrane tethers were intact.

The *ace-4* promoter is strongly expressed in L1 larvae, and downregulated in adults (Combes et al., 2003). The muscle cell GRASP GFP signal followed a similar time course, with a strong larval signal that disappeared in adult animals. Although GFP assembly is thought to be irreversible once it occurs (Kerppola, 2006), this observation suggests that the normal turnover of the CD4 tether protein can disrupt the refolded GFP or release it from cells. Weak GFP signals were sometimes observed in internal vesicles, suggesting the internalization of the refolded proteins.

GRASP can label synapses in wild-type animals

To generate markers for synapses, at least one of the two spGFP tether proteins should be localized to synaptic regions. The best-characterized presynaptic transmembrane protein in *C. elegans* is PTP-3A, a member of the LAR/receptor tyrosine phosphatase family with extracellular Ig repeats and Fibronectin type III repeats (Ackley et al., 2005). PTP-3A and related proteins affect synaptic development and morphology in *C. elegans, Drosophila,* and vertebrates (Ackley et al., 2005; Dunah et al., 2005; Kaufmann et al., 2002). *C. elegans* PTP-3A is expressed in many neuronal cell types, and in motor neurons is tightly localized to presynaptic active zones through interactions with the extracellular matrix component nidogen and the active zone protein SYD-2/liprin-alpha (Ackley et al., 2005). PTP-3A::spGFP was generated by inserting the small spGFP11 tag immediately after an artificial signal peptide followed by full-length PTP-3A (Figure 2.2A). In GRASP experiments, PTP-3A in presynaptic neurons was paired with the delocalized CD4::spGFP1-10 tether on postsynaptic partners.

Another potential way to visualize specific synapses between two neurons is to target both GRASP carriers to pre- and postsynaptic sites. To construct such a marker, Miri VanHoven and Kang Shen searched for transmembrane molecules that are targeted to synapses. In the vertebrate central nervous system, neuroligins are preferentially localized to postsynaptic sites, where they interact with presynaptic neurexins to affect synaptic maturation and function (Craig and Kang, 2007; Varoqueaux et al., 2006). *C. elegans* has a single neuroligin homolog, C40C9.5 (*nlg-1)*, that is widely expressed in the nervous systems (www.wormbase.org). A full-length NLG-1 cDNA was tagged with intact YFP and expressed in different neuronal cell types. Consistent with vertebrate findings, bright punctate staining was observed in dendritic (postsynaptic) regions (Figure 2.3). Surprisingly, clear punctate staining was also observed in presynaptic regions of each neuronal type. For example, in the DA9 motor neuron, bright NLG-1::YFP puncta were present in the ventral postsynaptic domain and dimmer puncta were present in the dorsal presynaptic region (Figure 2.3A-B). Puncta were excluded from the synapse-poor region between the cell body and dorsal presynaptic region, and from the anterior asynaptic region of the dorsal process. To further study the punctate staining in the presynaptic region, NLG-1::YFP localization was examined in animals expressing the tagged synaptic vesicle protein mCherry::RAB-3 in DA9. In the dorsal axon, NLG-1::YFP puncta partially colocalized with puncta containing mCherry::RAB-3, suggesting that NLG-1::YFP localization is perisynaptic (Figure 2.3C-E).

Like DA9, AVE interneurons and VA motor neurons have distinct presynaptic and postsynaptic regions. AVE interneurons have a dense postsynaptic region in the nerve ring and a sparse presynaptic region in the ventral nerve cord. VA motor neurons

Figure 2.3. *C. elegans* neuroligin localizes to both pre- and postsynaptic regions of neurons.

(A, B) NLG-1::YFP localizes to pre- and postsynaptic regions of DA9 motor neurons, but is more prominent in the postsynaptic region.

(C-E) NLG-1::YFP colocalizes with the synaptic vesicle marker mCherry::RAB-3 in DA9. (C) NLG-1::YFP. (D) mCherry::RAB-3. (E) Merge. Yellow arrowheads indicate colocalizing puncta, white arrows indicate RAB-3-only puncta. In A-E, DA9 expression was directed by the *mig-13* promoter.

(F, G) NLG-1 localizes to pre- and postsynaptic regions of AVE interneurons, labeled using the *opt-3* promoter. P, Pharynx.

(H, I) NLG-1 localizes to pre- and postsynaptic regions of VA motor neurons, labeled using the *unc-4* promoter.

Known synaptic domains (White et al., 1986) are indicated in schematic diagrams (A, F, H). Anterior is at left in all panels. Scale bars are 10 μm.

Figure 2.3

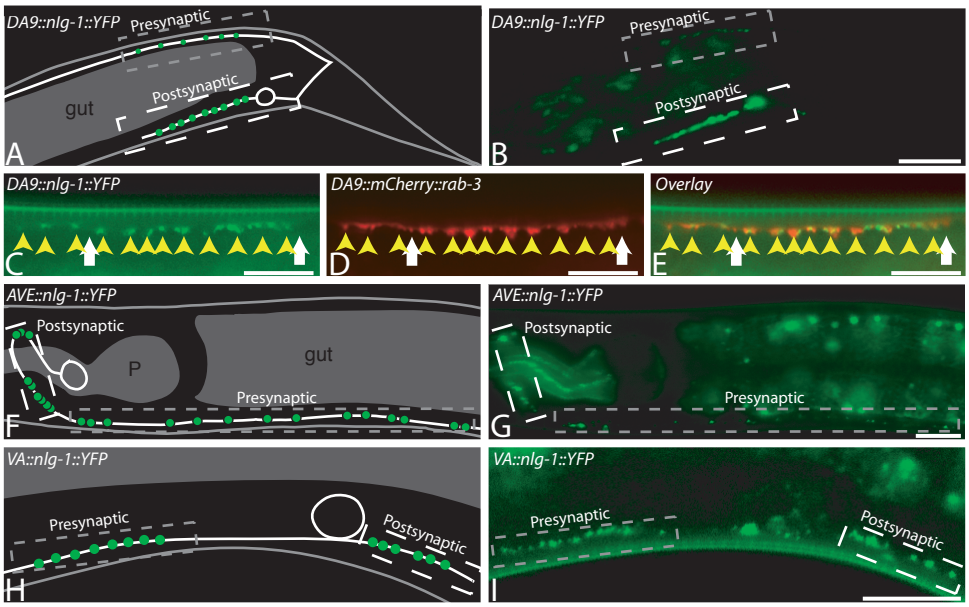
DA9::nlg-1::YFP
Presynaptic
gut
Postsynaptic
A
DA9::nlg-1::YFP
Presynaptic
Postsynaptic
B
DA9::nlg-1::YFP
C
DA9::mCherry::rab-3
D
Overlay
E
AVE::nlg-1::YFP
Postsynaptic
P
gut
Presynaptic
F
AVE::nlg-1::YFP
Postsynaptic
Presynaptic
G
VA::nlg-1::YFP
Presynaptic
Postsynaptic
H
VA::nlg-1::YFP
Presynaptic
Postsynaptic
I

have cell bodies in the ventral nerve cord and extend short dendrites posteriorly and longer axons anteriorly. NLG-1::YFP was present in both presynaptic and postsynaptic regions of each of these neuronal classes, but absent from asynaptic zones of the processes (Figure 2.3F-I). NLG-1 thus has the potential to label all synapses made by a single cell, both at presynaptic and at postsynaptic sites.

The activities of three different GRASP pairs – CD4:CD4, PTP-3A:CD4, and NLG-1:NLG-1 – were compared in a common set of synaptic partners. The AVA command neurons of *C. elegans* form synapses and gap junctions with VA and DA motor neurons along the entire length of the ventral nerve cord (Figure 2.4A-C) (White et al., 1976; White et al., 1986). One member of a GRASP pair was expressed in AVA neurons under either the *rig-3* promoter or the *flp-18* promoter, which are unique to AVA neurons in the ventral nerve cord (www.wormbase.org), and the other GRASP partner was expressed in VA and DA neurons using the *unc-4* promoter, which is limited to VA, DA, and VC motor neurons in the ventral nerve cord (Lickteig et al., 2001).

When AVA or VA/DA neurons were labeled with the complementary CD4:CD4 GRASP pair, GFP fluorescence was observed along the entire ventral nerve cord (Figure 2.4D-F). Labeling appeared uniform along most of the ventral cord, suggesting that the signal resulted from general proximity of axons and not from synapses or gap junctions, which should appear more punctate. No GFP fluorescence was detected with the individual AVA or VA/DA spGFP transgenes.

When the PTP-3A:CD4 GRASP pair or the NLG-1:NLG-1 GRASP pair (M. VanHoven and K. Shen) were used to label AVA and VA/DA neurons, discrete puncta of GFP fluorescence were visible along the mCherry-labeled VA/DA axons, in contrast with

Figure 2.4. GRASP labels neuronal contact sites and synapses *in vivo*.

(A) Schematic diagram of AVA neuron and VA and DA motor neurons. (B) mCherry-labeled VA neuron. (C) mCherry-labeled AVA neuron.

(D-F) CD4 GRASP smoothly labels AVA-to-VA/DA axon contacts. AVA expresses CD4::spGFP11, VAs and DAs express CD4::spGFP1-10 and mCherry. (D) mCherry. (E) GRASP GFP signal. (F) Merge.

(G-I) PTP-3A:CD4 GRASP labels punctate AVA-to-VA/DA synaptic contacts. AVA expresses PTP-3A::spGFP11, VAs and DAs express CD4::spGFP1-10 and mCherry (G) mCherry. (H) GRASP GFP signal. (I) Merge.

(J-L) NLG-1 GRASP requires both spGFP fragments. (J) NLG-1::spGFP1-10 expressed in AVA. (K) NLG-1::spGFP11 expressed in VA and DA. (L) Combined expression of NLG-1::spGFP1-10 in AVA and NLG-1::spGFP11 in VA and DA. Arrowheads flank GRASP GFP puncta.

(M-N) NLG-1 GRASP in a mosaic animal. (M) mCherry-labeled VA axons and cell bodies. (N) GRASP GFP signal. Anterior VA and DA neurons lacking NLG-1::spGFP11 are devoid of GRASP signals (white arrows), in contrast to posterior VA and DA neurons expressing NLG-1::spGFP11 (yellow arrowheads).

(O-Q) NLG-1 GRASP colocalizes with synaptic markers. (O) NLG-1 GRASP between AVA and VA and DA neurons. (P) Presynaptic mCherry::RAB-3 marker in AVA. (Q) Merge. Yellow arrowheads indicate colocalizing puncta, white arrows indicate RAB-3-only puncta. AVA was labeled using *rig-3* or *flp-18* promoters, VA and DA using the *unc-4* promoter. Anterior is at top center in C and at left in all other panels.

Figure 2.4

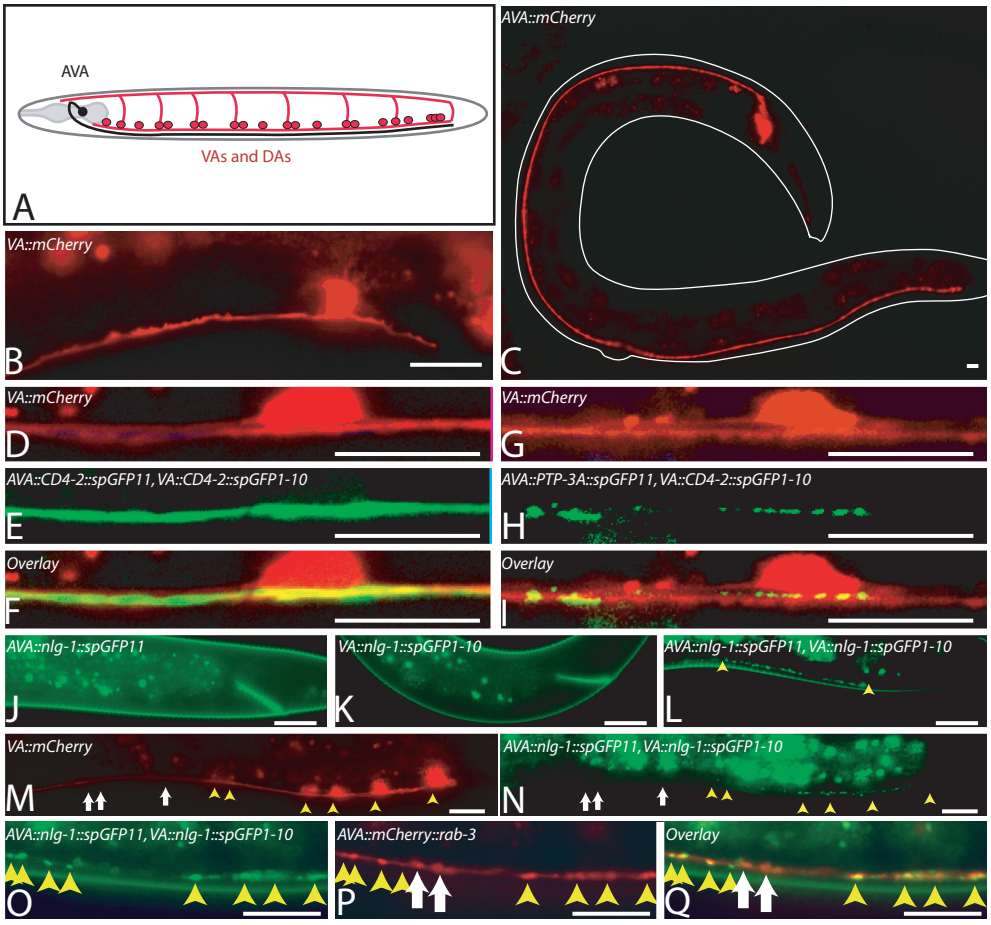
AVA
VAs and DAs
A
AVA::mCherry
VA::mCherry
B
C
VA::mCherry
D
VA::mCherry
G
AVA::CD4-2::spGFP11, VA::CD4-2::spGFP1-10
E
AVA::PTP-3A::spGFP11, VA::CD4-2::spGFP1-10
H
Overlay
F
Overlay
I
AVA::nlg-1::spGFP11
J
VA::nlg-1::spGFP1-10
K
AVA::nlg-1::spGFP11, VA::nlg-1::spGFP1-10
L
VA::mCherry
M
AVA::nlg-1::spGFP11, VA::nlg-1::spGFP1-10
N
AVA::nlg-1::spGFP11, VA::nlg-1::spGFP1-10
O
AVA::mCherry::rab-3
P
Overlay
Q

the uniform fluorescence seen with CD4:CD4 GRASP (Figure 2.4G-L). The GRASP signals appeared as clusters of ~10 puncta separated by gaps, as expected if a single cluster represents AVA connections with one motor neuron (White et al., 1976). Thus, synaptic localization of either one or both spGFP carriers can localize the reconstituted GFP signal to specialized membrane domains.

To confirm that GRASP signals were at synapses, and to distinguish between the chemical synapses and the gap junctions made between AVA and VA/DA neurons, a labeled RAB-3 synaptic vesicle protein was expressed in AVA neurons together with the NLG-1 GRASP partner. Most NLG-1 GRASP signals colocalized with RAB-3::mCherry puncta, suggesting that the GRASP signal corresponds to chemical synapses and not gap junctions (Figure 2.4M-O). However, some AVA RAB-3::mCherry puncta were not associated with NLG-1 GRASP signals, consistent with the fact that AVA makes synapses onto other neurons in the ventral nerve cord that do not express *unc-4*.

GRASP detects synaptic specificity mutants

AVA-to-VA synapses have been the subject of extensive genetic studies. A paired-type homeodomain protein, UNC-4, and a Groucho corepressor, UNC-37, are required in VA2-VA10 neurons to specify the correct pattern of presynaptic input from AVA neurons (White et al., 1992; Miller et al., 1992; Pflugrad et al., 1997). Other properties of VA neurons, including their morphologies, ability to express *unc-4,* axon guidance, and fasciculation are not affected by *unc-4* and *unc-37* mutations, nor are synapses from AVA onto the DA neurons affected. In the posterior *C. elegans* nerve cord, synapses from AVA to VA10 are localized between the VA10 cell body and the

DA7 cell body (Figure 2.5A-C)(White et al., 1976)(E. Chen, D. Hall, and D. Chklovskii, personal communication). The majority of synapses between AVA and *unc-4*-expressing neurons in this small region should be from AVA onto VA10 neurons. A small cluster of NLG-1 GRASP GFP signals was reliably present between VA10 and DA7 in wild-type animals, but was systematically lost in *unc-4* and *unc-37* mutants, consistent with the loss of AVA-to-VA synapses (M. VanHoven and K. Shen, Figure 2.5). A nearby cluster of GFP puncta behind the VA11 cell body was intact in mutants, as expected based on EM data showing that the *unc-4* mutation spares synapses between AVA and VA11 neurons (Figure 2.5C-G). These results indicate that GRASP labeling can be used to visualize differences in synaptic connectivity in the ventral nerve cord of wild-type and mutant animals.

A different set of genetically characterized synapses, those associated with the egg-laying motor neuron HSN, was analyzed using PTP-3A: CD4 GRASP in collaboration with Andres Bendesky. HSN forms synapses onto vulval muscles and VC4 and VC5 neurons in the middle of the body near the vulval opening (Figure 2.6A)(White et al., 1986). To examine HSN synapses onto muscles, the *tph-1* promoter was used to express PTP-3A::spGFP11 in HSN, and the *myo-3* promoter was used to express CD4::spGFP1-10 in vulval muscles and body wall muscles. Discrete GFP puncta were observed on HSN branches near the vulva, where HSNs synapse onto vulval muscles (Figure 2.6B-E). Although body wall muscles lie near HSN in the ventral nerve cord, HSN does not synapse onto them and no GFP signals were observed there (Figure 2.6B-E).

Figure 2.5. NLG-1 GRASP reveals synaptic defects in *unc-4* and *unc-37* mutants. (A) mCherry-labeled VA and DA neurons. (B) Schematic diagram of posterior VA and DA neurons shown in (A). (C) AVA-to-VA/DA NLG-1 GRASP of the animal in (A), showing GFP puncta at sites of AVA-to-VA/DA synapses. (D-G) *unc-4* and *unc-37* mutations disrupt AVA to VA10 synapses but not AVA to VA11 synapses. (D) Schematic diagram. (E,F) NLG-1 GRASP of *unc-4* (E) and *unc-37* (F) animals. (G) Quantification of GFP fluorescent puncta, as shown in C,E,F. Scale bars are 10 μm.

Figure 2.5

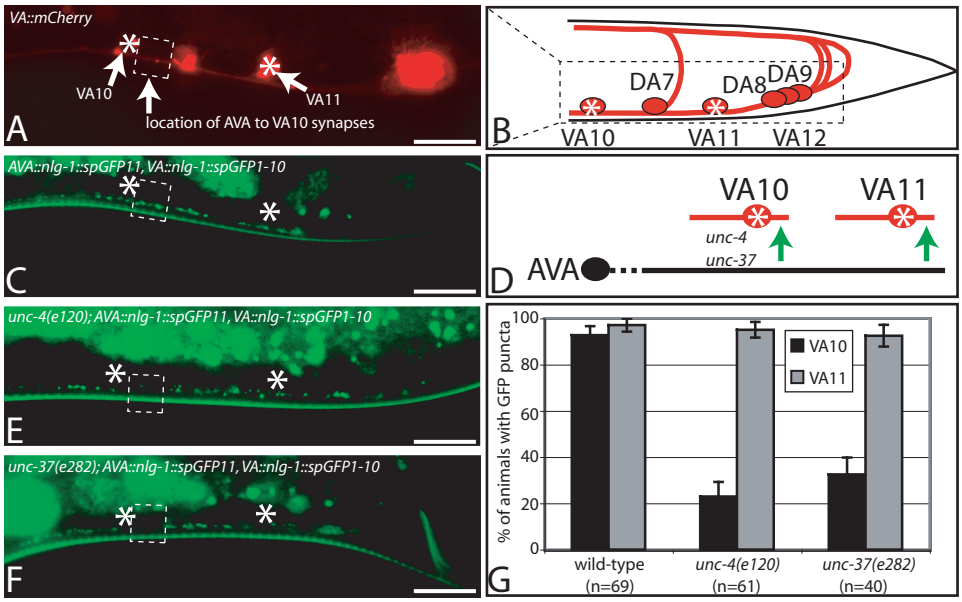
VA::mCherry
VA10
VA11
location of AVA to VA10 synapses
A
DA7
DA8
DA9
VA10
VA11
VA12
B
AVA::nlg-1::spGFP11, VA::nlg-1::spGFP1-10
C
VA10
VA11
unc-4
unc-37
AVA
D
unc-4(e120); AVA::nlg-1::spGFP11, VA::nlg-1::spGFP1-10
E
unc-37(e282); AVA::nlg-1::spGFP11, VA::nlg-1::spGFP1-10
F
% of animals with GFP puncta
100
80
60
40
20
0
VA10
VA11
wild-type
(n=69)
unc-4(e120)
(n=61)
unc-37(e282)
(n=40)
G

Figure 2.6. PTP-3A:CD4 GRASP identifies synaptic defects in *syg-1* mutants. (A-I) PTP-3A:CD4 GRASP between HSN and muscles. HSN expresses PTP-3A::spGFP11 and mCherry, and muscles express CD4::spGFP1-10. (A) Schematic diagram of positions of HSN neuron, vulval muscles (VM), VC neurons, select body wall muscle (BWM), and normal and ectopic synapses. (B-E) PTP-3A:CD4 GRASP in wild-type animal. (B) mCherry-labeled HSN axon. (C) GRASP GFP signal. (D) Merge. (E) Schematic diagram. White arrows mark GRASP-labeled synapses. Asterisks indicate vulval autofluorescence. (F-I) PTP-3A:CD4 GRASP in *syg-1(ky652)* mutant animal (F) mCherry-labeled HSN axon. (G) GRASP GFP signal. (H) Merge (I). Schematic diagram. Yellow arrowheads mark GRASP-labeled ectopic synapses. (J) Quantification of GRASP signals in the anterior HSN axon (dotted box in A) (n=11-12, $P < 0.01$, unpaired t-test). (K) Quantification of GRASP signal in the segment of the HSN axon near the vulva (dashed box in A)(n=11-12, $P<0.01$, unpaired t-test). HSN was labeled using the *tph-1* promoter, vulval and body wall muscles using the *myo-3* promoter. Anterior is at left and ventral is at bottom in all images. Scale bars are 10 μm.

Figure 2.6

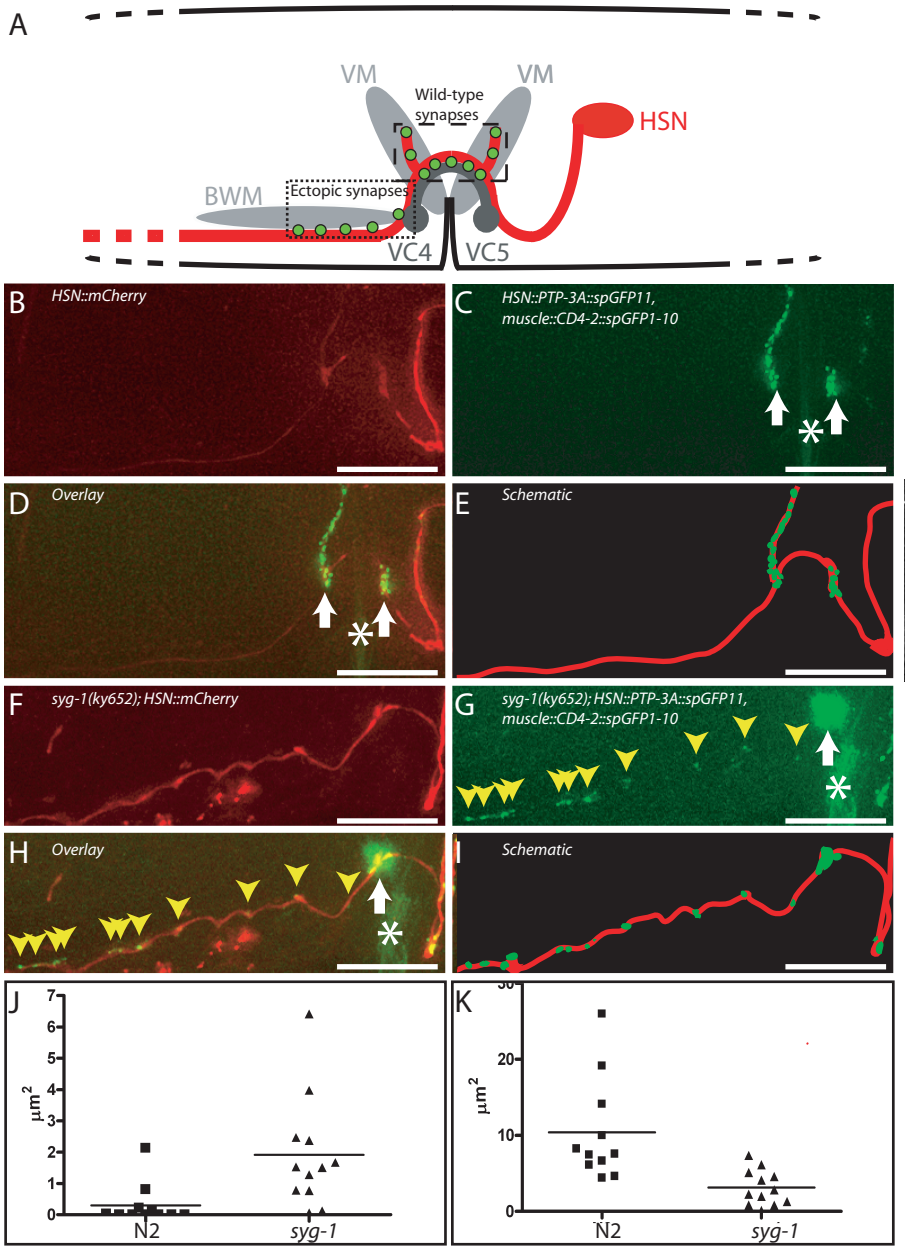
A
VM
VM
Wild-type synapses
HSN
BWM
Ectopic synapses
VC4
VC5
B HSN::mCherry
C HSN::PTP-3A::spGFP11, muscle::CD4-2::spGFP1-10
D Overlay
E Schematic
F syg-1(ky652); HSN::mCherry
G syg-1(ky652); HSN::PTP-3A::spGFP11, muscle::CD4-2::spGFP1-10
H Overlay
I Schematic
J
µm2
N2
syg-1
K
µm2
N2
syg-1

The synaptic specificity of HSN is disrupted by mutations in the genes *syg-1* and *syg-2,* which encode transmembrane proteins that are expressed in HSN and in guidepost cells that localize HSN synapse formation, respectively (Shen and Bargmann, 2003; Shen et al., 2004). In *syg-1* and *syg-2* mutants there is a partial loss of HSN synapses near the vulva and the ectopic appearance of anterior synapses onto body wall muscle. Both missing and ectopic synapses were reflected in the pattern of fluorescence using PTP-3A:CD4 GRASP in *syg-1* and *syg-2* mutants (Figure 2.6F-I). Quantification of signal intensity demonstrated a six-fold increase in anterior GRASP fluorescence and a four-fold decrease in vulval GRASP fluorescence in the *syg-1* strain compared to wild type (Figure 2.6 J-K). These results suggest that GRASP accurately recapitulates the underlying synaptic connectivity in wild-type and mutant HSN neurons.

GRASP detects the subcellular positions of specific synapses

HSN synapses onto VC neurons were visualized by pairing the presynaptic PTP-3A partner in HSN with *unc-4::CD4::spGFP1-10,* which labels VC, VA, and DA neurons. VC axons defasciculate dorsally from the ventral nerve cord near the vulva, so *unc-4* signals in this loop are exclusively from VC and not from VA or DA (Figure 2.6A). As expected from HSN connectivity, GRASP GFP fluorescence was observed only in this loop near the vulva, although HSN runs near many *unc-4*-expressing neurons in the ventral nerve cord. To my surprise, the GRASP pattern was different from that observed with the vulval muscle *myo-3::CD4::spGFP1-10* transgene (Figure 2.7A-F). Whereas HSN-to-vulval-muscle fluorescence was strongest at the two branch points or branches of the HSN axon that flank the vulval opening, HSN-to-VC fluorescence was concentrated

Figure 2.7. GRASP identifies subcellular locations of specific synapses

(A-C) PTP-3A:CD4 GRASP between HSN expressing PTP-3A::spGFP11 and mCherry, and vulval muscles expressing CD4::spGFP1-10. (A) mCherry-labeled HSN axon. (B) GRASP GFP signal. (C) Merge. (D-F) PTP-3A:CD4 GRASP between HSN expressing PTP-3A::spGFP11 and mCherry and VC neurons expressing CD4::spGFP1-10. (D) mCherry-labeled HSN axon. (E) GRASP GFP signal. (F) Merge. White arrows mark GRASP signal, asterisk indicates vulval autofluorescence.

(G) Location and postsynaptic partner of individual HSN synapses from a wild-type L4 animal, reconstructed from 2000 serial electron micrograph sections (Shen et al., 2004). The vulva is approximately 10 μm long.

(H-K) NLG-1 GRASP signals at synapses between AIY and RIA interneurons (H, I) and AIY interneurons and AFD sensory neurons (J, K). Schematic diagrams in H and J show cell positions and locations of specific synapses (White et al., 1986). AIY expresses NLG-1::spGFP1-10, and RIA (I) or AFD (K) express NLG-1::spGFP11. AIY was labeled using the *ttx-3* promoter, RIA using the *glr-3* promoter, and AFD using the *gcy-8* promoter. Scale bars are 10 μm. Anterior is at left and ventral is at bottom in all images.

Figure 2.7

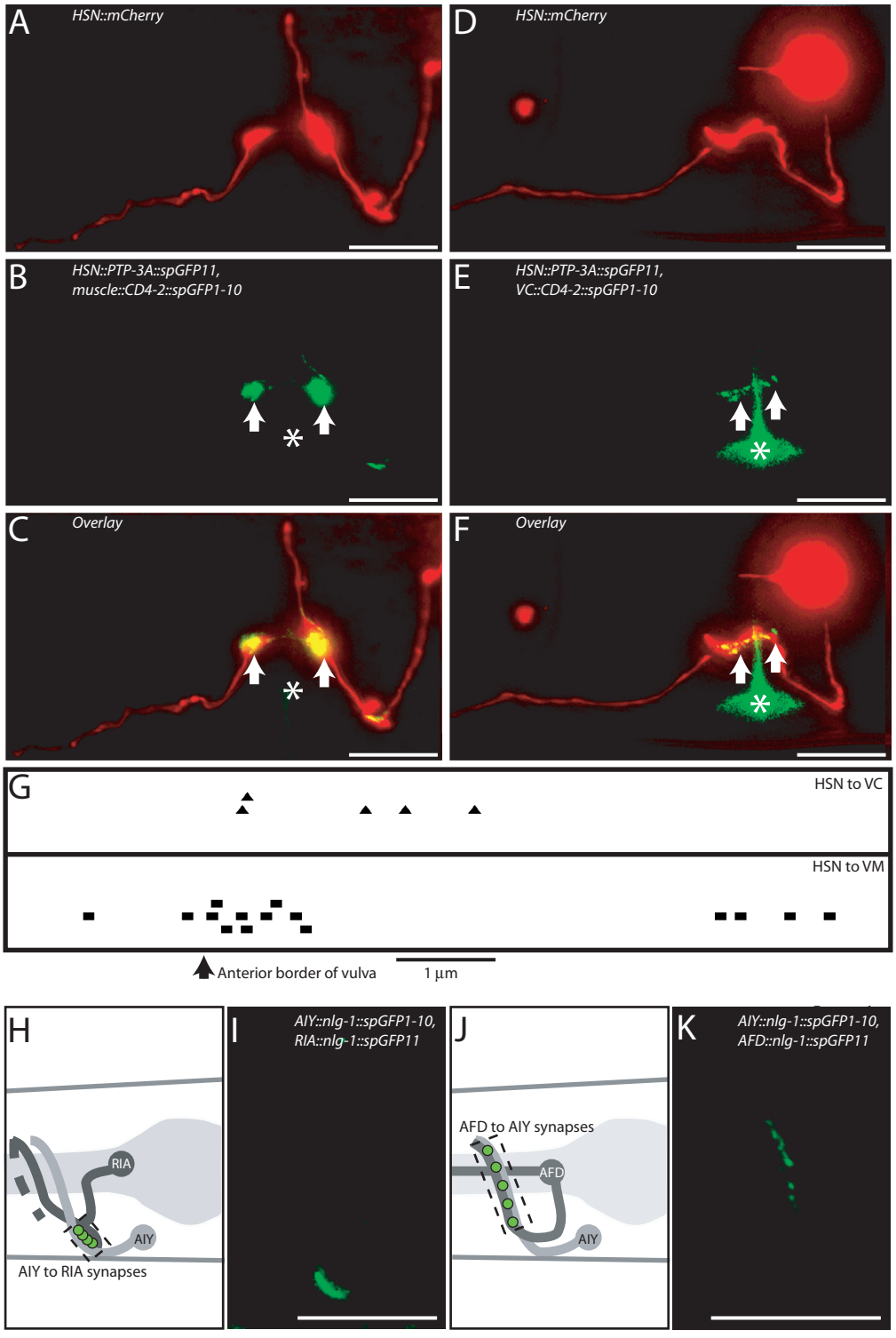
A
HSN::mCherry
D
HSN::mCherry
B
HSN::PTP-3A::spGFP11,
muscle::CD4-2::spGFP1-10
E
HSN::PTP-3A::spGFP11,
VC::CD4-2::spGFP1-10
C
Overlay
F
Overlay
G
HSN to VC
HSN to VM
Anterior border of vulva
1 µm
H
RIA
AIY
AIY to RIA synapses
I
AIY::nlg-1::spGFP1-10,
RIA::nlg-1::spGFP11
J
AFD to AIY synapses
AFD
AIY
K
AIY::nlg-1::spGFP1-10,
AFD::nlg-1::spGFP11

in the central axon region between the branches. Previous electron microscopic studies of wild-type HSN synapses were consistent with muscle synapses flanking central VC synapses, but only one animal had been reported and the effect was not absolute (White et al., 1986). Richard Fetter therefore examined 2000 serial-section electron micrographs of a second wild-type HSN, scoring the location of 20 synapses onto vulval muscles and VC neurons separately (Figure 2.7G). This analysis confirmed that HSN-to-VC synapses are centrally located around the vulva and are flanked by HSN-to-vulval muscle synapses.

This unexpected detail of HSN connectivity offers a glimpse of the potential of GRASP. Previous experiments in which HSN synapses were labeled with the synaptic vesicle protein SNB-1::GFP were sufficient to show the aberrant anterior synapses and, to a lesser extent, the loss of vulval synapses in *syg-1* and *syg-2* mutants (Shen and Bargmann, 2003; Shen et al., 2004). Electron microscopy was needed to detect the change in postsynaptic partners in *syg-1* and *syg-2* mutants, but using GRASP, it was possible to infer the change in partner choice by light microscopy. In addition, the fine structure of wild-type HSN synapse localization onto vulval muscles and VCs had been overlooked, but was revealed by GRASP.

To confirm that GRASP could differentially label distinct subsets of synapses made on one process, two classes of AIY interneuron synapses were labeled with NLG-1 GRASP by Miri VanHoven and Kang Shen. In the nerve ring, the AIY interneuron sends synapses to the RIA interneuron in a small ventral region of its axon, and receives synapses from the AFD sensory neuron in the dorsal part of its axon (White et al., 1986). To examine these synapses, NLG-1::spGFP1-10 was expressed in AIY neurons using the

ttx-3 promoter, and NLG-1::spGFP11 was expressed either in the RIA neuron using the *glr-3* promoter, or in the AFD neuron using the *gcy-8* promoter (Figure 2.7H-K). NLG-1 GRASP exclusively labeled the regions where synapses were expected based on EM reconstruction of AIY (White et al., 1986). Thus NLG-1 GRASP between AIY and RIA labeled only the ventral region of the AIY axon, whereas NLG-1 GRASP between AIY and AFD labeled only the dorsal region. The localized GRASP signal between AIY and RIA is distinct from the signal with a generic presynaptic marker for AIY; GFP::RAB-3 labels all AIY synapses, and therefore forms puncta along the entire AIY process (Colon-Ramos et al., 2007).

Discussion:

GRASP has the potential to greatly increase the ease of synaptic mapping. In these studies, I used a genetically accessible system with a well-defined synaptic map to establish the feasibility and accuracy of the method, but the greatest possibilities lie in more complex systems. *Drosophila* is the most straightforward system for extending this approach, because many promoter elements and GAL4 lines are available to direct GFP fragments to known cell types (Armstrong et al., 1995). *Drosophila* also provides one of the greatest opportunities for anatomical discovery, because the anatomy of the major brain centers is highly complex, with many branched processes packed into small regions, and CNS connectivity is virtually unknown. The application of this system to the optically transparent zebrafish should also be straightforward.

In vertebrates, the existence of large-scale projects for gene expression analysis should provide promoter elements to drive GRASP in many specific cell types (Lein et

al., 2007). Long-range connectivity in the vertebrate CNS can be analyzed with lectins and viruses, but local connectivity might be better defined using GRASP and promoters for individual excitatory or inhibitory cell types. Although detecting small GFP signals in vertebrate brains may prove optically challenging, GRASP should be immediately applicable in dissociated cells or slice cultures. GRASP fragments should act dominantly and noninvasively upon viral delivery or transfection, methods that are established in many experimental animals. Therefore, GRASP should be useful to study connectivity in animals that are not accessible to traditional genetic approaches.

Any transgene has the potential to be disruptive, and with GRASP it is possible that the trans-cellular association of GFP could promote cell adhesion. However, the ability of GRASP to detect normal and mutant synapses in *C. elegans* suggests that it reports existing intercellular connections, rather than creating new ones.

Even in *C. elegans,* where the synaptic map is known, GRASP should provide new information about synaptic variation, development, and remodeling. The molecular basis of synaptic specificity in HSN was already accessible to genetic studies because HSN makes synapses in a precise and anatomically simple region, but most *C. elegans* synapses are in more complex environments. In the nerve ring, a single neuron often forms groups of closely clustered synapses with multiple target cells in a small area. These connections represent only ~15% of the dozens of cells that one neuron contacts (White et al., 1986). GRASP-based genetic screens are an attractive future approach to discovering molecules that promote or prevent synapse formation in these complex environments.

Although my primary interest is in the nervous system, the ability to identify sites of muscle-muscle contact shows that GRASP could be used to probe cell contacts in many tissues. Cell migration, organogenesis, and other physiological processes require cells to form specialized contacts with appropriate target cells. Light microscopy can reveal cell adjacency, but the closer association required for GFP assembly may help identify bona fide recognition events. As shown here for synaptic labeling, the use of localized markers allows the selective visualization of specialized attachments and subcellular domains. I hope that variations of GRASP will be useful to probe many aspects of cell recognition.

Chapter 3

Identification and characterization of *ky957*, a mutation that disrupts ASH-to-AVA GRASP labeling

Summary

To probe mechanisms of synaptic specificity, I analyzed the formation of synapses between the ASH sensory neuron and AVA interneuron in the GRASP transgenic strain *kyIs501*. *kyIs501* was generated and characterized in wild-type animals, and found to provide robust GRASP labeling of ASH-to-AVA synapses consistent with predictions from serial section electron microscopy. A genetic screen was used to seek factors that govern synaptic target identification. A semi-clonal screen identified a recessive mutant, *ky957*, with a partially penetrant loss of ASH-to-AVA GRASP labeling in the absence of other obvious defects. *ky957* initially mapped to regions on both chromosomes IV and V, but subsequent analysis suggested a location on chromosome V with a possible modifier polymorphism on chromosome IV. Transgene rescue assays identified several genomic regions capable of suppressing *ky957*. However, both targeted sequencing of these fragments and whole-genome sequencing of *ky957* failed to identify a causative mutation. Whole-genome sequencing did identify the insertion site of *kyIs501* within the interval to which *ky957* mapped. Subsequent analysis suggests that

ky957 is a mutation that affects the multicopy integrated transgene itself, reducing its associated GRASP signal.

Introduction

C. elegans, with invariant cell lineage and a known synaptic wiring diagram, is an ideal system in which to apply the GRASP method. GRASP can reliably detect synaptic connectivity in wild-type and mutant animals, and therefore was applied to label synapses formed between the ASH sensory neuron and AVA interneuron in the *C. elegans* central nervous system, while all presynaptic sites in ASH were labeled with an additional fluorophore, mCherry, fused to the vesicle-associated GTPase RAB-3. In these animals, a forward genetic screen was performed to identify mutations that specifically disrupt GRASP labeling of ASH-to-AVA synapses. Mutagenesis was performed with ethyl methanesulfonate (EMS) because of its potency, relative lack of sequence specificity, and potential to create hypomorphic alleles. These features were expected to expedite screening and increase representation of genes that are transcribed at low levels or are essential or pleiotropic.

Following mutagenesis, GRASP labeling in F2 progeny of EMS-mutagenized animals was monitored in an attempt to identify mutants with altered ASH-to-AVA GRASP labeling. This screen was performed semi-clonally to enrich for mutants with reduced growth rates or fecundity. Several candidate classes of phenotypes could have been observed in this screen. Increased GRASP labeling could occur if ASH and AVA formed additional synapses, and the subcellular location of the GRASP labeling could shift if positional information for synaptic specificity is altered or if cell morphology

changed. In this screen, which was not performed to saturation, mutants with those phenotypes were not isolated. Instead, mutants were identified in which GRASP labeling is reduced or lost, and mCherry::RAB-3 labeling and other means were used to characterize candidate causative mechanisms. Mutations in genes involved in cell polarity or synaptogenesis, such as SAD-1, would perturb the synapse of interest and other synapses, leading to altered distribution of mCherry::RAB-3 (Crump et al., 2001). Axon guidance mutations that prevent the two cells from extending their axons to the appropriate sites could be distinguished by altered axonal morphology. Mutations that affect the differentiation of or gene expression in ASH or AVA could be identified through analysis of transgenes expressed in those cells. In this screen, four mutants with reduced ASH-to-AVA GRASP labeling were identified and characterized. One mutant, *ky957*, displayed reduced or absent GRASP labeling yet grossly normal ASH and AVA morphology, gene expression, and mCherry::RAB-3 localization, as would be expected in a mutant with altered synaptic specificity. Further characterization revealed that this mutation more likely affects GRASP transgene expression rather than synaptic specificity.

Results

Generation of *kyIs501*

Candidate neuronal pairs for using GRASP to study synaptic specificity in the central nervous system were identified by examining the *C. elegans* wiring diagram. The ASH sensory neuron forms three or four synapses onto the AVA command interneuron in

Figure 3.1. Identification of ASH-to-AVA synapses. (A) Schematic diagram showing an *en face* view of ASH-to-AVA synapses in the nerve ring AVA is black, ASH is gray, and ASH-to-AVA synapses are green. (B) Schematic diagram showing a sagittal view ASH-to-AVA synapses in the nerve ring AVA is black, ASH is gray, and ASH-to-AVA synapses are green. (C) DIC image of the head of a *kyIs501* L4 animal. (D) Presynaptic sites in ASH labeled with mCherry::RAB-3. Arrowheads indicate mCherry::RAB-3 puncta. (E) Wild-type ASH-to-AVA synapses labeled with GRASP in *kyIs501*. Synaptic puncta (arrowheads) are located in the lateral nerve ring. (F) Merge of C-E. Arrowheads indicate sites of GRASP colocalization with mCherry::RAB-3. Scale bar, 10 μm.

Figure 3.1

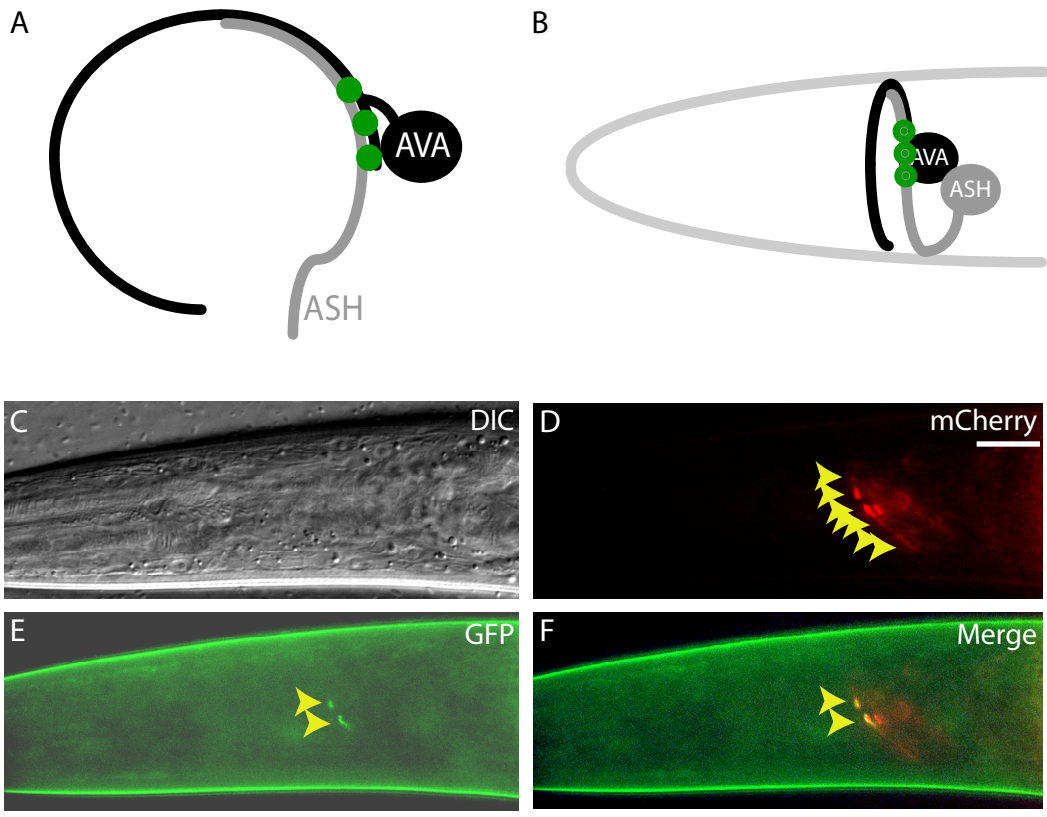

the lateral portion of the nerve ring, proximal to the AVA soma (White et al., 1986; Figure 3.1A-B). The relatively few synapses formed between ASH and AVA in wild-type animals might facilitate identification of perturbations that disrupt ASH-AVA synapse formation, alter the subcellular locations of those synapses, or increase the number of ASH-AVA synapses. In addition, sensory stimuli that activate ASH are known, and ASH and AVA responses to ASH stimuli have been recorded using electrophysiology and genetically encoded calcium indicators that measure intracellular calcium levels as a proxy for neuronal activity (Kahn-Kirby et al., 2004, Mellem et al., 2002). As synapses are fundamental units of interneuronal communication, the opportunity to relate changes in anatomy detected by GRASP to changes in neurophysiology was highly attractive. For these reasons, ASH-to-AVA synapses were selected for further investigation.

To study the ASH-to-AVA synapses, a suitable GRASP transgenic strain was required. Transgene expression in ASH was driven with the *sra-6* promoter, which is expressed in ASH and more weakly in ASI and PVQ neurons (Troemel et al., 1995), and expression in AVA was driven with the *flp-18* promoter, which is expressed in AVA and more weakly in the AIY, RIG, and RIM interneurons, and pharyngeal neurons (Rogers et al., 2003). Importantly, although expression driven by these promoters is not confined to single cells, both promoters are expressed most strongly in the cells of interest, and none of the more weakly expressing cells form synapses with ASH, AVA, or each other. In addition to GRASP labeling the ASH-to-AVA synapses, presynapstic regions in ASH were labeled with an additional fluorophore, mCherry fused to RAB-3, a small GTPase that associates with the readily-releasable pool of synaptic vesicles (Licktieg et al., 2001).

This marker could detect changes in ASH polarity, axon guidance, and overall synapse distribution in future studies. Post-synaptic sites in AVA were not labeled, mainly due to the paucity of proteins known to be exclusively postsynaptic in *C. elegans* and a lack of fluorescent proteins that could be distinguished from both GFP and mCherry..

ASH-AVA GRASP extrachromosomal arrays were generated by injection of dilution series of *sra-6::mCherry::RAB-3*, *sra-6::PTP-3A::spGFP11* or *sra-6::NLG-1::spGFP11*, and *flp-18::nlg-1::spGFP1-10* or *flp-18::CD4-2::spGFP1-10*. These plasmids were coinjected with *ofm-1::dsRed2*, a co-transformation marker expressed in coelomocytes, and bulk plasmid DNA to facilitate array formation. Coinjection of postsynaptic *flp-18*::CD4-2::spGFP1-10 with presynaptic *sra-6* PTP-3A or NLG-1 plasmids led to intracellular accumulation of cis-reconstituted spGFP throughout the ASH or AVA axons and in perinuclear regions. This may occur because of recombination between plasmids or transactivation across promoters that cause both spGFP fragments to be expressed in the same cell; under these circumstances, intracellular GFP reconstitution is too bright to permit visualization of the transcellular GRASP signal of interest. Intracellular GFP reconstitution was not observed with the postsynaptic NLG-1 GRASP carrier, in agreement with published findings (Feinberg et al., 2008). In several transgenic strains with postsynaptic NLG-1, the GRASP signal observed was bright and localized to the lateral nerve ring, consistent with the ASH-to-AVA synapses determined from serial-section electron microscopy (White et al., 1986). As expected, the GRASP puncta co-localized with a subset of the mCherry::RAB-3-labeled presynaptic sites in the ASH axon.

Like most transgenes in *C. elegans*, the high copy extrachromosomal GRASP arrays were subject to mosaic patterns of inheritance and variable expression levels. To address these problems, integrated arrays were generated from four extrachromosomal arrays displaying GRASP labeling ranging from dim to bright, two with presynaptic PTP-3A carriers and two with presynaptic NLG-1 carriers, using trimethyl psoralen (TMP) mutagenesis. Twenty integrated strains, several from each parental extrachromosomal array, were backcrossed to N2 four times to remove TMP-induced mutations unlinked to the transgene.

The outcrossed integrated strains were assessed for the brightness and specificity of the GRASP and mCherry labeling at the L4 stage in animals cultivated at 20 degrees. One strain with presynaptic PTP-3A and postsynaptic NLG-1 GRASP carriers, *kyIs501*, displayed the most consistent and bright GRASP labeling together with bright, punctate axonal mCherry::RAB-3 (Figure 3.1C-F). In *kyIs501* animals, bilateral GRASP labeling was observed in the lateral portion of the nerve ring, the predicted location of the ASH-to-AVA synapses (Figure 3.1C-F, White et al., 1986). Occasional animals displayed GRASP signal in the ventral portion of the nerve ring. This may reflect internalized GRASP-labeled protein complexes trafficking within the cell, or bona fide synapses that occasionally form between ASH and AVA in the ventral nerve ring.

Characterization of *kyIs501* in candidate developmental mutants

As a first-stage characterization of *kyIs501*, candidate mutants were used to identify phenotypes that might be observed in a genetic screen. Candidates were chosen from developmental regulators of cell differentiation, axon guidance, synaptic active zone

formation, and synaptic guidepost signals that might affect the formation of ASH-to-AVA synapses.

unc-42 encodes a homeodomain transcription factor that regulates the expression of multiple genes in both ASH and AVA, among other cells (Baran et al., 1999; Brockie et al., 2001). *unc-42* is required for *sra-6* expression in ASH but not other cells (Baran et al., 1999), and in agreement with these results, ASH-AVA GRASP labeling and ASH mCherry::RAB-3 were undetectable in *kyIs501;unc-42(e270)* animals. *unc-42* is believed to have developmental effects and might be required for ASH-to-AVA synapse formation, but this effect cannot be detected with *kyIs501* because of the defects in ASH gene expression.

kyIs501 was also examined in mutants that alter the cell biology of neurons and synapses by disrupting the polarized sorting of factors and the organization of the synaptic machinery (Zhen and Jin, 1999; Crump et al., 2001; Hallam et al., 2002). PTP-3A is known to interact with one of these factors, *syd-2*, via its intracellular domain, and loss of *syd-2* leads to a reduction in synaptic localization of PTP-3A (Ackley et a., 2005). In *kyIs501;syd-2(ju37)* animals, GRASP labeling was slightly dimmer than wild-type but detectable, and mCherry::RAB-3 labeling was reduced in some animals. Similar effects were observed in *kyIs501;sad-1(ky289)* and *syd-1(ju82);kyIs501* animals. These data indicate that *syd-1*, *syd-2*, and *sad-1* are not required for ASH-to-AVA recognition or trafficking of PTP-3A and NLG-1 to synapses in ASH and AVA, respectively.

Several guidance cues and cell-surface molecules regulate the specification of synaptic regions; therefore, *kyIs501* was examined in these mutants as well. The axon guidance receptor *sax-3(*ROBO) regulates nerve ring morphogenesis and axon guidance

(Zallen et al., 1998), but ASH-AVA GRASP labeling in *sax-3(ky123);kyIs501* animals was largely intact. In instances in which GRASP labeling was not detected, this could reflect misguidance of the axons of ASH or AVA. ASH misguidance was observed in many of these animals, but the morphology of unlabeled AVA axons could not be assessed in these animals. Interestingly, some animals with ventrally misguided ASH axons were GRASP labeled, suggesting that AVA accompanied ASH to form synapses at an ectopic site.

The guidance cues *unc-6*/Netrin and *unc-40*/DCC promote axon guidance and can provide synaptic guidepost signals (Hedgecock et al., 1990; Colon-Ramos et al. 2007). GRASP signals were lost from a few *kyIs501;unc-6(ev400)* and *unc-40(e271);kyIs501* animals, but most animals were largely normal. Labeling of AVA axons in these mutants could help to determine whether the moderate defects in *unc-6*, *unc-40*, and *sax-3* arise from changes in ASH-to-AVA axon guidance, target selection, or both processes.

syg-1 and *syg-2* guidepost signals specify formation of synapses along a portion of the HSNL axon (Shen and Bargmann, 2003; Shen et al., 2004). GRASP and mCherry::RAB-3 labeling in *kyIs501;syg-1(ky652)* and *kyIs501;syg-2(ky671)* were indistinguishable from those of wild-type animals. These data indicate that *syg-1* and *syg-2* synaptic guideposts are not required for ASH-to-AVA synapse formation.

To explore the requirement for synaptic activity in ASH-AVA target recognition, *kyIs501* was examined in mutants with defects in synaptic transmission. *unc-13* encodes a factor that docks synaptic vesicles in classical neurotransmitter exocytosis, and *unc-13(e450)* hypomorphs are paralyzed (Hammarlund et al 2008). Nevertheless, ASH-to-AVA GRASP labeling in *unc-13(e450);kyIs501* animals appeared normal, suggesting

that classical neurotransmission is not required for ASH-to-AVA synapse formation. *unc-104* encodes a kinesin required for anterograde traffic of classical synaptic vesicles and dense-core vesicles into axons (Hall and Hedgecock, 1991; Zahn et al., 2004). As expected, mCherry::RAB-3 was absent from the axons of *unc-104(e1265);kyIs501* animals, but GRASP labeling was intact. With the qualification that *unc-13(e450)* and *unc-104(e1265)* are hypomorphic alleles that do not completely abrogate neurotransmitter release, these results suggest that classical synaptic activity is likely not required for the specification of ASH-to-AVA synapses, although other forms of neural activity could be involved.

A genetic screen for synaptic specificity mutants identifies *ky957*

In principle, GRASP offers a means to identify mutants with altered fine-scale synaptic connectivity, so I performed a forward genetic screen to seek molecules that regulate ASH-to-AVA synapse formation. *kyIs501* P0 animals were mutagenized with ethyl methane sulfonate (EMS) and their F1 progeny screened semi-clonally to increase the likelihood of including mutations with low penetrance or reduced viability. Five mutagenized F1 hermaphrodites were placed on a culture plate, allowed to self fertilize, and three days later the available L4 F2 (on average, between twenty and fifty) progeny were examined under the compound microscope. Any animals displaying an abnormal GRASP phenotype were recovered and their progeny maintained and examined. Roughly 2000 F1 animals, or approximately 4000 haploid genomes, were screened. In a screen of this size, there was an 86% probability that a loss of function mutation in a given gene was present in an F1. If an average of four F2s per F1 were scored, there was

a ~63% chance that one was homozygous for new mutation; if ten F2s were screened per F1, this rose to roughly 90%. Therefore, if a homozygous mutation in a gene of interest causes a 100% penetrant GRASP phenotype, there was a 59-80% chance of identifying that mutant in the screen. If a homozygous mutation in a gene of interest causes a 50% penetrant phenotype, there was a 35%-64% chance of identifying that mutant. ~130 abnormal animals were picked, of which only four displayed a heritable phenotype. These strains were backcrossed to *kyIs501* four times to remove background EMS mutations. The mutant alleles from this screen were *ky957*, *ky958*, *ky959*, and *ky960*. *ky957* will be discussed below. *ky958* animals display a variable loss of either or both GRASP and mCherry::RAB-3 labeling, while *ky959* animals display faint GRASP and mCherry::RAB-3 labeling. *ky960* animals were subviable and could not be propagated to allow characterization.

Characterization of *ky957*

After backcrossing, *ky957* showed a reproducible abnormal GRASP phenotype in the absence of any noticeable *mCherry::RAB-3* or *ofm-1::dsRed2* defects. *ky957* animals have grossly normal growth rate, morphology, fecundity, mating capacity, and locomotion. *ky957* is a recessive mutation causing complete loss of GRASP labeling in approximately thirty percent of animals and unilateral GRASP labeling in approximately forty percent of animals (Fig. 3.2 A-D, I). Among animals in which GRASP labeling was detectable, three broad phenotypic classes were observed (Figure 3.2J). One fourth of the GRASP labeling observed was wild-type in pattern and brightness. Another fourth of the GRASP labeling was confined to a much smaller area than in wild-type animals,

Figure 3.2. *ky957* alters GRASP labeling of ASH-to-AVA synapses in *kyIs501*. (A) DIC image of the head of a *ky957 kyIs501* L4 animal. (B) Presynaptic sites in ASH labeled with mCherry::RAB-3 are indicated with arrowheads. (C) GRASP-labeled ASH-to-AVA synapses are not detected in this animal. (D) Merge of B-C. Scale bar, 10 μm. (E) DIC image of the head of a *ky957 kyIs501* L4 animal. (F) Presynaptic sites in ASH labeled with mCherry::RAB-3 are indicated with arrowheads. (G) Reduced area of ASH-to-AVA GRASP labeling (arrowhead) in *ky957 kyIs501*. (H) Merge of F-G. Scale bar, 10 μm. (I) Quantification of ASH-to-AVA GRASP labeling phenotypes in *ky957 kyIs501* (n=100). Labeling was bilateral in 100% of wild-type *kyIs501* animals examined. (J) Quantification of different forms of ASH-to-AVA GRASP labeling in *ky957 kyIs501* (n=200). WT, wild-type. Labeling was 100% wild-type in the *kyIs501* animals examined.

Figure 3.2

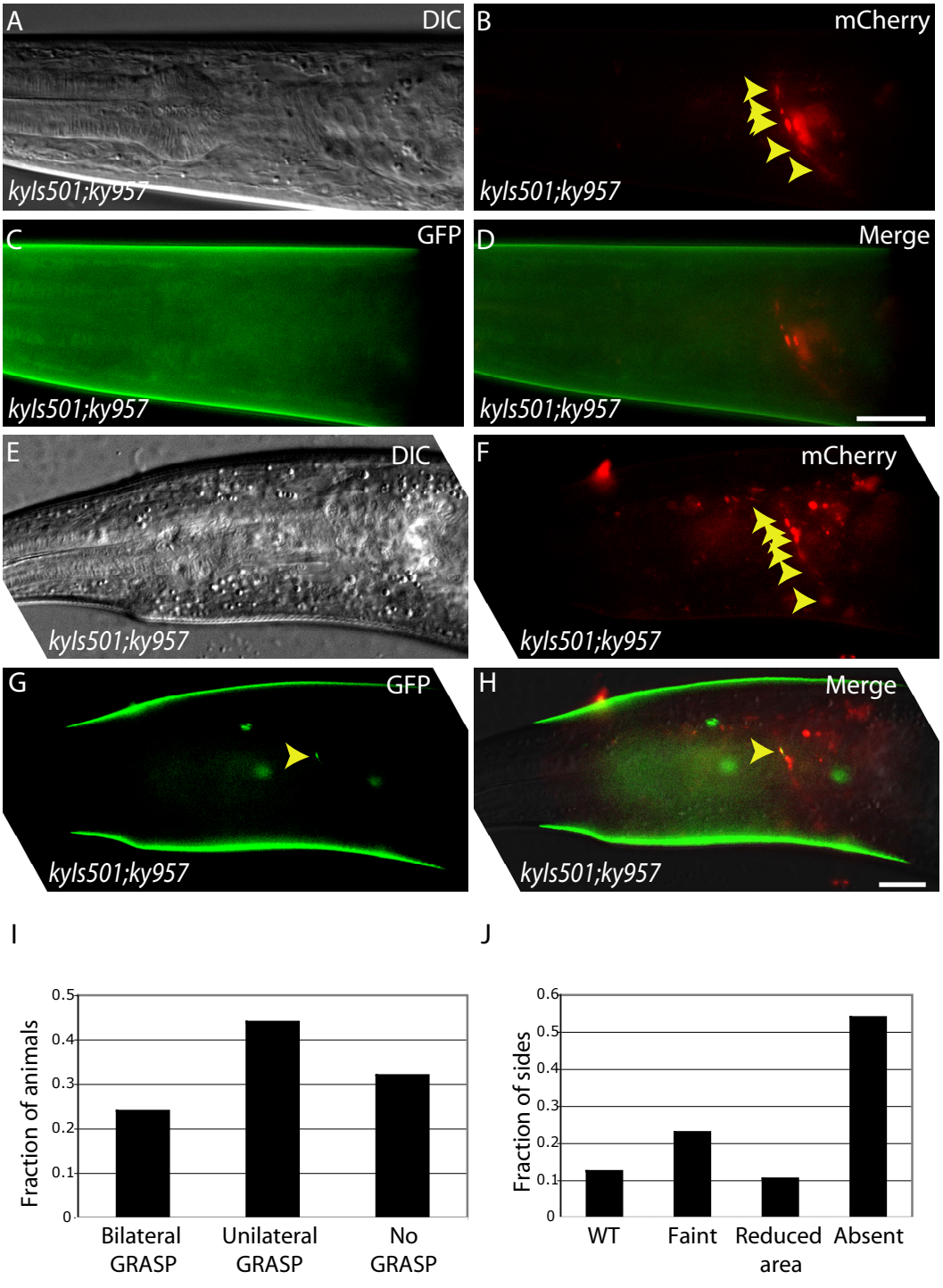
A
DIC
kyIs501;ky957
B
mCherry
kyIs501;ky957
C
GFP
kyIs501;ky957
D
Merge
kyIs501;ky957
E
DIC
kyIs501;ky957
F
mCherry
kyIs501;ky957
G
GFP
kyIs501;ky957
H
Merge
kyIs501;ky957
I
Fraction of animals
0.5
0.4
0.3
0.2
0.1
0
Bilateral GRASP
Unilateral GRASP
No GRASP
J
Fraction of sides
0.6
0.5
0.4
0.3
0.2
0.1
0
WT
Faint
Reduced area
Absent

often a single punctum (Fig. 3.4 E-H), and the remaining half of the GRASP labeling was faint or barely detectable. The GRASP phenotype on the two sides of each animal were not correlated, and no obvious lateral biases were observed for any of these phenotypes.

To determine whether *ky957* altered ASH or AVA cell fate, like *unc-42*, *ky957* animals were injected with *sra-6::GFP* and *flp-18::mCherry* plasmids. Bright expression of both promoters was seen in *ky957* animals, indicating that a large-scale change in cell identity had not occurred for either cell. To determine whether *ky957* altered the morphology, migration, or axon guidance of ASH or AVA, the *ky957 sra-6::GFP* and *ky957 flp-18::mCherry* lines were examined under the compound microscope; no significant defects were observed.

Mapping *ky957* on chromosome IV

ky957 was mapped with an approach based on polymorphisms between the laboratory strain N2, in which *kyIs501* was generated, and the wild strain CB4856 (Davis et al., 2005). During mapping with candidate mutants, *kyIs501* heterozygotes and their progeny displayed variable silencing of the transgene that was stronger than expected from a two-fold reduction in transgene copy number. To avoid this problem, *kyIs501* was introgressed and homozygosed in all strains used for mapping, and specifically was introgressed into CB4856 for ten successive crosses, after which greater than 99% of the DNA unlinked to *kyIs501* should be derived from CB4856. This strain was subsequently crossed to *kyIs501;ky957* animals, and hermaphrodite F1 cross progeny were allowed to self-fertilize to produce recombinant F2 animals. Due to the partially penetrant nature of *ky957*, F2 animals were assessed in a manner similar to that used in the genetic screen.

Individual animals displaying a strong loss of the GRASP phenotype were identified under 630x magnification and recovered, and their F3 progeny scored clonally to confirm that the isolated F2 was a homozygous mutant. Genomic DNA was isolated from 30 F2 mutant animals and 30 non-mutant F2 animals. DNA from wild-type and mutant animals were combined into separate pools, and SNP genotyping was performed to determine polymorphisms at which the mutants showed relative enrichment for N2 DNA. This analysis found strong enrichment of N2 DNA on the left arm of chromosome IV, and weak enrichment on the left arm of chromosome V in *ky957*. No linkage was observed to other regions of chromosomes, with the important caveat that *kyIs501* is located on the right arm of chromosome V, and as such the *kyIs501*;CB4856 animals were homozygous for N2 DNA and uninformative for mapping in this region.

Although linkage to two chromosomes was observed, *ky957* was inherited in a simple, monoallelic pattern suggesting that a single locus was mutated. Clonal F2 progeny of a cross between *ky957;kyIs501* and kyIs501 were isolated and phenotypes scored in F3 progeny. 6/20 animals were homozygous wild-type, 9/20 were heterozygous, and 5/20 were homozygous mutants. Based on the strong linkage to the left arm of chromosome IV, which was strongest between –24 and –17 map units (cM), interval mapping was performed by genotyping individual F2 *ky957* recombinants at these and intervening SNPs. In this manner, a ~300kb interval over which 49/49 recombinants carried homozygous N2 DNA was found between 1.3 and 1.6 Mb (Figure 3.3 A).

Linkage of *ky957* to chromosomes IV and V was tested directly. Previous members of the Bargmann laboratory had found that an olfaction mutant phenotype

Figure 3.3. Interval mapping of *ky957* and a potential modifier on chromosomes IV and V. (A) Identification of an interval linked to *ky957* in mapping of *ky957;kyIs501* with *kyIs501*;CB4856. Red and blue indicate DNA with CB4856 or N2 SNPs, respectively. Brackets indicate the interval of the mutation deduced from the recombinants. Number of animals carrying recombination breakpoints between two SNPs are shown above each class of recombinant. (B) Identification of an interval linked to *ky957* in mapping of *ky957 kyIs501* with *kyIs501*. Red and blue indicate DNA regions with *kyIs501* or *ky957 kyIs501* EMS SNPs, respectively. Brackets indicate the interval deduced from the recombinants. Number of animals carrying recombination breakpoints between two SNPs are shown above each class of recombinant. (C) Breakpoints in recombinant animals identified by genotyping. 140 animals were screened to identify 4 *ky957 kyIs501* F2 animals with recombination breakpoints between 17.9 Mb and 18.7 Mb.

Figure 3.3

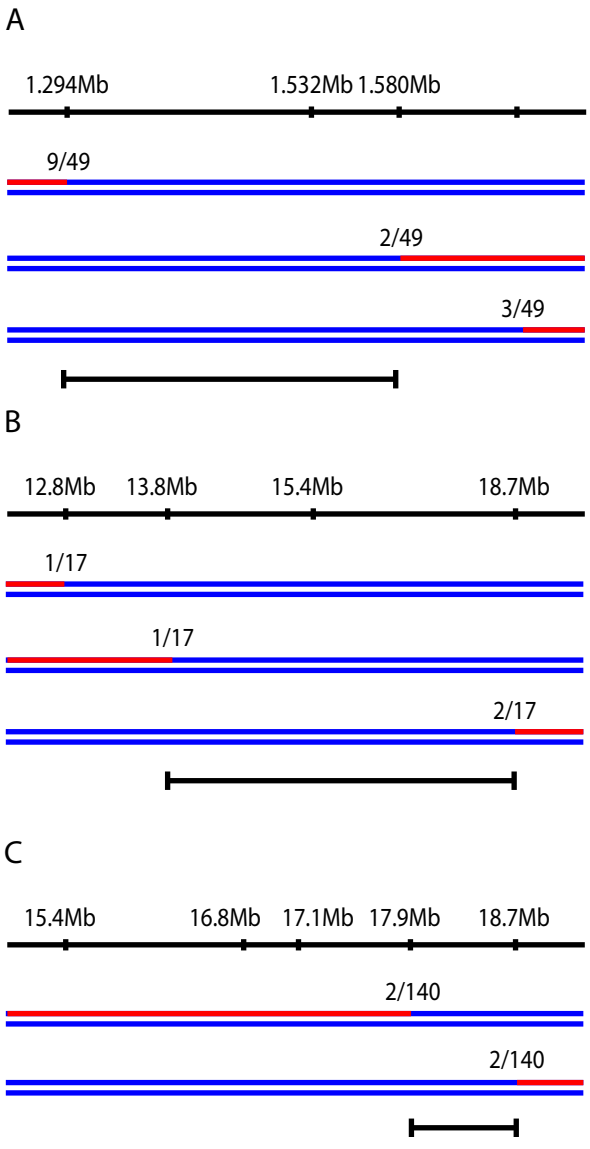
A
1.294Mb
1.532Mb 1.580Mb
9/49
2/49
3/49
B
12.8Mb
13.8Mb
15.4Mb
18.7Mb
1/17
1/17
2/17
C
15.4Mb
16.8Mb
17.1Mb
17.9Mb
18.7Mb
2/140
2/140

identified in N2 could be suppressed in a CB4856 background (M. Tsunozaki, personal communication). Mapping of this mutant with CB4856 showed linkage to two chromosomes, one containing the mutation and the other containing the modifier polymorphism. Therefore, it was possible that a modifier polymorphism could explain the observed linkage of *ky957* to chromosomes IV and V. Although *ky957* had appeared most strongly linked to chromosome IV in CB4856 mapping, linkage to the left arm of chromosome V was observed, and linkage to the right arm of chromosome V could not be ascertained. To examine these regions further, *ky957* was mapped in an N2 background with dominant visible markers on chromosomes IV and V, *dpy-13* and *unc-70*, respectively. *ky957* was crossed with *kyIs501*;*dpy-13* and *kyIs501*;*unc-70* animals, F1 hermaphrodites were allowed to self-fertilize, and individual non-Dpy or non-Unc F2 progeny were isolated. The F3 progeny of each F2 were scored to determine whether the F2 animal was homozygous *ky957*, heterozygous, or homozygous wild-type. *dpy-13* is located 19 map units from the region identified in CB4856 mapping; if *ky957* were located 19 map units from *dpy-13*, 23/35 non-dpy F2s should be homozygous *ky957*. However, only 6/35 non-*dpy-13* animals were homozygous *ky957*, suggesting that *ky957* is not linked to *dpy-13* and therefore not located on chromsome IV ($\chi 2 > 30$, $P < .0001$). By contrast, 26/35 non-*unc-70* animals were homozygous *ky957*, suggesting that *ky957* is linked to *unc-70* on chromosome V at a distance of 14 cM. To determine on which arm of chromosome V *ky957* resides, similar experiments were performed with the recessive mutants *unc-34* and *rol-9*, located at the far left and right ends of chromosome V, respectively. 11/29 non-Unc F2 progeny were homozygous for *ky957*, while 27/34 non-Rol F2 progeny were homozygous for *ky957*. These data were in good agreement and

assigned *ky957* to the right arm of chromosome V between 14 and 18 cM. Overall, these data indicated that *ky957* is located on V and that the linkage to chromosome IV seen in CB4856 mapping likely reflects a modifier polymorpism.

A new approach was needed to map *ky957* on V. The right arm of chromosome V carries few visible markers that could be used for three-point crosses. Integrated transgenes inhibit recombination when placed in trans with wild-type chromosomes (Hammarlund et al., 2005), and the insertion of *kyIs501* on this arm of chromosome V precluded interval mapping with commonly used polymorphic strains such as CB4856. Illumina sequencing (see below) identified many polymorphisms between *ky957;kyIs501* and *kyIs501*, and I reasoned that these polymorphisms could be could be used for mapping, much like single-nucleotide polymorphisms between N2 and CB4856. This approach would permit interval mapping, and recombination suppression due to the transgene should not arise between *ky957;kyIs501* and *kyIs501*. GRASP-defective mutant F2 progeny of a *ky957;kyIs501* x *kyIs501* cross were isolated, and after their phenotypes were confirmed in the F3 progeny, animals were genotyped at SNPs along chromosome V. 17/17 GRASP-defective isolates were homozygous for the *ky957* alleles of SNPs on the right arm of V, with a few animals heterozygous for SNPs at the center and extreme right end of chromosome V. This mapping placed *ky957* between 13.8 and 18.7 megabases (Mb) on chromosome V (Figure 3.3B). To generate additional recombinants, F2 animals were cloned blind to phenotype and genotyped at SNPs at 9.8 and 18.7 Mb. GRASP phenotypes were scored in the F3 progeny of F2 animals carrying recombinant chromosomes. This analysis identified two animals that were heterozygous for *ky957* SNPs at 17.1 Mb, one of which was also heterozygous at 17.9 Mb. Several

recombinants were heterozygous at 18.7 Mb. To confirm these boundaries, recombinants between 17.9 and 18.7 Mb were identified as above and phenotyped. These recombinants confirmed that *ky957* lies in the ~800kb region between 17.9 and 18.7 Mb (Figure 3.3C). This physical position corresponds to 13.3 to 17.3 cM, a close match to the position of 14 to 18 cM deduced from mapping with visible markers.

Transgenic rescue of *ky957*

Rescue experiments were undertaken on chromosomes IV and V in the intervals identified above. A few fosmids were available for the intervals on IV and V, but most of the injection rescue was attempted with long PCR products. PCR products 12 kilobases (kb) in length, each overlapping the next by 2 kb, were amplified from N2 DNA to cover this interval and injected into *ky957 kyIs501* animals in contiguous pools spanning 50 kb of genomic sequence. Each pool overlapped the next pool by 20-30 kb. Two overlapping pools out of ten tested from chromosome IV rescued the *ky957* GRASP mutant phenotype. These fragments overlapped by ~20 kb, and included two complete predicted genes, *clp-7* and *Y77E11A.3*, and a portion of another gene, *clp-6* (Figure 3.4A).

Surprisingly, sequencing failed to identify any differences in these genes between *ky957* and *kyIs501*, but did identify one mutation common to both strains and absent in the reference N2 DNA sequence. The mutation was present in some but not all wild-type N2 strains in use in the Bargmann laboratory, suggesting that it arose spontaneously during ongoing lab cultivation. This mutation, now called *ky982,* affected the coding region of the *clp-6* gene, which encodes an atypical calpain (Figure 3.4B). Calpains are

Figure 3.4. Suppression of *ky957* by transgenic rescue with three non-overlapping genomic regions. (A) Region of chromsome IV containing *clp-6* that can suppress *ky957* when overexpressed. Green line indicates DNA fragment contained in array in E. Image from www.wormbase.org. (B) Structure of *clp-6* and location of *ky982* G to R missense mutation at a conserved site. Alignment to nearest *C. elegans* homologs in this region, *clp-3* and *clp-4*, shown. Mutated residue marked with gray box and asterisk. (C) Region of chromsome V between 18.168 and 18.20 Mb that can suppress *ky957* when overexpressed. Green line indicates DNA fragment contained in array in E. Image from www.wormbase.org. (D) Region of chromsome V between 18.168 and 18.20 Mb that can suppress *ky957* when overexpressed. Green line indicates DNA fragment contained in array in E. Image from www.wormbase.org. (E) Quantification of ASH-to-AVA GRASP labeling in *ky957 kyIs501* carrying transgenic arrays containing three different genomic regions. Data are summed for three separate extrachromosomal arrays corresponding to each region. Asterisks, significantly different from ky957 (two-tailed P<.001, Fisher's exact test) (F) Quantification of ASH-to-AVA GRASP labeling in *kyIs501* and *ky957 kyIs501* animals carrying the *clp-6* alleles c*lp-6(ky982)* and *clp-6(ok1779)*.

Figure 3.4

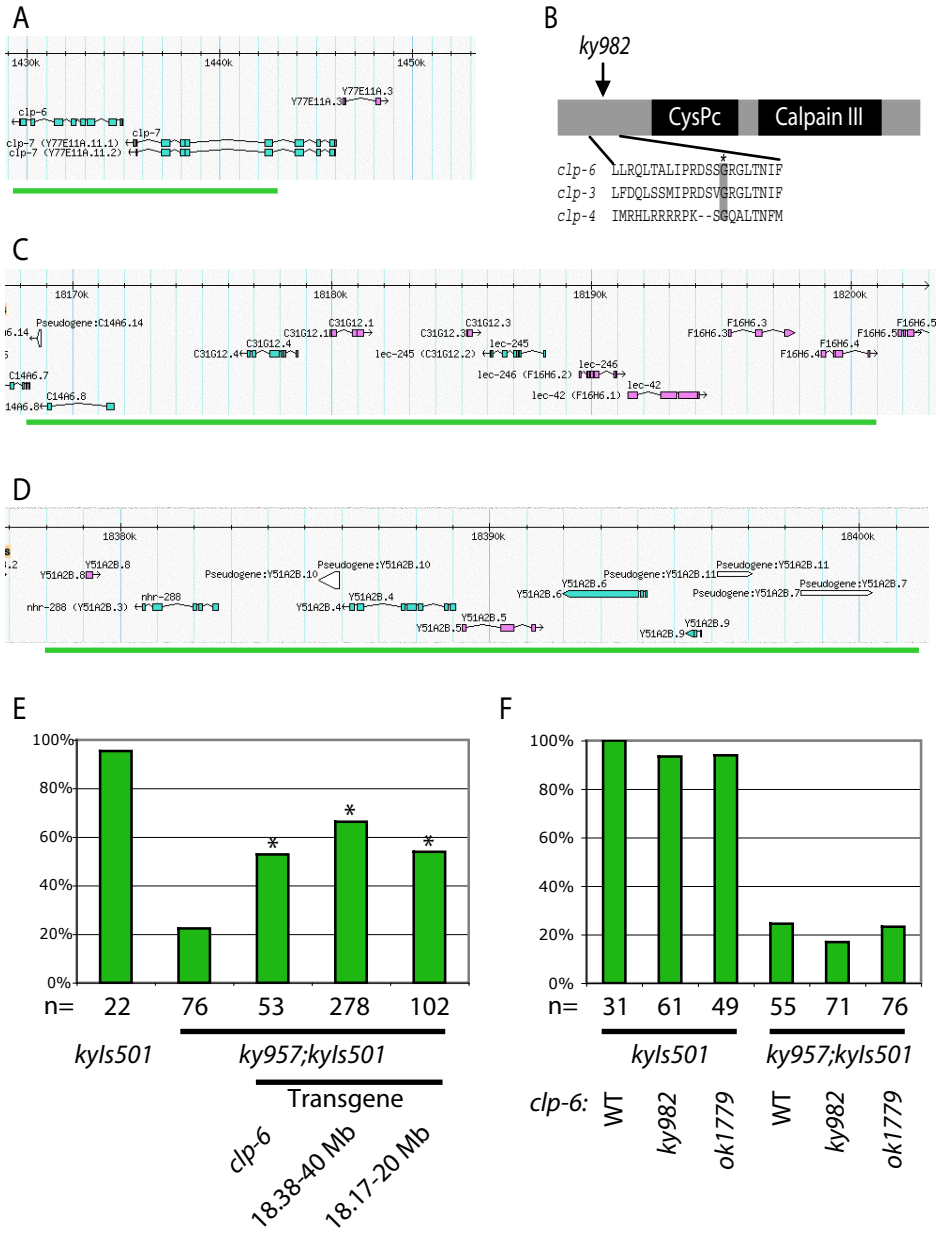
A
1430k
1440k
1450k
Y77E11A.3
clp-6
clp-7
clp-7 (Y77E11A.11.1)
clp-7 (Y77E11A.11.2)
B
ky982
CysPc
Calpain III
clp-6 LLRQLTALIPRDSSGRGLTNIF
clp-3 LFDQLSSMIPRDSVGRGLTNIF
clp-4 IMRHLRRRRPK--SGQALTNFM
C
18170k
18180k
18190k
18200k
Pseudogene:C14A6.14
C31G12.1
C31G12.3
F16H6.3
F16H6.5
C31G12.4
lec-245
F16H6.4
lec-246
lec-42
C14A6.7
C14A6.8
D
18380k
18390k
18400k
Y51A2B.8
Pseudogene:Y51A2B.10
Pseudogene:Y51A2B.11
Pseudogene:Y51A2B.7
nhr-288
Y51A2B.4
Y51A2B.6
Y51A2B.5
Y51A2B.9
E
100%
80%
60%
40%
20%
0%
n= 22 76 53 278 102
kyIs501
ky957;kyIs501
Transgene
clp-6
18.38-40 Mb
18.17-20 Mb
F
100%
80%
60%
40%
20%
0%
n= 31 61 49 55 71 76
kyIs501
ky957;kyIs501
clp-6: WT ky982 ok1779 WT ky982 ok1779

calcium-dependent intracellular proteases that have been implicated in a variety of cellular processes in both health and disease. *clp-6(ky982)* substitutes arginine for glycine in an N-terminal domain believed to be involved in substrate recognition. The CB4856 strain used for mapping does not bear the *clp-6(ky982)* allele, so this sequence variant could lead to chromosome IV linkage in crosses with CB4856 strains but not all N2-derived strains, the result observed in the genetic crosses described above.

Injection of a PCR product containing the wild-type *clp-6* gene rescued GRASP signals in *ky957 kyIs501* mutants. To determine more rigorously whether expression of the *ky957* phenotype was affected by *clp-6*, *kyIs501* and *ky957 kyIs501* animals were crossed to N2 animals carrying wild-type alleles of *clp-6* and to animals carrying a presumed null allele of *clp-6* identified in the *C. elegans* knockout project, *clp-6(ok1779)*. The *clp-6* genotype was determined using standard PCR-based genotyping, and *ky957* animals were identified by genotyping with SNPs at 17.9 and 18.7 Mb on chromosome V. Surprisingly, replacement of *clp-6(ky982)* with either the wild-type *clp-6* allele or the *clp-6(ok1779)* allele had no effect on GRASP signals, either in the *kyIs501* strain or the *kyIs501 ky957* strain (Figure 3.4F). Moreover, crossing clp-6(ky982) back into the N2 strain did not reconstitute the phenotype (Figure 3.4F). These results suggest that *clp-6(ky982)* is not a modifier polymorphism of *ky957*, although a modifier polymorphism between *ky957 kyIs501* may be present on IV. The rescue observed is best explained as second-site suppression of the *ky957* GRASP phenotype, and not complementation of the mutant with the wild-type allele.

Similar rescue experiments were conducted using DNA from chromosome V between 17.9 and 18.7 Mb. 21 Pools of genomic DNA spanning fifty to sixty kb were

injected into *ky957 kyIs501* animals, and several transgenic lines were isolated and scored for each injection pool. These injections identified three pools capable of rescuing the GRASP phenotype of *ky957*. One pool of PCR products located between 18.17 and 18.20 Mb rescued significantly, but exon sequencing failed to identify any mutations (Figure 3.4 C, E). The other rescuing DNA pools spanned 18.35 to 18.40 Mb and 18.38 to 18.43 Mb. Their region of overlap, 18.38 to 18.40 Mb, significantly rescued *ky957*, as did the 12 kb from 18.388 to 18.40 Mb, containing the genes *Y51A2B.5*, *Y51A2B.6*, and *Y51A2B.9* (Figure 3.4 D-E, Figure 3.5 B). The 22 kb region from 18.378 to 18.40 Mb was fully sequenced but no coding or non-coding mutations were found.

Although no mutations were identified in *Y51A2B.5*, *Y51A2B.6*, or *Y51A2B.9,* Illumina sequencing (see below) identified another mutation located in an intron of the lipase *ZK262.3*, approximately twenty kb from *Y51A2B.5*, *Y51A2B.6*, and *Y51A2B.9* (Figure 3.5 A). Fosmids containing *ZK262.3* did not rescue the GRASP phenotype of *ky957*, indicating that *ky957* is not an allele of *ZK262.3* (Figure 3.5 B). This non-coding mutation could have disrupted an enhancer and reduced expression of *Y51A2B.5*, *Y51A2B.6*, or *Y51A2B.9,* in which case high-copy transgenes carrying additional copies could have restored expression of *Y51A2B.5*, *Y51A2B.6*, or *Y51A2B.9* to wild-type levels. This explanation would predict that expression of one or more of *Y51A2B.5*, *Y51A2B.6*, and *Y51A2B.9* is altered in *ky957* mutants. This possibility was explored by quantitative reverse-transcription PCR (qRT-PCR), which failed to identify any significant changes in mRNA levels of either gene in *ky957* animals (Fig 3.5C). It is possible that the *ZK262.3* SNP could alter tissue-specific expression of one of these genes in a manner that would be below the detection threshold for RT-PCR. Overall, however, these experiments

Figure 3.5. A SNP in a *ZK262.3* intron is likely not the causative mutation in *ky957 kyIs501*. (A) Genomic region containing *ZK262.3*. The arrow indicates the location of the *ZK262.3* SNP. Green line indicates the nearby minimum genomic DNA fragment that suppresses *ky957* as a transgene. Image from www.wormbase.org. (B) Quantification of suppression of *ky957* by the genomic DNA indicated by the green line in A or a fosmid encompassing *ZK262.3*. Asterisk, significantly different from *ky957* (two-tailed P<.001, Fisher's exact test). n.s., not significantly different from *ky957*. (C) Quantitative RT-PCR expression analysis of genes contained in area indicated by green line in A.

Figure 3.5

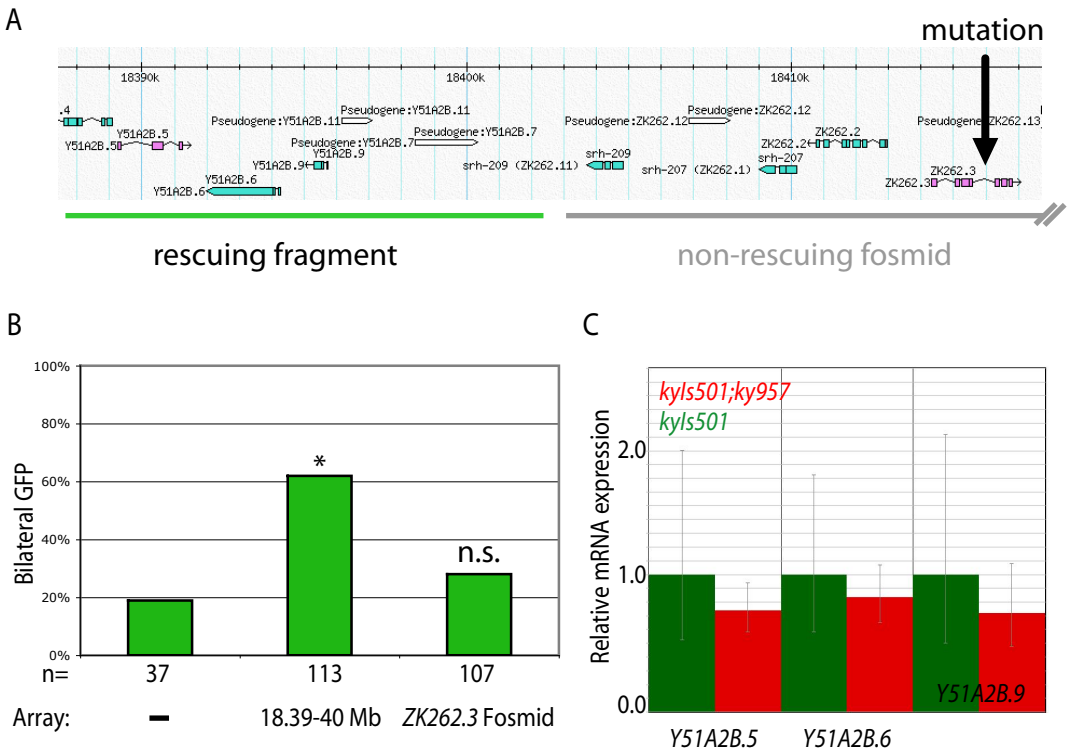
A
mutation
18390k
18400k
18410k
Pseudogene:Y51A2B.11
Pseudogene:Y51A2B.7
Pseudogene:ZK262.12
Pseudogene:ZK262.13
Y51A2B.5
Y51A2B.9
Y51A2B.6
srh-209
srh-207
ZK262.2
ZK262.3
rescuing fragment
non-rescuing fosmid
B
Bilateral GFP
100%
80%
60%
40%
20%
0%
*
n.s.
n=
37
113
107
Array:
18.39-40 Mb
ZK262.3 Fosmid
C
kyIs501;ky957
kyIs501
Relative mRNA expression
2.0
1.0
0.0
Y51A2B.9
Y51A2B.5
Y51A2B.6

further suggested that rescue reflected second-site suppression of *ky957* by the rescuing array rather than complementation of the mutation, a conclusion similar to that obtained with *clp-6* rescue.

These results indicate that several genes or genomic regions are able to suppress *ky957* when introduced as high-copy transgenes. However, they failed to identify a candidate for the underlying mutation in *ky957,* which would require the combination of a biologically significant mutation present in *ky957* and a rescuing fragment. It was possible that a mutation was hidden in the corresponding DNA for one of these regions but was somehow undetected. Alternatively, it was possible that although these rescue experiments could identify overexpression suppressors of *ky957*, rescue by complementation was not possible. Rescue could fail due to dosage sensitivity, for example, or lack of adequate cis-regulatory regions in the injection pools.

Genome sequencing of *ky957;kyIs501*

Whole-genome sequencing was undertaken as an unbiased approach to identify mutations in *ky957*. In the first experiment, Illumina sequencing was performed to generate approximately fourteen-fold coverage of the genome. Thirty-two bp sequence reads were aligned to the reference N2 genome using Maq (mapping and assembly with quality) to identify point mutations (Li et al., 2008). These data were compared to that obtained for other mutants generated in the Bargmann laboratory to subtract background SNPs present in Bargmann laboratory N2. New mutations were verified by PCR amplification and Sanger sequencing. This analysis identified eight point mutations on chromosome V that changed the coding sequence of predicted genes (Table 3.1), none of

Table 3.1. Coding mutations identified in *ky957;kyIs501*.

Gene	Chromosome and Position(Mb)	Mutation	PCR rescue	Fosmid Rescue
F38E1.11	V, 8.37	E to K	-	-
F41E6.11	V, 8.62	G to K	-	-
ZC455.1	V, 12.77	A to V	-	-
dpf-1	V, 15.47	T to I	-	-
phy-3	V, 16.84	P to S	-	NA
nhr-241	V, 18.70	P to G	-	NA
gcy-22	V, 20.82	E to K	-	-
clp-6	IV, 1.43	G to R	+	

which fell between 17.9 and 18.7 Mb. (These point mutations were the SNPs used in the section on genetic mapping, above, to localize *ky957* to the 17.9-18.7 Mb interval.)

Roughly one quarter of EMS mutations can be small deletions, which are not detected through the alignment approach. If small deletions included unique sequences, they would likely be reflected as gaps in sequencing coverage. At 14x coverage, over 100 such gaps were present between 17.9 and 18.7 Mb, of which three fell within predicted coding regions. PCR amplification and sequencing of *ky957* genomic DNA determined that the three coverage gaps in coding regions were not deletions. Therefore, Illumina sequencing failed to identify any verified point mutations or deletions between 17.9 and 18.7 Mb, although *ky957* should have been found.

The standard Maq analysis of Illumina whole-genome sequencing is based on alignment of 32 bp reads with a reference genome (Li et al., 2008). Non-unique sequences are aligned randomly, precluding identification of mutations in sequences that are duplicated in the genome. New inserted sequences are not identified at all; they simply fall into pool of unaligned sequence reads. Deletions of one base pair are detectable, deletions of more than one base pair are not detected efficiently (Li et al., 2008). To provide tools to seek deletions and insertions, paired-end sequencing was attempted, in which thirty-two bp reads are generated from both ends of a ~200 bp genomic DNA fragment. The additional information provided by this approach can facilitate alignment of ambiguous reads and uncover insertions, deletions, and other rearrangments. The paired-end sequencing failed due to faulty reagents from Illumina, but as a result approximately forty-fold single-end coverage was generated. The increased coverage enabled identification of two additional non-coding SNPs between

17.9 and 18.7 Mb, one in an intron of *ZK262.3* (see above). The increased coverage also drastically reduced the number of gaps in coverage. To validate the gaps and address the possible sequence changes mentioned above, I worked with Patrick McGrath to develop an algorithm to improve deletion and insertion identification. Reads that Maq could not align along their full length to the *C. elegans* genome were examined to determine whether portions align with the DNA within the *ky957* interval. Sequence reads spanning a newly created junction at the site of a deletion or insertion would be expected to align perfectly to reference sequence on one side of the junction, but should not align to the reference sequence on the other side. In this manner, reads spanning a putative junction were identified and aligned to create contiguous sequence representing DNA unique to *ky957*.

When this approach was applied to the ~800 kb *ky957* interval, reads meeting these criteria could be identified at a single location, 18.35 MB. The algorithm was able to assemble a fifty bp sequence on one end of the gap, reflecting the need for further refinement of the parameters. Detailed analysis found that this sequence corresponded to the site of the *kyIs501* insertion. Basic local alignment search tool (BLAST) found that 22 bp of this sequence corresponded to the genomic sequence at this position on chromosome V, while the remaining sequence derived from chromosome I, in the *ofm-1* promoter (Figure 3.6A). A larger fragment could be amplified from *kyIs501* and *ky957*, but not N2, to confirm the predicted junction and identify additional unique flanking sequence. Sequencing of this fragment confirmed the juxtaposition of the *ofm-1* promoter with chromosome V DNA at this site (Figure 3.6B). These data indicate that

Figure 3.6. Identification of the *kyIs501* integration site on chromosome V. (A) 50 bp sequence assembled from Illumina sequence reads. 22 bp derive from chromosome V (red), and 28 bp derive from the *ofm-1* promoter on chromosome I (blue). One nucleotide (purple) at this junction could not be unambiguously assigned to chromosome V or *ofm-1*. (B) Sequencing of an extended PCR product that spans the junction of chromosome V (red) and the *kyIs501* transgene (blue) confirms the identification of the insertion site.

Figure 3.6

A

B

TCCCTCCACAAGCTTCCTAATTCCAAGGGGTCTTCCACAAATCGCTTCA
GCCTCGAATCTTGTCATATTCGGCGGAGAATTAATGTACATTGGGCATTT
TTCATGTCAAACTTTAGGTGAGATTTTTTCACCGTAATACATATATTTTTC
TAGGTAATACTCACTTTTGAATAGTCCACAAATA

kyIs501 fell within the interval to which *kyIs957* mapped. No other deletions or insertions were found.

Chromosomal rearrangments in *ky957*

Illumina sequencing failed to identify mutations between 17.9 and 18.7 Mb on chromosome V. This could reflect a rearrangement on chromosome V caused by TMP or EMS mutagenesis. Chromosomal rearrangments such as inversions or translocations could have moved the DNA carrying one or both of the mapping SNPs at 17.9 and 18.7 Mb, or could have inserted a segment of DNA between these SNPs (Yandell et al., 1991; Herman et al., 1976). If this were true, one of the SNPs identified on Chromosome V that fall outside of the ~800 kb *ky957* interval with in the reference genome could be translocated between these SNPs in *ky957*. In this way, one of these SNPs could be the causative mutation. This possibility was first explored through rescue experiments. Fosmids and long PCR products spanning coding regions and several kb of flanking cis-regulatory sequence for each of the coding SNPs on V were injected into *ky957 kyIs501* animals, but no rescue was observed (Table 3.1). Although these results suggest that *ky957* is not one of the identified coding SNPs on chromosome V, it did not exclude the possibility that an unidentified mutation fell within a rearrangment.

The possibility of a rearrangement on chromosome V was also consistent with the relatively low number of silent EMS-induced mutations near the predicted site of *ky957*. EMS mutagenesis of *C. elegans* by the standard protocol has been shown to induce an average of one point mutation per twenty to forty kilobases in previous whole-genome sequencing studies. Although *ky957* was backcrossed to *kyIs501* four times to remove

most unlinked mutations, recombination in *C. elegans* generates only one crossover per chromosome pair per meiosis. Therefore, the area tightly linked to *ky957* was unlikely to have recombined with wild-type chromosomes, and should retain these densely packed mutations. Based on these predictions, within the ~800 kb interval defined by mapping, *ky957* and an additional twenty to forty mutations should have been observed, instead of the two discovered here. The absence of these predicted mutations could reflect one or a few of several possibilities. First, it is possible that after four backcrosses to *kyIs501,* EMS-induced mutations near *ky957* were lost. For example, the integrated transgene *kyIs501* is linked to *ky957,* and the repetitive nature of the transgene could promote recombination in this interval (both strains in the backcross carried the transgene, allowing free recombination). Second, the mutagenesis performed that yielded *ky957* could have been substantially less potent than the mutageneses used to calibrate the published mutation frequency. Both of these possibilities would explain the low mutation frequency observed between 17.9 and 18.7 Mb, but would not explain the failure to identify *ky957* in this interval. Third, chromosome V could be rearranged in *ky957* animals in a way that provides misleading linkage data. If that were the case, one would expect to observe more densely clustered mutations at another region in the genome. We examined this possibility by aligning all potential mutants in *ky957* mutants with the reference genome, in a way that allowed easy assessment of mutation density (Figure 3.7A). One region with an increased density was found on V far from *ky957*, but no other region of the genome of the backcrossed *ky957* strain showed a mutation frequency approaching 1/20,000 bp (Figure 3.7A).

Figure 3.7. Distribution of EMS-like mutations in the *ky957* genome. Illumina sequencing data from two mutants, *ky777* and *ky957*, were compared to identify unique single-base changes in each strain that would be consistent with EMS mutagenesis. The slope of the gray lines corresponding to each chromsome indicates the density of mutations in that area, likely reflective of genetic drift or sequencing errors. (A) A graph of unique SNPs in *ky957* against genomic position. Two regions (red lines) with higher density of EMS mutations are observed in the *ky957* genome, one short region on II and another on V. Neither region corresponds to the *ky957* interval. The slope of the right arm of V indicates that theoverall density of mutations along this region is higher than that of the remainder of the genome.(B) The unique mutations in the genome of *ky777* are graphed against their positions on the chromosome. The red line indicates a region on X with a slope indicative of a high density of mutations. The causative mutation in *ky777* lies in this region of increased density (B. Lesch, personal communication).

Figure 3.7

A

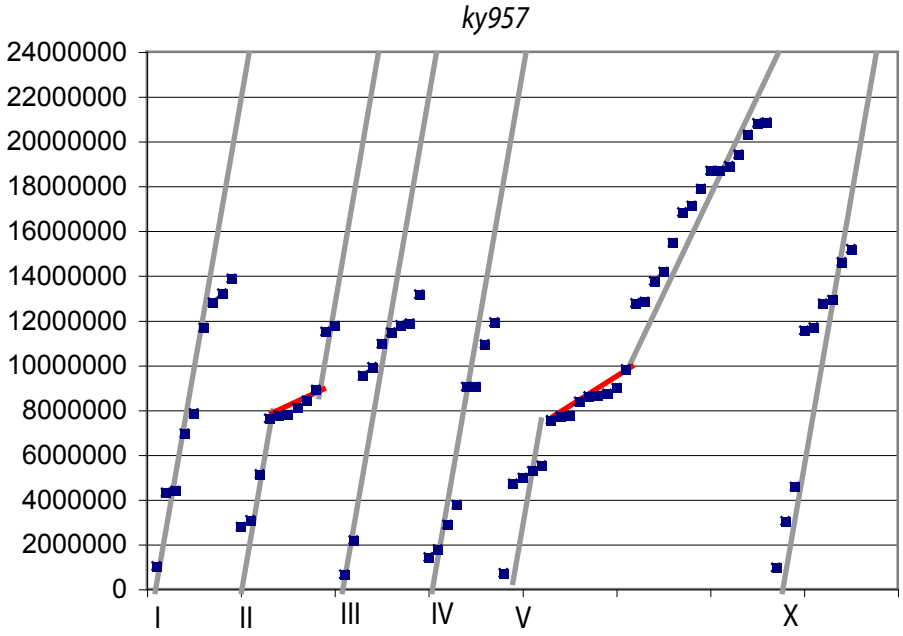
ky957
24000000
22000000
20000000
18000000
16000000
14000000
12000000
10000000
8000000
6000000
4000000
2000000
0
I
II
III
IV
V
X

B

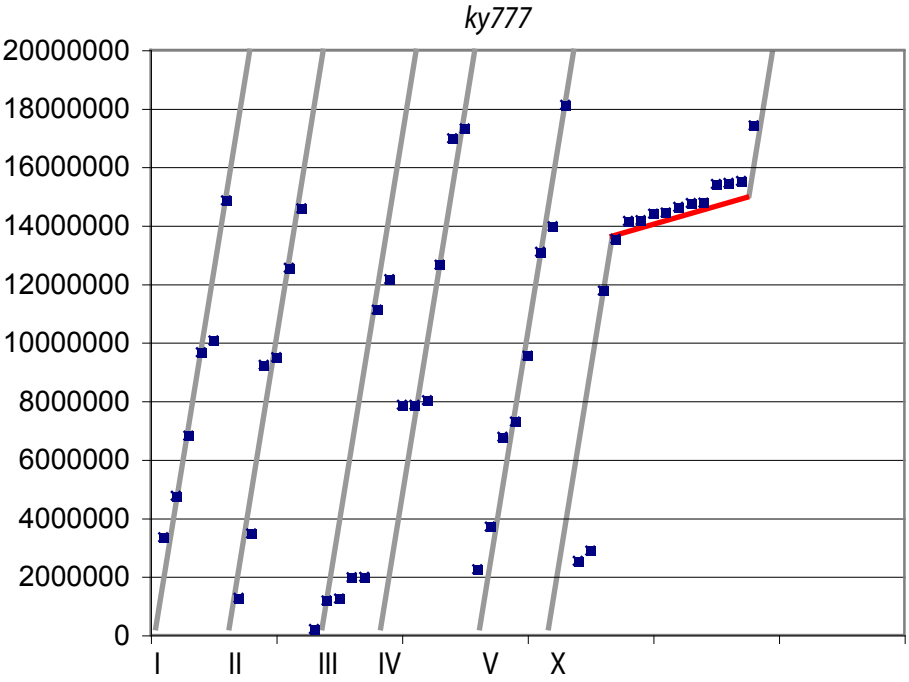
ky777
20000000
18000000
16000000
14000000
12000000
10000000
8000000
6000000
4000000
2000000
0
I
II
III
IV
V
X

A large rearrangement would interfere with identification of recombinants along that chromosome, but many recombinants between *ky957 kyIs501* and *kyIs501* were observed using markers along chromosome V. If there were a large rearrangement, therefore, it would be present in *kyIs501*. Alternatively, a small deletion, insertion, or translocation could have arisen in *ky957*. Recombination between visible mutants or SNPs and *kyIs501* was observed with markers distributed across most of chromosome V, including a few markers spanning the region with the highest EMS mutation frequency (Figure 3.8). A region of recombination suppression was observed near the predicted *ky957* region (Figure 3.8), in keeping with the recombination suppression observed surrounding transgene integration sites (Hammarlund et al., 2005). These data suggested that no large rearrangements are present on chromosome V in *kyIs501*, although smaller rearrangments remained possible.

To search for small rearrangments such as deletions, duplications, or DNA insertions, microarray comparative genomic hybridization (array CGH) was performed in collaboration with the Moerman laboratory at the Univeristy of British Columbia. In this approach, DNA from *kyIs501* and *ky957; kyIs501* were hybridized to microarrays containing roughly 400,000 50-mer oligonucleotides, located on average once every 250 bp (Maydan et al., 2007). Relative binding intensities at each position were measured to determine the relative copy number. Array CGH found one significant copy number variation between N2, *kyIs501*, and *ky957* on chromosome V, a ~16 kb deletion in *ky957* encompassing multiple cytochrome P450 family members and the seven-transmembrane olfactory receptor *str-247* (Figure 3.9A). This deletion is located at 3.95 Mb, almost 14 Mb from where *ky957* mapped, but it was possible that through a rearrangement this

Figure 3.8. Recombination map of V indicates the absence of any large rearrangements of chromosome V in *kyIs501*. Black line indicates chromosome V sequence. Open diamonds indicate locations of EMS SNPs. Green triangles represent mutations in N2 background and SNPs in a CB4856 background that recombined with *kyIs501*. Red triangles indicate the positions of SNPs and visible markers that did not recombine with *kyIs501*. Gray bar indicates the region shown in figure 3.7 with the highest density of EMS SNPs. Arrowheads indicate EMS SNPs flanking the ky957 genetic interval. The region of recombination suppression is consistent with that caused by an integrated transgene (Hammarlund et al., 2005).

Figure 3.8

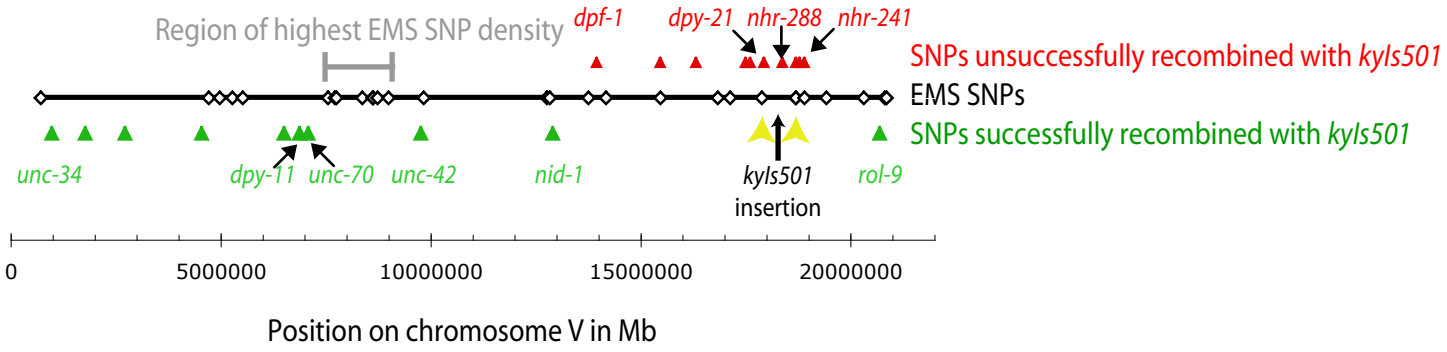
Region of highest EMS SNP density
dpf-1
dpy-21
nhr-288
nhr-241
SNPs unsuccessfully recombined with kyIs501
EMS SNPs
SNPs successfully recombined with kyIs501
unc-34
dpy-11
unc-70
unc-42
nid-1
kyIs501
insertion
rol-9
0
5000000
10000000
15000000
20000000
Position on chromosome V in Mb

Figure 3.9. Array CGH identifies a 16 kilobase deletion that is likely not the causative mutation in *ky957 kyIs501*. (A) Genomic location of 16 kb deletion. Red line indicates extent of deletion. (B) Quantification of ASH-to-AVA GRASP labeling in *ky957* animals carrying extrachromosomal arrays containing fosmids spanning the deletion. n.s., not significantly different from *ky957*.

Figure 3.9

A

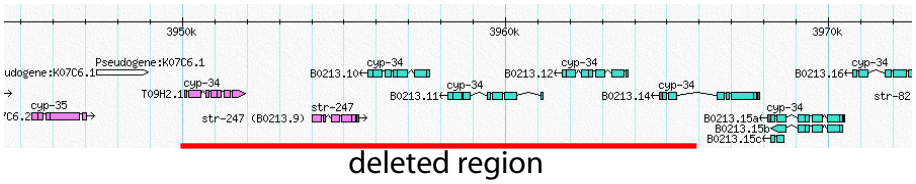
3950k
3960k
3970k
Pseudogene:K07C6.1
cyp-34
cyp-35
str-247
str-247 (B0213.9)
deleted region

B

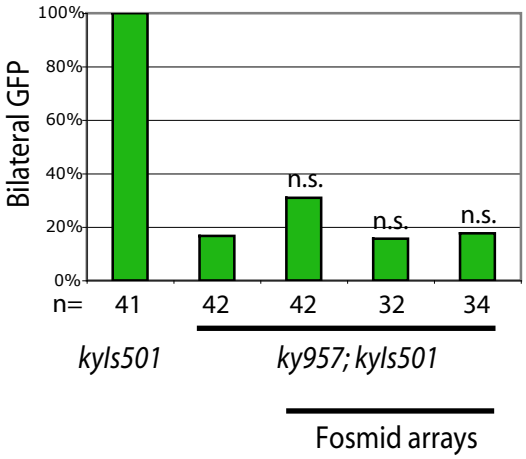
Bilateral GFP
100%
80%
60%
40%
20%
0%
n.s.
n.s.
n.s.
n=
41
42
42
32
34
kyIs501
ky957; kyIs501
Fosmid arrays

deletion was the causative mutation. Fosmids spanning the deletion failed to rescue, however, indicating that it is probably not the causative mutation in *ky957* (Figure 3.9B).

Array CGH data was examined to determine whether a duplicated genomic region could have masked an important mutation in one of the two copies. An existing example of this problem in the N2 strain involves the gene *rpm-1,* which consists of one complete copy accompanied by one perfect duplication of most of the gene (Zhen et al., 2000; Schaefer et al., 2000). This genomic arrangement complicated efforts to identify the causative mutation in alleles that overlapped the duplicated region. Similarly, if a gene in the *ky957* interval were present in two copies and only one copy of the gene was mutated, this could give rise to a phenotype but would be difficult to identify by sequencing. Array CGH data on V identified no duplications among the selected probes, suggesting that this explanation is unlikely, although small duplications or insertions could be present.

ky957 affects *kyIs501* rather than ASH-to-AVA synapse formation

The identification of *kyIs501* within the region containing *ky957* raised the possibility that *ky957* was a mutation associated with *kyIs501* itself. Array CGH found no significant difference in the copy number of any of the transgenes in *ky957* as compared to *kyIs501*, indicating that *ky957* is not a deletion within *kyIs501*(Don is assembling this data for me, but they were having software problems and said I might have to wait until after the holidays, it'll be good to have this, and to present what you find out about the structure of the integrant). Alternatively, point mutations within *kyIs501* could alter expression or function of the transgenes contained therein, by

repressing expression or by creating a dominant-negative form of one of the transgenes. Alignment of Illumina sequencing reads to the sequences of the plasmids in *kyIs501* found numerous potential point mutations at abundances that correspond to that expected for mutations in a single copy of that plasmid in the array. The functional significance of any of these potential SNPs is difficult to ascertain. Therefore, I sought to perform functional assays to address whether *ky957* is associated with *kyIs501*.

If *ky957* affects *kyIs501* rather than ASH-to-AVA synapse formation, GRASP labeling of ASH-to-AVA synapses by other transgenes might be unaffected in a *ky957* background. *kyIs491,* like *kyIs501*, is an integrant of the extrachromosomal array *kyEx2718*. *kyIs491* is integrated at an unknown site in the genome, but inheritance patterns indicate that it is unlinked to *kyIs501*. It is expected that 1/4 of the *ky957 kyIs501* F2 progeny of a *ky957 kyIs501* by *kyIs491* cross will be homozygous for *kyIs491*, and 1/2 will be heterozygous for *kyIs491*. 92 F2 progeny from a *ky957 kyIs501* by *kyIs491* cross were genotyped at EMS SNPs on chromosome V to identify 20 strains homozygous for *ky957*, and their F3 progeny were scored. In four of twenty strains, ASH-AVA GRASP labeling was wild-type in greater than ninety percent of animals. These four strains are probably derived from *kyIs491* homozygous F2 animals. In eleven of twenty strains, ASH-AVA GRASP labeling was wild-type in over fifty percent of animals, but some *ky957*-like labeling was observed. These animals are likely the progeny of *kyIs491* heterozygous F2 animals. The nearly Mendelian observed frequency of GRASP phenotypes, 4:11:5, is consistent with two interpretations: *kyIs491* was inherited as expected and labeling from this transgene is normal in *ky957 kyIs501* animals, or an unlinked synthetic mutation was segregating in these crosses. To address

this possibility, *ky957 kyIs501* was crossed to a different integrated strain that does not carry GRASP transgenes, *kyIs479* (Saheki and Bargmann, 2009), and *kyIs501* homozygous F2s were identified. All homozygous *kyIs501* F2 progeny displayed the *ky957* phenotype. Therefore, the *kyIs491* strain segregates a suppressor of *ky957* that it is not present in the *kyIs501* strain that derived from the same integration event that yielded *kyIs491*. This suppressor is most likely to be *kyIs491* itself.

To further explore whether *ky957* specifically affects *kyIs501*, extrachromosomal arrays carrying the intestinal marker *elt-2::mCherry* and the GRASP plasmids *sra-6::PTP-3A::spGFP11* and *flp-18::nlg-1::spGFP1-10* were generated to label ASH-to-AVA synapses in N2. These arrays were crossed into *ky957 kyIs501*, F1 animals were allowed to self-fertilize, and mutant F2 animals were isolated. *ky957* animals bearing the arrays displayed bright bilateral GRASP labeling similar to *kyIs501* controls, in contrast to their array-negative siblings that resembled *ky957 kyIs501* controls (Figure 3.10A,C). This results supports the conclusion that the defect in *ky957* is specifically associated with the *kyIs501* array. To alleviate the potential concern that overexpression of GRASP transgenes might result in non-specific, extrasynaptic labeling throughout the ASH and AVA axons, extrachromosomal arrays providing dim GRASP labeling were used for these experiments. In array-bearing *ky957 kyIs501* animals, labeling was confined to the lateral nerve ring, where GRASP labeling occurs in *kyIs501* (Figure 3.10E). As an additional control, the arrays were crossed into *kyIs501* animals. GRASP labeling in these animals was similar to that of array-negative siblings, suggesting that the combined expression of GRASP transgenes from *kyIs501* and the arrays does not produce an obvious overexpression effect (Figure 3.10F). These results indicate that the observed

Figure 3.10. Suppression of *ky957* by extrachromosomal arrays carrying coding and non-coding GRASP constructs similar to those in *kyIs501*. (A) Schematic of coding GRASP transgenes used in C. These transgenes are identical to those in *kyIs501*, and encode a signal sequence (SS) followed by split GFP fragments and GRASP carriers. Signal sequence cleavage generates the mature GRASP spGFP-carrier molecules. (B) Schematic of non-coding GRASP transgenes used in (D). Stop codons were inserted between the signal sequence and the spGFP fragments in the GRASP transgenes. Translation of the resultant mRNA yields a signal sequence but no GRASP proteins. (C) Transgenes described in (A) suppress *ky957 kyIs501*. For each array, array-bearing animals and their array-negative siblings were scored to control for *ky957* genotype. Asterisk, significantly different from array-negative siblings (two-tailed P<.001, Fisher's exact test) (D) Transgenes described in (B) suppress *ky957 kyIs501*. For each array, array-bearing animals and their array-negative siblings were scored to control for *ky957* genotype. (E) GRASP labeling (arrowheads) of ASH-to-AVA synapses in *ky957 kyIs501* animals carrying array 3 from (C). (F) GRASP labeling (arrowheads) of ASH-to-AVA synapses in *kyIs501* animals carrying array 3 from C. (G) GRASP labeling (arrowheads) of ASH-to-AVA synapses in *ky957 kyIs501* animals carrying array 3 from (D). Scale bars, 10 μm.

Figure 3.10

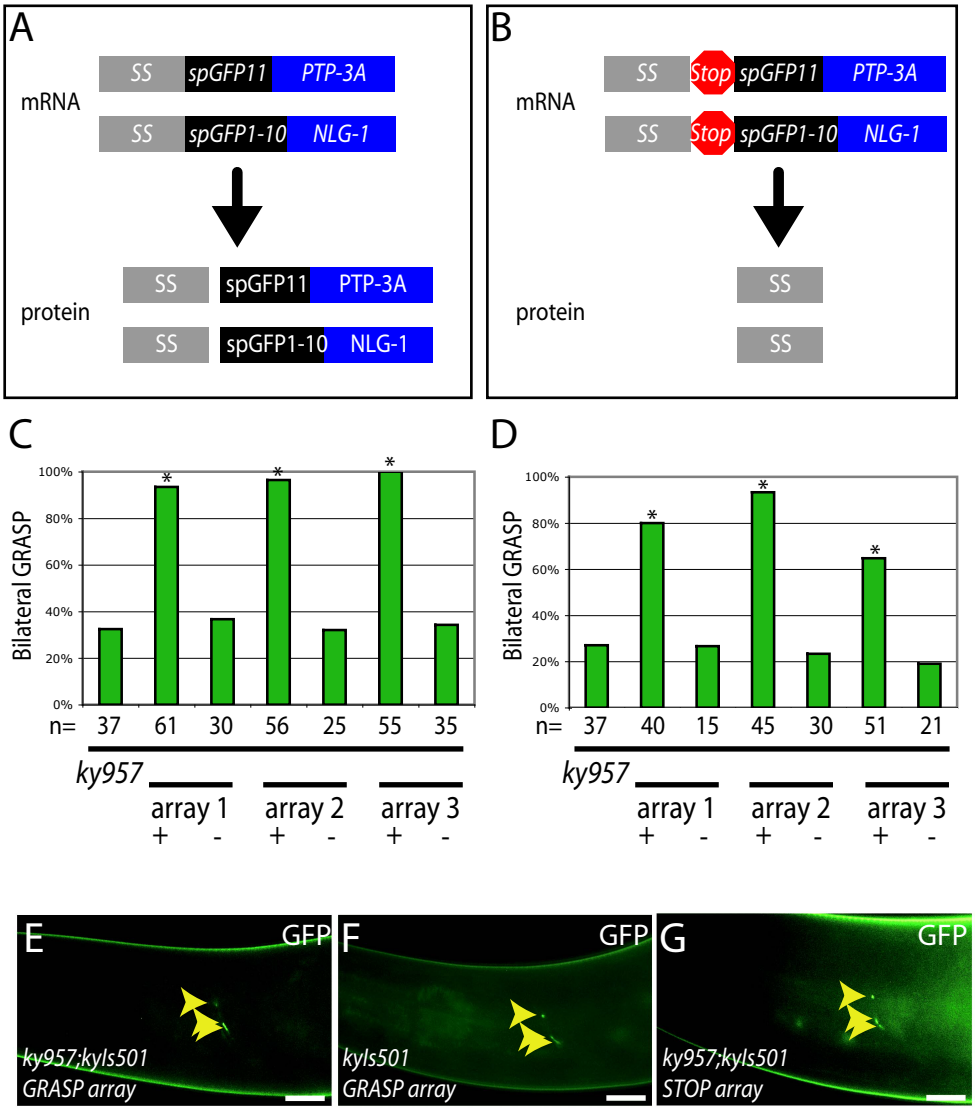
A
mRNA
SS
spGFP11
PTP-3A
SS
spGFP1-10
NLG-1
protein
SS
spGFP11
PTP-3A
SS
spGFP1-10
NLG-1
B
mRNA
SS
Stop
spGFP11
PTP-3A
SS
Stop
spGFP1-10
NLG-1
protein
SS
SS
C
Bilateral GRASP
100%
80%
60%
40%
20%
0%
n= 37 61 30 56 25 55 35
ky957
array 1
array 2
array 3
+ - + - + -
D
Bilateral GRASP
100%
80%
60%
40%
20%
0%
n= 37 40 15 45 30 51 21
ky957
array 1
array 2
array 3
+ - + - + -
E
GFP
ky957;kyIs501
GRASP array
F
GFP
kyIs501
GRASP array
G
GFP
ky957;kyIs501
STOP array

labeling reflects intact ASH-AVA synapses in *ky957* animals, and that *ky957* reduces GRASP signals by its effects on *kyIs501* itself.

These results, combined with the overexpression rescue observed with several DNA fragments from Chromosome IV and V, raised the possibility that *ky957* could be suppressed by interactions between *kyIs501* and other arrays. To test this possibility, *sra-6::PTP-3A::spGFP11* and *flp-18::NLG-1::spGFP1-10* transgenes were each modified by the introduction of a single nucleotide to generate a frameshift and premature stop codon immediately prior to the the spGFP; the only protein expressed from these transgenes should be a signal peptide (Figure 3.10B). These transgenes were injected into N2 animals, and as predicted did not display any GRASP labeling. However, these arrays were able to suppress the *ky957* GRASP defect (Figure 3.10D,G). This result indicates that *ky957* is associated with *kyIs501*, and that its effects can be suppressed through interactions with other DNA sequences.

The association of *ky957* with *kyIs501* could reflect decreased expression of the GRASP transgenes. Silencing of repetitive transgenes occurs in several classes of mutants such as *tam-1* and involves the RNA interference (RNAi) pathway, a process termed RNAi transcriptional gene silencing (RNAi-TGS) (Hsieh et al., 1999., B. Lesch, personal communication). I had previously observed reduced or absent GRASP and mCherry::RAB-3 labeling in *kyIs501* in the RNAi-hypersensitive mutant *eri-1(mg366);lin-15b(n744)*. Although this phenotype was not as specific to the GRASP label as *ky957*, it seemed possible that the *ky957* GRASP phenotype might be caused by RNAi-TGS-like silencing of *kyIs501*. RNAi of chromatin remodeling factors such as *mes-4* and *mrg-1* or pharmacologic inhibition of histone deacetylases (HDAC) can

relieve RNAi-TGS (Cui et al., 2006; Grishok and Sharp, 2005). In preliminary experiments, *ky957* was not suppressed by RNAi of *mes-4* or *mrg-1*, although this negative result might reflect the neuronal refractoriness to RNAi (Wang et al., 2005), or the HDAC inhibitors n-butyrate and trichostatin A. These results, although not conclusive, suggest that *ky957* may exert its effects on *kyIs501* through a mechanism distinct from RNAi-TGS.

Discussion

In this work, I found that several regulators that act at earlier steps or other cells during neural development are dispensable for ASH-to-AVA synapse formation. For example, the *syg-1* and *syg-2* guidepost molecules are required for synaptic specificity in the HSN neuron (Shen et al., 2004), and *syg-1* is expressed in other neurons as well (Shen and Bargmann, 2003). However, *syg-1* and *syg-2* are not required for ASH-to-AVA synapse formation, suggesting that other guidepost signals might aid in the formation of ASH-to-AVA synapses. Mutations of the axon guidance molecules *unc-6*/Netrin and *sax-3*/ROBO disrupted ASH-to-AVA synapse formation in some animals, but often the ASH axon appeared misguided, which could preclude interaction with AVA. A systematic analysis of GRASP labeling in animals with labeled AVA axons could allow determination of whether *unc-6* and *sax-3* play roles outside of axon guidance in ASH-to-AVA synapse formation.

SNPs identified with Illumina sequencing proved useful for multiple steps in mapping beyond mere mutation identification. First, Bluma Lesch's work showed that whole-genome sequencing was able to identify a region of increased mutation density to

which a relevant mutation, *ky777*, maps. This mutation rate approach may be of general use and could expedite mapping of future mutants. Second, a concern when mapping any mutant is that mapping strains might alter the mutant phenotype, particularly the highly polymorphic CB4856 strain used in many studies. SNPs identified with Illumina sequencing allowed mapping of *ky957 kyIs501* against the parental strain *kyIs501*, minimizing any background-dependent effects.

The mutant described here, *ky957*, alters ASH-to-AVA GRASP labeling. *ky957* appears to be associated with *kyIs501*, and does not appear to affect ASH-to-AVA synapse formation. GRASP depends on transgene expression, and mutations that increase or decrease transgene expression or alter expression patterns may alter GRASP labeling without altering synaptic connectivity. Future studies using GRASP will need to address this problem, perhaps by incorporating additional markers into GRASP transgenes to minimize the identification of these mutants, or by secondary screens for behavioral or physiological phenotypes.

The molecular basis of the *ky957* phenotype appears to be associated with *kyIs501*, but the exact lesion is unclear. Transgene silencing has been described in several genetic backgrounds, and is often observed in the mutants that increase the sensitivity of neurons and other cells to RNAi (Hsieh et al., 1999; Grishok et al., 2005; Wang et al., 2005). Interestingly, when *kyIs501* was introduced into an RNAi sensitized strain, *eri-1(mg366);lin15(n744)* (Wang et al., 2005), a variable phenotype was observed in which GRASP labeling was reduced in some animals without a loss of mCherry::RAB-3 signal, a phenotype reminiscent of *ky957*. Whether *ky957* affects *kyIs501* expression in a similar way remains to be seen.

ky957 may represent one of many possible mutants that could affect GRASP phenotypes without affecting ASH-to-AVA synapse formation. Altered GRASP labeling in the absence of ASH-to-AVA synapse defects might also be caused by mutations that alter expression of the promoters used in the GRASP transgenes, such as *unc-42*, or mutations that alter the function or localization of the GRASP carriers. In future screens, the GRASP carriers could be tagged with fluorophores, such as mCherry or uv-GFP, to monitor their expression and localization. Mutants with altered GRASP labeling could be rescreened to exclude mutants with obvious defects in carrier expression or localization. In addition, after initial mapping a new GRASP transgene, as used in figure 3.10, could allow determination of whether the GRASP signal is truly disrupted.

Chapter 4

Discussion and future directions

This work establishes a new approach to the longstanding question of how neurons identify their synaptic targets. GRASP enables the visualization of specific synapses in live animals, permitting analyses on a scale that was previously unattainable. In these studies, GRASP was applied to the study of one set of synapses in the CNS, the synapses between ASH sensory neurons and AVA interneurons. These experiments illustrate the potential of GRASP for future studies of the mechanism of synapse formation, including the discovery of molecules and mechanisms of synaptogenesis. However, new approaches and methodologies may need to be merged with further refinements of GRASP to solve the problem of synaptic specificity.

Intersectional gene expression with Cre recombinase

Despite years of intensive study, unique promoters are lacking for many of the 120 neuron classes in *C. elegans*. To fully harness the power of *C. elegans* genetics in the study of neural circuits, a method to produce single-cell expression of transgenes for rescue, gain of function, and functional imaging methods was needed. In this thesis, I developed a Cre-loxP based toolkit for confining gene expression to single cells (Macosko et al., 2009). Cre-based methods are likely to be useful for a number of other applications. However, expression of transgenes after Cre-mediated stop excision was

weaker than expression of comparable transgenes in multicopy arrays. This reduced expression suggests that several iterations of Cre-mediated recombination within an array result in reduced copy numbers of plasmids within the transgene, or that recombination between distal loxP sites excises several intervening copies of that plasmid (Figure 4.1A). The problem of successive recombination events might be minimized through the use of mutant loxP sites. Distinct mutations could be introduced into the 5' and 3' loxP sites flanking the stop sequence to generate a substrate that is competent to undergo only one recombination event because the resultant hybrid loxP site cannot be recognized by Cre (Arakawa et al., 2001, Figure 4.1B). This method would extend the utility of Cre-loxP expression tools to applications requiring higher transgene expression levels.

Cre-loxP tools could be used to facilitate genetic rescue experiments in *C. elegans*. In typical transgene rescue experiments, sites of expression sufficient for rescue can be identified by injecting *C. elegans* mutants with wild-type cDNA driven by cell-specific promoters. More rarely, the converse experiment has been performed by identifying sites of expression necessary for rescue using mosaic analysis with unstable genetic elements. Genetic mosaic analysis can be slow for single-worm assays and prohibitive for population assays, and as this method is lineage-based, it is hard to use in the nervous system where the left and right members of a neuronal pair are usually unrelated by lineage. In other organisms, tissue-specific conditional knockouts can be generated using site-specific recombinases such as Cre (Gu et al., 1994). Similarly, worm conditional knockouts could be made through rescue of a mutant with a loxP-flanked transgene driven by a broadly expressed promoter (Figure4.1C). Cre expression

Figure 4.1. Applications of Cre-loxP technology. (A) Effects of Cre-mediated recombination on multicopy transgenes. A loxP-stop-loxP transgene construct is contained in a multicopy array. Cre expression leads to successive rounds of Cre-mediated recombination that result in reduced copy number and corresponding reduced transgene expression. Triangles represent loxP sites. (B) Modified loxP sites (truncated triangles) recombine to generate a non-functional hybrid loxP site that is not competent for subsequent recombination. In this way, Cre removes fewer copies of the transgene to maintain strong transgene expression. (C) Cre-mediated conditional knockout in *C. elegans*. Wild-type cDNA corresponding to a gene of interest is flanked by loxP sites and introduced into the mutant in that gene. Cre-mediated recombination deletes the cDNA in cells of interest.

Figure 4.1

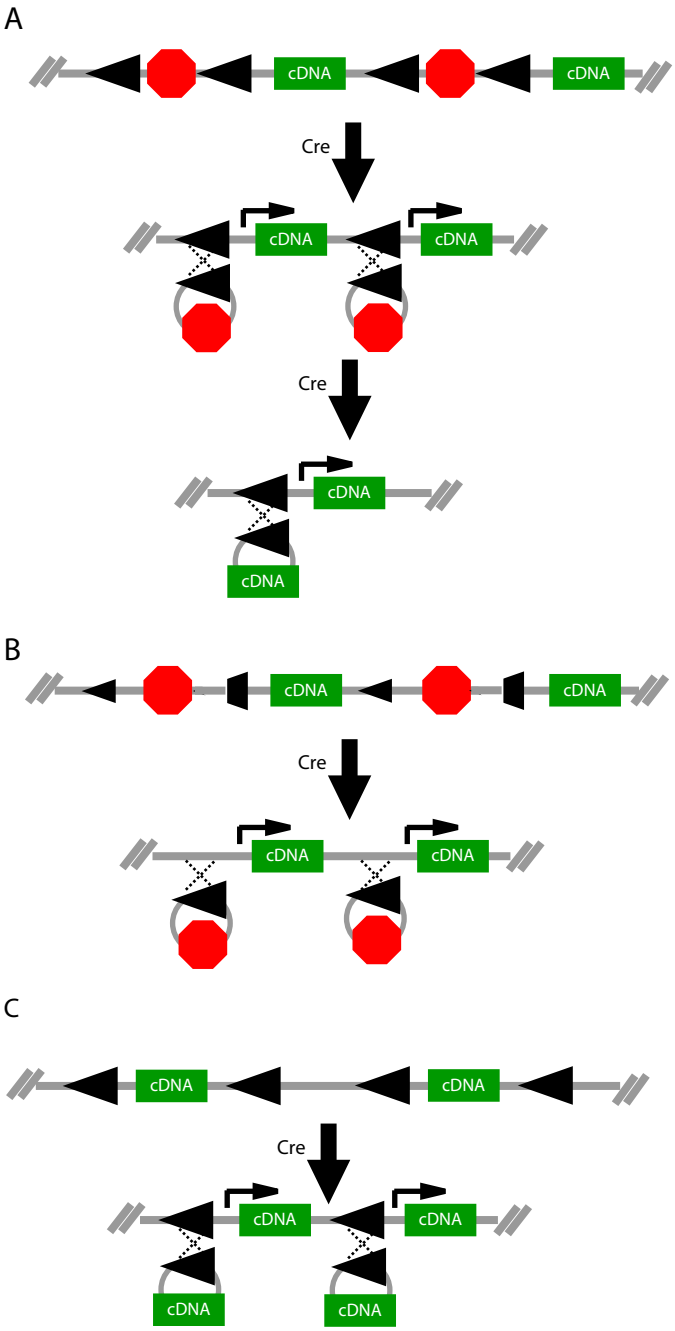
A
cDNA
cDNA
Cre
cDNA
cDNA
Cre
cDNA
cDNA
B
cDNA
cDNA
Cre
cDNA
cDNA
C
cDNA
cDNA
Cre
cDNA
cDNA
cDNA
cDNA

in cells of interest should delete the transgene in those cells so that necessity can be assessed.

Finally, Cre-loxP tools could be useful in the study of essential genes. Many pleotropic mutations cause phenotypes such as embryonic lethality that preclude their study in the adult nervous system. The use of conditional knockouts would allow investigation of the functions of these essential genes in the adult nervous system.

Applications of GRASP

In *C. elegans*, the classical analysis of the nervous system by serial section electron microscopy (EM) and synaptic reconstruction of a few animals discovered a striking but not absolute connectivity stereotypy. First, although most of the CNS is bilaterally symmetric, systematic comparison of EM data from two animals measured substantial variation within bilateral neuron pairs in each animal (Durbin, 1987). The probability that two neurons were connected by a chemical synapse if their contralateral homologs were connected was 79% in one animal and 87% in the other animal, with a slightly higher likelihood for gap junctions. Second, animal-to-animal variation was found. When two neurons formed multiple synapses in one animal, those neurons were 95% likely to synapse in the second animal. However, if two neurons formed one synapse in one animal, they were only 75% likely to be connected in the other animal. In 137 instances, chemical synapses were observed between two cells on one side in one animal and not observed on either side of the other animal, while in 32 instances two neurons were connected bilaterally in one animal and unilaterally in the other. These and other measurements suggest that *C. elegans* synaptic connectivity is not fully invariant,

and that the wiring diagram derived from these serial section EM reconstructions samples a portion of the synaptic spectrum that animals display. Relevant to my work, ASHL formed two synapses onto AVAL in one animal and one synapse in the other, and ASHR formed four synapses onto AVAR in both animals. This variability is consistent with the range of GRASP labeling observed in *kyIs501* animals. However, GRASP signal was also present in the ventral portion of the nerve ring in occasional *kyIs501* animals. This signal may reflect an artifact of the GRASP method, such as internalized GRASP-labeled protein complexes, or alternatively bona fide synapses that may occasionally form between ASH and AVA in the ventral nerve ring. The rare presence of this ventral signal in the absence of labeling in the lateral nerve is consistent with the latter possibility, which could be tested by examining additional pre- and postsynaptic markers.

A comprehensive picture of the range of connectivity patterns in a circuit of interest could be developed with GRASP. Variability could be compared within laboratory wild-type and mutant strains, and among wild strains isolated from different environments. This system could also be used to assess how environmental experience, such as dauer development, impacts the structure of the mature nervous system. It is possible that this approach could identify molecules that function to constrain variability.

The variability observed with GRASP labeling might offer a means to explore how connectivity determines function. Synapses of interest could be GRASP labeled, and animals displaying different GRASP patterns could be sorted and assayed by behavior. This approach might be a useful way to determine the roles of classes of synapses or numbers of synapses, and more generally to probe the question of how neuroanatomy dictates function.

The studies described here focused on synapses at a defined point in development, but synapses can be highly plastic in living nervous systems. Numerous studies have identified alterations in neural architecture as result of activity (Shatz and Stryker, 1988; Zhao and Nonet, 2000), and the ability to monitor changes in synaptic connectivity dynamically would be of great use for studies of learning and memory as well as aging and disease models. My results suggest that GRASP labeling should appear as synapses form and disappear as synapses are lost. spGFP reconstitution is rapid but is believed to be essentially irreversible, which could lead to a persistent signal long after a synapse is lost (G. Waldo, personal communication). However, the disappearance of muscle GRASP labeling as the *ace-4* promoter was extinguished in late larval stage animals suggests that cells are able to degrade GRASP complexes in the course of normal protein turnover. GRASP signal may disappear as a result of transcytosis of the transcellular GRASP complexes, proteolytic liberation of the reconstituted GFP from one of its linkers and subsequent dissociation, or GFP dissociation or degradation. This result may be carrier-dependent, and further examination is needed. The stability of GRASP labeling could be measured in HSN, where wild-type early L4 animals form synapses anterior of the vulva that are eliminated in a *syg-1*-dependent manner (Ding et al., 2007), or in DD motor neurons, which remodel their axons to shift from innervating ventral muscles to innervating dorsal muscles in late L1 stage animals (White et al., 1978). Should GRASP signals prove highly stable, dynamic gain and loss of synapses might be studied by photobleaching and recovery experiments (Jacobson et al., 1976), or through the development of split, superfolding versions of the fluorescent timer protein E5, which

spontaneously shifts its emission from green to red with defined kinetics (Terskikh et al., 2000).

The intersectional approach used in GRASP might point to a way to manipulate individual synapses. For example, reconstitution of a split molecule that modifies synaptic signaling synaptic components might be used to suppress activity at a single synapse. An attractive target for synaptic manipulation is the presynaptic voltage-gated calcium channel (VGCC), through which calcium influx triggers vesicle exocytosis. Nature has provided numerous protein-based inhibitors of these channels, such as the conotoxins from snails, but perhaps the most attractive comes from the clinic. Lambert-Eaton myasthenic syndrome (LEMS) is an autoimmune disorder in which autoantibodies target and inhibit presynaptic VGCCs to cause progressive weakness (Lang and Vincent, 2009). These antibodies form a bipartite extracellular toxin, with antigen binding requiring the interaction of the separately encoded heavy chain (HC) and light chain (LC). Although HC and LC are typically co-expressed and assembled in the secretory pathway in B cells, in pathological conditions like multiple myeloma, B cells secrete free HC or LC, and LC can be secreted from fibroblasts in the absence of HC, suggesting that single chains can fold and exit the ER (Gonzalez et al., 2007; Dul et al., 1996). In theory, PTP-3A::HC expressed in a presynaptic cell and NLG-1::LC expressed in a postsynaptic cell would culminate in formation of a tethered antibody at sites of intersection and silencing of that synapse through interference with presynaptic VGCCs. This is just one example of how intersectional protein reconstitution methods hold the potential to change how individual synapses are labeled and manipulated *in vivo*.

A systematic approach to synaptic specificity in *C. elegans*

GRASP permits monitoring of only one set of synapses per anatomical region in each animal. Faster and more systematic assessment of synaptic connectivity would require the ability to monitor several synapses at once. Existing split superfolding cyan and yellow fluorescent proteins could expand the GRASP palette to allow simultaneous and independent visualization of two sets of synapses. spYFP1-10 and spCFP1-10 reconstitute with spGFP11, so that one pre- or post-synaptic cell, and two or synaptic partners, could be differentially labeled in one strain. For example, differential labeling of HSN-to-VC and HSN-to-vulval muscle cells synapses could allow screens for mutations that differentially regulate one of two sets of synapses.

Comprehensive analysis of synaptic connectivity in *C. elegans* will require a suite of strains in which different synapses are labeled. Titrating the expression of both pre- and post-synaptic GRASP carriers in extrachromosomal arrays is a tedious process that must be repeated for each synapse of interest. Moreover, repetitive extrachromosomal arrays are subject to silencing and other phenomena that could produce spurious signals. To create a modular GRASP system, a set of two newly developed single-copy transgenesis techniques could be of use. One method, MosSCI, enables single-copy transgene insertion at defined chromosomal loci (Frokjaer-Jensen et al., 2008). MosSCI could be used to insert a transgene containing a pan-neuronal promoter driving a loxP-STOP-loxP presynaptic GRASP construct carrier, and a second transgene containing a pan-neuronal promoter driving a FRT-STOP-FRT::postsynaptic GRASP line (Davis et al., 2008). Expression of Cre in a presynaptic cell of interest and FLP in a postsynaptic interest should lead to excision of the stop sequences in those cells and expression of the

corresponding GRASP markers. Different Cre and FLP lines could be crossed into the GRASP strains to label different sets of synapses. Importantly, the catalytic activity of Cre and FLP has an all-or-none quality, so that these transgenes might not need to be titrated. The second potentially useful transgenic method, MosTIC, enables modification of genes at their endogenous loci (Robert and Besserau, 2007). LoxP- and FLP-dependent expression constructs could be introduced at the PTP-3A and NLG-1 loci to enable conditional expression of GRASP transgenes under the control the endogenous promoters of the carrier molecules, reducing concerns of overexpression artifacts. A potential limitation of these techniques is that expression from single transgenes can be dim. This issue could be addressed through the use of strong constitutive promoters with MosSCI transgenes. Signal amplification could also be accomplished through incorporation of several tandem spGFP fragments per carrier molecule, as has been performed with the dim pH sensor phluorin (Zhu and Stevens, 2008). Should single-copy expression methods fail to provide a sufficiently bright signal, multicopy transgenesis using the variant loxP sites described above could prove a viable approach.

The genetics of synaptic specificity in *C. elegans*

The problem of synaptic specificity has been recognized for decades, yet our understanding of this process is incomplete. Identifying specific synapses *in vivo* is challenging, and it is difficult to perturb those synapses. The studies presented here offer a potential solution to the former, and it is worth considering whether they are informative with regard to the latter. The genetic screen in which *ky957* was identified was not saturated, but it is still notable that only a few mutants were identified. In

Figure 4.2 Single-copy transgenic toolkit for GRASP. (A) MosSCI allows insertion of single copies of loxP-stop-loxP and FRT-stop-FRT GRASP transgenes driven by strong constitutive promoters. Expression of Cre or FLP leads to excision of the corresponding stop sequence and expression of the GRASP transgenes in the cells of interest. Black triangles represent loxP sites, and purple triangles represent FRT sites. (B) MosTIC allows modification of the endogenous locus for the GRASP carriers. In this case, the *ptp-3a* locus is modified by insertion of a copy of exon 1 with spGFP11 inserted at the appropriate position in an inverted orientation with respect to the gene. Exon 1 and the spGFP11-fused exon 1 are flanked by mutant loxP sites in opposite orientations. In the absence of Cre, PTP-3A is expressed normally. In the presence of Cre, a single recombination event occurs to invert the exon 1 cassette, placing the spGFP11 form on the same strand as *ptp-3a*. This results in expression of PTP-3A::spGFP11 in those cells driven by the endogenous *ptp-3a* promoter. Truncated triangles indicate mutant loxP sites.

Figure 4.2

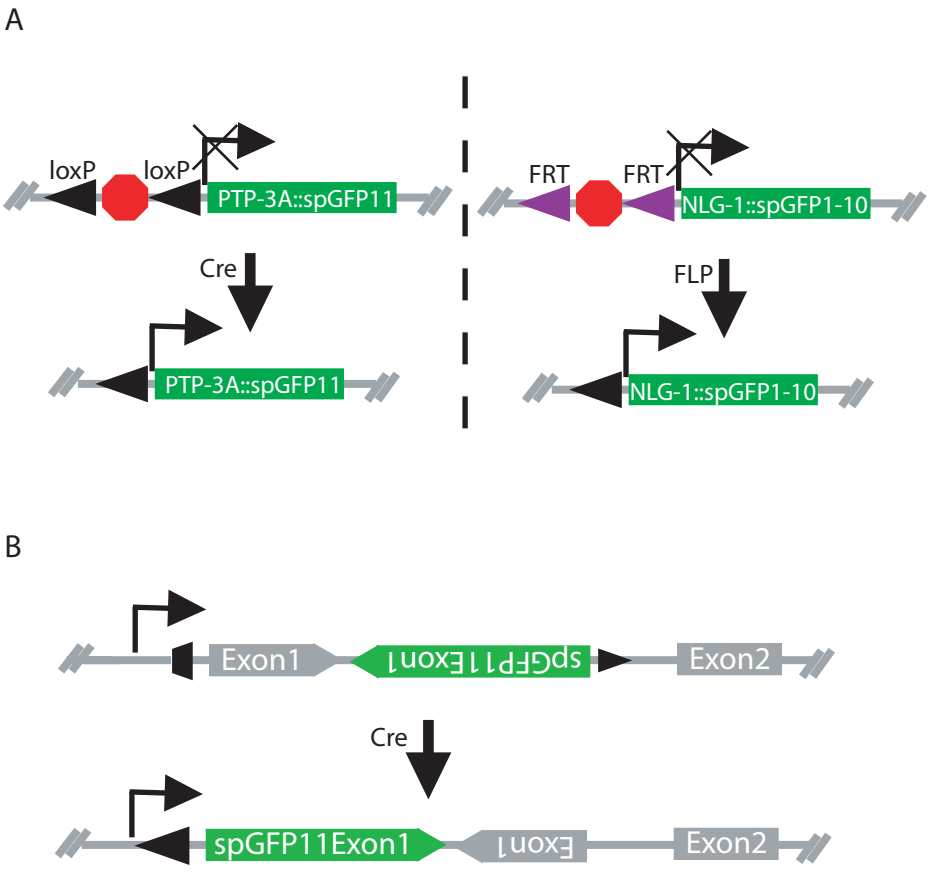
A
loxP
loxP
PTP-3A::spGFP11
Cre
PTP-3A::spGFP11
FRT
FRT
NLG-1::spGFP1-10
FLP
NLG-1::spGFP1-10
B
Exon1
spGFP11Exon1
Exon2
Cre
spGFP11Exon1
Exon1
Exon2

addition to cell surface recognition molecules required for targeting, transcription factors, RNA binding proteins, non-coding RNAs and other factors that shape a cell's repertoire of connectivity determinants could have been identified in this screen, along with intracellular components involved in signaling downstream of target recognition. This screen identified four mutants with heritable phenotypes out of ~4,000 genomes, only one of which, *ky957*, displayed wild-type mCherry::RAB-3 labeling and mutant GRASP labeling. These results suggest that subsequent screening may need to be made more sensitive.

A concern when performing a new screen is that the phenotype scored may not reflect the underlying biology. In particular, GRASP labeling could be artificially robust in a manner that masked *bona fide* specificity mutants. The analyses of HSN-to-VC and vulval muscle synapses and AVA-to-VA synapses found that GRASP labeling detected specificity mutants in these test cases, but in the absence of a similar mutant it is difficult to validate the sensitivity of a GRASP strain that labels a different set of synapses. At present, comparison of the observed labeling to that found in serial section EM remains the best means to identify suitable GRASP strains, but it is possible that strains meeting these visual criteria could suffer from overexpression artifacts nonetheless. Overexpression artifacts might produce spurious GRASP labeling at extrasynaptic contacts between ASH and AVA, so that only mutants with loss of ASH to AVA fasciculation would be identified. This phenotype is worth studying independently, using CD4 GRASP, but was not the goal of the screens described here. The use of single-copy transgenesis methods described above could reduce overexpression effects and increase the sensitivity of GRASP screens.

This screen also could have failed to identify mutants due to two commonly observed genetic phenomena, redundancy and pleiotropy. Redundancy, reduced penetrance defects in single mutant due to overlapping gene function, and pleiotropy, defects in multiple processes, can interfere with identification of mutants of interest. Modifications of screen design could address these concerns.

If ASH-to-AVA synapse formation involves redundant factors, identification of a mutant phenotype would require simultaneous loss of several recognition factors. Although redundancy is frequently observed in genetic pathways, the historical success of forward genetics argues that at least some non-redundant factors in a pathway can usually be identified. Significant redundancy would reflect the presence of parallel recognition molecules that signal through distinct pathways. The best-characterized examples of redundant parallel pathways in *C. elegans* are the synthetic multivulval (synMuv) pathways. Generation of a synMuv phenotype requires the loss of at least two factors from independent pathways that inhibit ras signaling (Jorgensen and Mango, 2002). Genes with redundant loss-of-function mutations can sometimes be identified by gain-of-function mutations. Gain-of-function mutations are induced more rarely than loss-of-function mutations, but could be identified in an F1 GRASP screen.

Limited candidate mutant analysis did not identify any factors with highly penetrant defects in ASH to AVA synapse formation, but it is possible that the mutants with mild defects or other untested mutants in various signaling pathways could be used as a sensitized background for a GRASP screen. Among previously analyzed candidate mutants, double and triple mutant analysis may uncover redundant interactions that could be studied and used to generate sensitized strains.

Another reason that this screen failed to identify mutants may be pleiotropic effects of the genes involved in synaptic specificity. As described earlier, specificity mutants in genes that function at several steps in circuit formation, or in essential genes, may not be identified in a stringent specificity screen. Temperature-sensitive alleles can be used for temporal control of gene activity, and this approach allowed identification of new roles of *glp-1*, which in null mutants causes sterility due to impaired germ cell production, in later steps in embryogenesis (Priess et al., 1987). However, temporal segregation of early stages in development at which embryonic-lethal genes act from stages at which synapses form may be minimal. Therefore, a temperature-sensitive screen might be of greater use in studying synapse formation by neurons that are born post-embryonically, such as the PQR sensory neuron or HSN. Mutant animals could undergo embryonic development at a permissive temperature and be shifted to a restrictive temperature shortly after hatching and for the remainder of development. Although this approach may prove fruitful, temperature-sensitive alleles are less common than standard null alleles and are not obtainable for all genes.

To facilitate identification of synthetic GRASP mutants, temperature-sensitive alleles, or rare dominant alleles, increased screening throughput is essential. The current throughput of GRASP-based screening is roughly 200 genomes per day. At this throughput, a synthetic mutant likely would not be identified for years. Therefore, technologies such as microfluidic devices and a commercially available worm sorter, which can increase screening throughput by a few orders of magnitude (Crane et al., 2009; Pulak, 2006), should be investigated. The low sensitivity of these automated approaches may require extensive optimization, but the potential benefits make this a

worthwhile investment of effort. Alternatively, a bipartite labeling system such as Tango might be used to detect cell contact and provide signal amplification for an initial automated screen for mutants with reduced cell contact (Barnea et al., 2008), which could be followed with a GRASP-based secondary screen.

Another way to increase the throughput of a GRASP-based screen for rare mutants would be through a behavioral prescreen. The ultimate purpose of synaptic connections is to permit neurons to communicate and generate behavior. Therefore, it would be reasonable to assume that perturbation of these synapses would result in behavioral deficits. ASH detects noxious stimuli, and AVA generates avoidance responses, yet previous screens for mutants defective in ASH-mediated avoidance failed to identify factors required for the formation of these synapses. This may reflect the difficulty of predicting the function of a synapse from wiring or redundancy in the function of individual synapses in a circuit. For example, *syg-1* and *syg-2* synaptic mutants have milder defects in egg laying than those seen after ablation of HSN (Shen and Bargmann, 2003; Shen et al., 2004). Moreover, animals in which HSN fails to reach the vulva have similarly mild defects in egg-laying (C. Bargmann, personal communication). For this reason, *syg-1* and *syg-2* may not have been identified in behavioral screens. Circuit redundancy may hinder further efforts to identify specificity mutant through behavioral screens, but more detailed analysis may identify subtle but quantifiable behavioral consequences of the loss of a certain synapses. In this context, a high-throughput, quantitative behavioral screen might allow prescreening of mutant animals for a GRASP screen.

Reverse genetics can facilitate the study of both pleiotropic and redundant genes. This approach might be focused by conducting gene expression analysis of the cells of interest, such as ASH and AVA, through RNA sequencing methods (Wilhelm and Landry, 2009). Genes enriched in those cells could be studied with loss-of-function alleles or RNAi. This approach would considerably reduce the pool of genes from which to generate double or triple mutants, aiding in the discovery of redundant interactions. Candidate genes with pleiotropic effects such as embryonic lethality could be rescued with conditional loxP alleles of the wild-type gene, then characterized for their roles in specificity through Cre-mediated deletion in those cells or at developmental times of interest. Another reverse genetic approach that may be of use in studying these phenotypes is RNAi. RNAi has proven difficult in some neurons, and RNAi-sensitized strains are sensitive to transgene silencing, but the use of these sensitized strains in a single-copy GRASP transgenic strain should minimize silencing (Hsieh et al., 1999). To minimize pleiotropic effects, RNAi can be initiated through feeding, soaking, injection, or hairpin transgene induction at the developmental time point of interest. Pleiotropic effects could be further rescued by confining RNAi to neurons by conducting RNAi in an *rde-1* mutant background in which *rde-1*, which functions cell autonomously (Tabara et al., 1999), is rescued in neurons. Each of these approaches to studying redundancy and pleiotropy may facilitate identification of certain forms of mutants and prevent identification of other mutants, and as such should be viewed as complementary.

Finally, it is possible that different assumptions or screening strategies should be used. In axon guidance, more repulsive than attractive cues are known (Tessier-Lavigne and Goodman, 1996). By analogy, there might be many more repulsive than attractive

cues in synaptic specificity. As an alternative approach to the GRASP screen done here, a genetic screen could be performed to identify factors that prevent synaptogenesis. Analysis of serial-section EM has identified many fasciculated neurons that do not synapse (Durbin, 1987). In wild-type animals, GRASP should fail to identify synapses between these cells, but in mutants in which the cells synapse, a GRASP label would appear. A search for a signal in an unlabeled strain allows investigators to screen more quickly. In a more fanciful analysis, this approach might be partnered with a behavioral screen for mutants that acquire a new behavior consistent with the functions of those cells.

The genetic nature of the *ky957* mutation

The *ky957* mutation was identified in a genetic screen as a mutation that disrupts ASH-to-AVA GRASP labeling. *ky957* maps to a small region that contains *kyIs501*, and the ability of different ASH-to-AVA GRASP transgenes to suppress *ky957* suggests that it is associated with *kyIs501*. The *ky957* phenotype of reduced GRASP labeling would be consistent with reduced functionality of the protein products in the transgene or reduced expression of the GRASP transgenes.

An EMS mutation in one or several of the GRASP transgenes in *kyIs501* could cause a loss-of-function allele that reduces GRASP labeling at ASH-to-AVA synapses. *kyIs501* carries multiple copies of the pre- and post-synaptic PTP-3A::spGFP11 and NLG-1::spGFP1-10 transgenes, so the *ky957* GRASP phenotype could require loss-of-function mutations in several copies of that transgene or a mutation in the most highly expressed copy. In this model, other GRASP arrays restore GRASP labeling through functional replacement of the mutated forms. The effects of the non-coding GRASP

transgenes may be explained by alterations in transgene expression. Transgene expression in *kyIs501* is likely dictated by a balance of transcriptional activators recruited to promoters in the array and repressors that target repetitive DNA non-selectively. If repressors are present in limiting qualities, as has been proposed in other contexts (Grewal et al., 1998), the presence of an additional non-coding repetitive array may titrate away the repressor activity and boost expression of the intact GRASP transgenes in *kyIs501* to suppress *ky957*.

A dominant-negative mutation in a single copy of either PTP-3A::spGFP11 or NLG-1::spGFP1-10 could interfere with the function of other wild-type copies of that carrier. The partial penetrance of *ky957* suggests that if there is a dominant-negative form of one of the GRASP carriers present in *ky957 kyIs501*, it is not a complete suppressor. Therefore, wild-type GRASP constructs could suppress such a mutatiotn by titrating the effects of the dominant negative allele. As described above, increased expression of *kyIs501* due to titration of repressive factors to this array could increase expression of the GRASP transgenes and GRASP labeling.

Another genetic mechanism by which *ky957* could affect *kyIs501* is through reduced expression of the GRASP transgenes. Array CGH suggests that *ky957* is not a large deletion in *kyIs501*, but *ky957* could be a mutation that creates a binding site for a transcriptional repressor such as a chromatin remodeling factor that binds and represses *kyIs501*. Alternatively, *ky957* might disrupt a promoter element in *kyIs501*. Suppression by other GRASP arrays or titration of repressors by non-coding arrays is easily reconciled with this model. In this model, GRASP carriers expressed from other arrays can functionally substitute for the silenced copies in *kyIs501* to suppress *ky957*.

Repetitive transgenes are particularly susceptible to transcriptional silencing, and non-coding GRASP arrays might recruit away limiting repressive factors to derepress *kyIs501* and suppress *ky957*.

Illumina sequencing identified many point mutations in coding and non-coding sequences of the single copies of the GRASP plasmids present in *kyIs501*, but the functional consequences of any of these mutations remains unclear. Determining which, if any, of these point mutations causes *ky957* may not be possible with current methods. Instead, characterization of the functional mechanism might be possible through antibody staining of GRASP carrier protein localization and quantitative RT-PCR of the GRASP carrier expression.

Although *ky957* was identified in a genetic screen, *ky957* could represent an epigenetic allele that silences only the integrated *kyIs501* transgene. Heritable epigenetic mutations have been identified in numerous systems, including plants and mice, in a phenomenon termed paramutation. Paramutation has been observed at repetitive endogenous and transgenic loci, and involves stably transmitted repression of genomic regions (Suter and Martin, 2009). Paramutation in several organisms is known to involve short template-derived RNAs and silencing through CpG methylation of DNA . Although *C. elegans* is believed to lack the ability to methylate DNA, RNA-based gene silencing in *C. elegans* is well documented. RNA interference (RNAi), in which double-stranded RNAs initially induce gene silencing through degradation of homologous mRNAs, can also trigger transcriptional gene silencing (RNAi-TGS) (Grishok and Sharp, 2005). *C. elegans* RNAi-TGS is propagated for >80 generations in the absence of the trigger dsRNA (Vastenhouw et al., 2006). RNAi-TGS-like silencing of transgenes in the

absence of exogenous dsRNA triggers has been observed in several mutants such as *tam-1* (Hsieh et al., 1999; Wang et al., 2005). *tam-1* contains a RING finger motif, which in *Drosophila* are found in transcriptional repressors, and belongs to the synMuvB class of genes that have been shown to mediate transcriptional repression. Some, but not all, repetitive transgenes expressed in numerous somatic tissues, including neurons, are silenced in *tam-1* mutants. SynMuvB mutants such as *tam-1* can enhance RNAi in somatic tissues, including neurons, and this enhancement may potentiate RNAi-TGS of repetitive transgenes (Wang et al., 2005).

Subsequent studies of RNAi-TGS have begun to elucidate pathways downstream of small RNAs that enact silencing in numerous organisms. In fission yeast, RNAi-TGS of centromeric regions involves *dicer*- and *argonaute*-dependent generation of small interfering RNA (siRNA) that leads to Clr-4-dependent methylation of Histone 3 lysine 9 which is recognized by Swi6, a chromodomain protein (Hall et al., 2002; Volpe et al., 2002). The *C. elegans* argonaute *rde-1* is required for RNAi-TGS (Cui et al., 2006), and the *C. elegans* Swi6 homolog, *hpl-2*, is a synMuvB gene, suggesting that these components of the RNAi-TGS pathways are shared in *C. elegans* (Couteau et al., 2002). RNAi-TGS in *C. elegans* is dependent on *mes-4* and *mrg-1* and histone deacetylases (HDAC) (Grishok and Sharp, 2005; Cui et al., 2006), but *ky957* is not suppressed by *mes-4* or *mrg-1* RNAi, although neurons are often refractory to RNAi. *ky957* is also not suppressed by the HDAC inhibitors n-butyrate and Trichostatin A. Importantly, studies of the effector mechanism of RNAi-TGS were performed on transgenes expressed in non-neuronal tissues, and it is possible, given the different RNAi activity observed in

neurons, that *tam-1*-dependent silencing in neurons involves a different but unknown mechanism.

Exogenous ASH-to-AVA GRASP transgenes and three distinct genomic DNA fragments from Chromosomes IV and V were able to suppress the *ky957* mutant phenotype in *kyIs501*. In the former case, the DNA sequence of the GRASP transgene alone appears sufficient to suppress *ky957*. The role of DNA sequence in suppression by the genomic DNA from Chromosomes IV and V could be tested with arrays carrying null mutations in the genes such as *clp-6* that are located in these genomic DNA fragments. BLAST alignment did not identify any large regions of DNA sequence homology in these genomic regions, but motif identification software may identify short sequences enriched in those areas that could be used to identify binding proteins and the mechanism by which these arrays suppress *ky957*.

Summary

Neuroscientists have marveled at the intricate and exquisitely precise architecture of neural circuits for over a century. Our understanding of how these circuits form and function is incomplete; moreover, the connectivities of many circuits remain elusive. A significant hurdle in the study of these circuits has been the scarcity of methods to allow rapid and fine-scale mapping of circuits. This thesis describes the GRASP method, a genetic tool that enables visualization of specific synapses in the central nervous systems of live animals. GRASP is able to detect altered connectivity in *C. elegans*, and has proven useful in circuit mapping in other nervous systems (Gordon and Scott, 2009).

GRASP and related applications should enable insights into fundamental questions in many areas of neuroscience.

Chapter 5

Methods

Strains

Nematodes were cultured according to standard techniques at 20-25°C (Brenner et al., 1974). The following mutations were used: LGI, *unc-40(e271)*, *unc-37(e262), unc-13(e450));* LGII, *unc-104(e1265),syd-1(ju82), unc-4(e120);* LGV, *unc-42(e270), him-5(e1490);* LGX*, sax-3(ky123), unc-6(ev400), syg-1(ky652), syd-1(ju37), sad-1(ky289), syg-2(ky671).* Transgenes were *kyEx1833[myo-3::nls::CFP::lacZ (10 ng/µl), myo-3::CD4-1::spGFP1-10 (50 ng/µl), myo-3::CD4-2::spGFP1-10 (50 ng/µl)]; kyEx1834[myo-3::mCherry (10 ng/µl), myo-3::GFP11::CD4-1 (50 ng/µl), myo-3::CD4-2::spGFP11 (50 ng/µl)]; kyEx1904[ace-4::mCherry (10 ng/µl), ace-4::CD4-1::spGFP11 (50 ng/µl), ace-4::CD4-2::spGFP11 (50 ng/µl), odr-1::DsRed2 (20 ng/µl)]; kyEx1905[him-4::nls::CFP::lacZ (50 ng/µl), him-4::CD4-1::spGFP1-10 (25 ng/µl), him-4:CD4-2::spGFP1-10 (25 ng/µl), rol-6 (100 ng/µl)]; kyEx1731[rig-3::PTP-3A::spGFP11 (10 ng/µl), rol-6 (100 ng/µl)] kyEx1718[unc-4::CD4-2::spGFP1-10 (50 ng/µl), unc-4::mCherry (5 ng/µl), odr-1::dsRed (15 ng/µl)]; kyEx1710[rig-3::CD4-2::spGFP11 (50 ng/µl), rol-6 (100 ng/µl)]; kyEx1935[unc-4::CD4-2::spGFP1-10 (50 ng/µl), odr-1::dsRed2 (20 ng/µl)]; kyEx1939[myo-3::CD4-2::spGFP1-10 (50 ng/µl), odr-1::dsRed2 (20 ng/µl)];*

kyEx1941[myo-3::CD4-2::GFP1-10 (50 ng/µl), odr-1::dsRed2 (20 ng/µl)]; kyEx2003[tph-1::SL2::PTP-3A::spGFP11 (50 ng/µl), tph-1::SL2::mCherry (5 ng/µl), flp-17::mCherry (2 ng/µl)]; kyEx2004[tph-1::SL2::PTP-3A::spGFP11 (50 ng/µl), tph-1::SL2::mCherry (5 ng/µl), flp-17::mCherry (2 ng/µl)]; kyEx2005[tph-1::SL2::PTP-3A::spGFP11 (50 ng/µl), tph-1::SL2::mCherry (5 ng/µl), flp-17::mCherry (2 ng/µl)]. wyEx1346[mig-13::nlg-1::YFP (5 ng/µl), odr-1::DsRed2 (50 ng/µl)], wyEx1957[mig-13::nlg-1::YFP (5 ng/µl), mig-13::mCherry::rab-3 (5 ng/µl), odr-1::DsRed2 (50 ng/µl)], wyEx1345[opt-3::nlg-1::YFP (20ng/µl), odr-1::DsRed2 (5 ng/µl)], wyEx1955-1956[unc-86::nlg-1::YFP (1ng/µl), unc-86::mCherry:rab-3(0.5 ng/µl), odr-1::DsRed2(50 ng/µl)], wyEx1915[unc-4::nlg-1::YFP (25 ng/µl), unc-4::mCherry (5 ng/µl), odr-1::DsRed2 (50 ng/µl)], wyEx1973[flp-18::mCherry (5 ng/µl), unc-122::GFP (20 ng/µl)], wyEx1334-1344[flp-18::nlg-1::spGFP11 (30ng/µl), odr-1::DsRed2 (50 ng/µl)], wyEx1968-1972[unc-4::nlg-1::spGFP1-10 (20ng/µl), odr-1::DsRed2 (50 ng/µl)], wyEx1845[unc-4::nlg-1::spGFP1-10 (20ng/µl), flp-18::nlg-1::spGFP11 (30 ng/µl), unc-4::mCherry (5 ng/µl), odr-1::DsRed2 (50 ng/µl)], wyEx1914[unc-4::nlg-1::spGFP1-10 (20 ng/µl), flp-18::nlg-1::spGFP11 (30ng/µl), flp-18::mCherry::rab-3 (10 ng/µl), odr-1::DsRed2 (50 ng/µl)], wyEx1733[ttx-3::nlg-1::spGFP1-10 (80 ng/µl), glr-3::nlg-1::spGFP11 (40 ng/µl), unc-122::DsRed2 (20 ng/µl)], wyEx1503[gcy-8::nlg-1::spGFP11 (10 ng/µl), ttx-3::nlg-1::spGFP1-10 (60 ng/µl), unc-122::DsRed2 (20 ng/µl)], kyIs491[sra-6::ptp-3a::spGFP11 (6 ng/µl), flp-18::nlg-1::spGFP1-10 (15 ng/µl), sra-6::mCherry::rab-3 (1ng/µl), pSM (40 ng/µl), ofm-1::DsRed2 (7 ng/µl)], kyIs501[sra-6::ptp-3a::spGFP11 (6 ng/µl), flp-18::nlg-1::spGFP1-10 (15 ng/µl), sra-6::mCherry::rab-3 (1ng/µl), pSM (40 ng/µl), ofm-1::DsRed2 (7 ng/µl)], kyEx3587 [sra-

6::ptp-3a::spGFP11 (6 ng/µl), flp-18::nlg-1::spGFP1-10 (15 ng/µl), flp-18::mCherry (1ng/µl), pSM (40 ng/µl), elt-2::mCherry (7 ng/µl)], kyEx3587 [sra-6::stop::ptp-3a::spGFP11 (6 ng/µl), flp-18::stop::nlg-1::spGFP1-10 (15 ng/µl), flp-18::mCherry (1ng/µl), pSM (40 ng/µl), elt-2::mCherry (7 ng/µl)], .

Cell Culture

Primary cell culture of embryonic *C. elegans* muscles and neurons was performed essentially as described (Christensen et al., 2002). Briefly, gravid hermaphrodites were lysed with 0.5M NaOH and 0.5% NaOCl to release embryos, which were digested with ~2 U/mL *Serratia marcescens* chitinase (Sigma, St. Louis, MO) to dissolve the eggshell. Cells were separated by trituration and passed through a 5 µm Durapore syringe filter (Millipore, Bedford MA). The cell preparation was rocked overnight in microcentrifuge tubes at room temperature to allow differentiation and aggregation. The next day, cells were transferred to poly-L-lysine-coated glass slides (Polysciences, Warrington, PA) and allowed to adhere for at least one hour in humidified chambers before coverslips were added and sealed with clear nail polish.

Molecular biology

Split GFP fragments

For CD4 GRASP and PTP-3A:CD4 GRASP, *spGFP1-10* cDNA was synthesized from published sequences (Cabantous et al, 2005), using cDNA codons optimized for *C. elegans* (BioBasic, Toronto, Canada). *spGFP11* was generated from complementary oligonucleotides with the sequences 5'-

GCTAGCCGTGACCACATGGTCCTTCATGAGTATGTAAATGCTGCTGGGATTAC AGGTGGCGGCGGAAGTGGAGGTGGAGGCTCGGTCGAC-3' and 5'-GTCGACCGAGCCTCCACCTCCACTTCCGCCGCCACCTGTAATCCCAGCAGCAT TTACATACTCATGAAGGACCATGTGGTCACGGCTAGC-3'. For NLG-1 GRASP, fragments of spGFP1-10 and spGFP11 were kind gifts of L. Looger.

To ensure that this split GFP would function properly in *C. elegans,* which is cultivated at a lower temperature than mammalian cells or bacterial cells, spGFP1-10 and spGFP11 were coexpressed under the muscle cell-specific *myo-3* promoter in transgenic strains. Strong fluorescence was observed within the cytoplasm of muscle cells expressing both fragments, but no detectable GFP fluorescence was observed when either spGFP1-10 or spGFP11 was expressed on its own (data not shown).

CD4 carriers

CD4 cDNA was a gift from P. Dhadialla. *CD4-1* and *CD4-2* were amplified with the oligonucleotides 5'-ATCATCGTCGACAGAGCCACTCAGCTCCAG-3' and 5'-ATCATCGTCGACTTCCAGAAGGCCTCCAGC-3', respectively, with the common reverse oligonucleotide 5'-ACTCACGATATCCTAGCGCCTTCGGTGCCGGCACCT-3'. These fragments were inserted into the SalI-EcoRV sites of pSM-PAT-3, a variant of the *C. elegans* expression vector pSM containing a 5' signal sequence. To generate this plasmid, the PAT-3 signal sequence and signal peptide cleavage signal from pPD122.39 were amplified with oligonucleotides 5'-TCGTATGTTGTGTGGAATTGTGAGCGGATA-3' and 5'-TATAGCTAGCAGTGACTTCTCCAGTCTTCC-3' and ligated as an XmaI/NheI fragment into the XmaI-NheI sites of pSM, with the signal peptide peptide cleavage site

immediately followed by an in-frame NheI site. *CD4-1::spGFP1-10, CD4-2::spGFP1-10, CD4-1::spGFP(11), and CD4-2::spGFP11* were generated by cloning *spGFP1-10* and *spGFP11* sequences into the NheI-SalI sites of pSM-PAT-3::CD4-1and pSM-PAT-3::CD4-2.

For experiments in neurons, CD4 transgene expression was increased by codon-optimizing the CD4 sequence for *C. elegans* and adding synthetic intron sequences. A *CD4-2::spGFP11* construct was synthesized from ~50-mer oligonucleotides according to the GeneDesign protocol (Richardson et al., 2006) with the substitution of PfuTurbo polymerase (Stratagene, La Jolla, CA) for ExTaq polymerase. Two ~500 bp products were fused by overlap-extension PCR, cloned into TopoBlunt (Invitrogen, Carlsbad, CA), and recloned into pSM-PAT-3. Introns were introduced into the *spGFP1-10* cDNA by overlap extension PCR, and this product fused to codon-optimized *CD4-2* by another round of overlap extension PCR.

PTP-3A carriers

An Asp718/AvrII fragment containing the *ptp-3a* minigene and 3' untranslated region (a kind gift of B. Ackley and Y. Jin) were cloned into the Asp718 and SpeI sites of pSM. An AscI-SpeI fragment containing the *pat-3* signal sequence, *spGFP11*, a glycine-serine linker, and a short 5' segment of the *ptp-3a* minigene was cloned into the AscI and SpeI sites of this vector to generate the *pat-3* signal sequence*::spGFP11::ptp-3a* chimeric minigene. This construct was subsequently modified to remove intron sequences that could modify transgene expression using quickchange to generate ptp-3aΔI.

NLG-1 carriers

An *nlg-1::GFP* construct was generated by M. VanHoven and K. Shen (Stanford) in two steps. First, the *GFP* in pSM-GFP was replaced with a fragment generated by amplifying the *nlg-1* signal sequence predicted by SMART and *GFP,* using a 5' primer adding an NheI site and a 3' primer adding an EcoRI site. The remainder of *nlg-1* cDNA was amplified with primers adding 5' EcoRI and SacI sites and a 3' EcoRI site and subcloned into the EcoRI site. *nlg-1::spGFP1-10* and *nlg-1::spGFP11* were generated by replacing the NheI-SacI fragment in *nlg-1::GFP* with a fragment generated by amplifying *spGFP1-10* or spGFP11 using primers that added 5' NheI and 3' SacI sites.

Promoters for GRASP:

Most promoters were cloned into pSM vectors using standard methods. To generate *flp-18::nlg-1::spGFP1-10, unc-4::nlg-1::spGFP1-10, ttx-3::nlg-1::spGFP1-10, glr-3::nlg-1::spGFP11,* and *gcy-8::nlg-1::spGFP11* SphI-SmaI fragment containing the *flp-18, ttx-3,* or *gcy-8* promoter, or SphI-AscI fragments containing the *unc-4* or *glr-3*(a gift of M. Margeta) promoter were subcloned into the multiple cloning site in *nlg-1::spGFP1-10* or *nlg-1::spGFP11*.

To create a *tph-1* promoter expressed in HSN, ~3kb of *tph-1* promoter and the first four exons and three introns of the *tph-1* gene were amplified from N2 genomic DNA, a stop codon was introduced by PCR, and this fragment was fused to an SL2 sequence by overlap-extension PCR. This plasmid creates a bicistronic mRNA in which the SL2 element initiates an inserted RNA of interest (Coates and de Bono 2002).

nlg-1::YFP

cDNAs in attL-containing pDONR201 vector (OpenBiosystems, Huntsville, AL) encoding NLG-1 (C40C9.5) were recombined (K. Shen) into the C-terminal YFP pSM Gateway Destination vector with LR Clonase (Invitrogen, Carlsbad, CA) containing the *mig-13* promoter (Klassen et al., 2007), *opt-3* promoter, or *unc-86* promoter (Patel et al., 2006). The *unc-4::nlg-1::YFP* plasmid was created by replacing an SphI-AscI fragment containing the *opt-3* promoter in *opt-3::nlg-1::YFP* with an *unc-4* promoter fragment from *unc-4::mCherry* (a gift from V. Poon).

***mCherry::rab-3, mCherry,* and nuclear *CFP* clones**

mig-13::mCherry::rab-3 (Klassen et al., 2007) and *unc-86::mCherry::rab-3* (Patel et al., 2006) were previously described. To generate the *flp-18::mCherry::rab-3* construct, the *flp-18* promoter (Rogers et al., 2003) was amplified from N2 genomic DNA, adding 5' SphI and 3' SmaI sites, and subcloned into the SphI-SmaI fragment from *ttx-3::mCherry::rab-3* (a gift from D. Colón-Ramos), replacing the *ttx-3* promoter. The *flp-18::mCherry* construct was made by replacing the *ttx-3* promoter in *ttx-3::mCherry* (a gift from D. Colón-Ramos) with the *flp-18* promoter. Other mCherry constructs were generated by introducing promoters into pSM-mCherry (a gift of N. Pokala).

Nuclear CFP plasmids were generated from pPD133.45, a plasmid containing *myo-3::nls::CFP::LacZ*. The *ttx-3* promoter was introduced into this plasmid as a HindIII/XbaI fragment, replacing the *myo-3* promoter, to create a nuclear CFP vector suitable for FseI-AscI promoter fragments.

Non-coding GRASP transgenes

Non-coding GRASP transgenes were made by inserting a single A immediately 5' to the NheI site after the *pat-3* signal sequence in *sra-6::ptp-3a::spGFP11* and *flp-18::nlg-1::spGFP1-10*. These mutations create a stop codon and place the GRASP carriers out of frame with the signal sequence.

Cre-Lox transgenes

A NcoI-SacI fragment containing nCre (gift of R. Axel) was introduced into the NcoI and SacI sites of pSM to generate pSM-nCre.

To generate pSM loxP, a ~3.5 kb LacZ cDNA fragment from pJM67 was amplified with oligonucleotides 5'-TACCGTTCGTATAGCATACATTATACGAAGTTATATGGTCGTTTTACAACGTCGTG-3' and 5'-AGTAGTGGATCCTATTATTTTTGACACCAGAC-3' and 5'-GAGAGAGCTAGCTACCGTTCGTATAGCATACATTATACG-3'. The stop sequence was amplified using oligonucleotides 5'-GCGCAGAGATCTAATAAAGAATAAAGAATAAATTT-3' and 5'-GAGAGAGCTAGCTACCGTTCGTATAATGTATGCTAT-3' from template oligonucleotides with the sequence 5'-GATCTAATAAAGAATAAAGAATAAATTTTTTTTGAAACATGAAACATAACTTCGTATAGCATACATTATACGAAGTTATA-3' and 5'-

CCGGTATAACTTCGTATAATGTATGCTATACGAAGTTATGTTTCATGTTTCAA AAAAAATTTATTCTTTATTCTTTATTA-3' . The LacZ and stop fragments were digested with BglII, ligated with T4 DNA ligase, and used as template for PCR with oligonucleotides 5'-GAGAGAGCTAGCGATAACTTCGTATAGCATACAT-3' and 5'-GAGAGAGCTAGCGATAACTTCGTATAATGTATGC-3'. The resulting PCR product was digested with NheI and ligated into the NheI site of pSM-GFP.

Germline transformation and analysis of transgenes

Transgenic strains were generated as previously described (Mello and Fire, 1995). Transgenic arrays were generated in either N2 or *him-5* backgrounds.

In CD4::spGFP and PTP-3A::spGFP GRASP experiments, presynaptic transgenes and postsynaptic transgenes were injected separately, demonstrated not to generate GFP fluorescence individually, and then crossed to each other at the F3 generation or later. In some NLG-1::spGFP GRASP experiments, both transgenes were injected together, and mosaic analysis of transgenic animals was used to ensure that GFP was only observed when both pre-and post-synaptic cells carried the transgenes. These controls indicated that GFP signals were not artefactually caused by recombination between plasmids during generation of the transgenes.

Light microscopy

Animals were mounted on 2% or 4% agarose pads containing 0.01% tetramisole or 1 mM levamisole. Most images were collected with a 63x objective on a Zeiss Axioskop or Axioplan2 equipped with DIC and epifluorescence and a Hamamatsu C2400 CCD camera. Experiments in Chapter 3 were performed on a Zeiss AxioimagerZ.1 with a

Axiocam MRm camera and analyzed with Axiovision software. Images of HSN-to-VC and HSN-to-vulval muscle GRASP labeling were acquired on a DeltaVision Image Restoration Microscopy system on an Olympus IX-70 microscope with a 60x objective. For quantification, a sub-stack that included all synaptic puncta was thresholded to yield the best signal to noise ratio by an investigator blind to the animal's genotype. The total area of fluorescence of each region of the HSN axon was then quantified using ImageJ 1.37v. Images were processed in Metamorph and Adobe Photoshop.

Electron microscopy

Electron microscopy was performed by Richard Fetter (Janelia Farms Research Campus). An N2 L4 hermaphrodite was prepared for conventional transmission electron microscopy as described (Shen et al., 2004) by fixation in 0.8% glutaraldehyde, 0.8% osmium tetroxide in 0.1M Na-cacodylate buffer, pH 7.4, postfixation with 0.5% osmium tetroxide in 100 mM Na-cacodylate buffer at 4º C, and staining *en bloc* with 1% aqueous uranyl acetate prior to debydration and embedding in Eponate 12 resin. Serial 50 nm sections were cut with a Leica Ultracut T microtome, collected on Formvar coated slot grids and stained with uranyl acetate and Sato's lead, and photographed with a JEOL 1200 EX/II TEM operated at 80 kV.

Mutagenesis

kyIs501 was generated by psoralen/UV integration of synchronized L4 *kyEx2718*. EMS mutagenesis was performed according to standard procedures (Brenner, 1974). Several hundred mutagenized *kyIs501* P0 animals were placed at high density on seeded 6cm

Petri dishes to lay eggs. Animals exhausted available food before their progeny hatched, so that F1 progeny arrested L1s 24 hours later. F1 L1 progeny were collected, resuspended in freezing medium (Brenner, 1974), aliquoted in cryovials containing >100 animals each, and frozen at –80 degrees. For screening, 1-2 vials were thawed each day animals allowed to recover and grow. Two days later, 5 independent adult F1 animals were picked to each of 20-30 plates. L4 F2 progeny were screened 72 hours later.

Mapping

SNP mapping with CB4856 was performed according to standard procedures (Davis et al., 2005) SNP mapping of *ky957* with *kyIs501* was performed using validated SNPs identified in whole-genome sequencing. For identification of recombinants blind to *ky957* phenotype, F2 progeny of a *ky957 kyIs501* x *kyIs501* cross were plated singly and allowed to lay eggs for 48 hours. F2 animals were then removed and genotyped at EMS SNPs on chromosome V. The ASH-to-AVA GRASP phenotypes were scored in the F3 progeny of F2 animals with recombination breakpoints in the *ky957* interval.

Genomic complementation rescue

Olignucleotides were designed with Primer3 (http://frodo.wi.mit.edu) and used to amplify 12 kb PCR products from purified N2 genomic DNA with Expand DNTPack Long Template (Roche). PCR products were analyzed on 1% agarose gels stained with ethidium bromide to confirm amplification of the desired products. PCR products were purified with Zymospin columns (Zymo) and concentrations were determined with a Nanodrop 1000 spectrophotometer (Thermo Scientific). Fosmid clones (Geneservice)

were cultured and fosmids were induced with CopyControl (Epicentre) and prepared by Miniprep (Qiagen). Fosmids and PCR products were combined in pools spanning 50-60 kb with each 12 kb of DNA at 5-10 ng/µl, along with 1-3 ng/µl *elt-2::mCherry* coinjection marker and 40-50 ng/µl pSM as bulk DNA, and injected into *ky957 kyIs501* animals. For each pool, ASH-to-AVA GRASP labeling was scored in at least three generations in at least three and typically five or more independent lines.

Whole-genome sequencing

Genomic DNA was isolated from several thousand mixed-stage *ky957 kyIs501* animals and purified through 3 phenol-chloroform extractions followed by ethanol precipitation. Purified genomic DNA was then sheared and ligated to adapters to generate a paired-end library. Whole-genome sequencing was performed in the Rockefeller Genomics Resource center using Solexa-Illumina Genome Analyzer technology. Fastq sequences were aligned to the WormBase refersence sequence WS195 and single-base changes were predicted with the MAQ program (http://maq.sourceforge.net). Predicted mutations were validated by PCR and conventional sequencing in *ky957 kyIs501* and *kyIs501* DNA.

Identification of *kyIs501* integration site

Each of the single end Illumina reads was mapped to the WS195 version of the *C. elegans* genome using MAQ 0.7.1. To identify possible structural changes between *ky957* and the reference N2 genome within the rescuing interval, such as insertions, deletions, inversions, and translocations, we queried the set of reads that MAQ was

unable to align to the *C. elegans* reference genome for partial matches to the *ky957* genetic interval. Partial matches were defined as reads with unique exact matches of 18 or more nucleotides starting from the beginning or end of the read, which were then used as anchors to assemble the rest of the read. Partially matched reads were then aligned and regions with more than 3 partial matches were manually inspected. If the majority of the reads aligned outside of the anchor region, the consensus sequence was aligned to the *C. elegans* reference by BLAST. This inspection identified one region that matched the *ofm-1* promoter. Subsequent analyses revealed a smaller region that matched the *flp-18* promoter, suggesting that both ends of *kyIs501* have been determined.

Quantitative RT-PCR

Total RNA was extracted from ~1000 mixed-stage *kyIs501* and *ky957 kyIs501* on two successive days using Trizol (Invitrogen). RNA was reverse transcribed with iScript (BioRad). Oligonucleotides predicted to amplify 70-120 bp sequences from spliced mRNA were designed for *Y51A2B.5*, *Y51A2B*.6, *Y51A2B*.9 with Primer3 (http://frodo.wi.mit.edu). Reactions were prepared with Fast SYBR Green kit (Applied Biosystems) and prepared in 96-well plates and analyzed on a LightCycler 480 System (Roche). Specificity of each oligonucleotide pair was determined with dilution series and dissociation curves. Expression of each gene relative to *act-3* controls was calculated with SDS2.3 and RQManager1.2 software (Applied Biosystems).

RNAi

Oligonucleotides corresponding to several hundred bases of exon sequence of *unc-22*,

mes-4, and *mrg-1* were designed with primer3 (http://frodo.wi.mit.edu) and the T7 polymerase promoter sequence (TAATACGACTCACTATAGGG) was placed at the 5' end of each oligonucleotide. These olignucleotides were used to amplify transcription templates from N2 genomic DNA and were purified with Zymospin columns (Zymo) and quantified with a Nanodrop 1000 (Thermo Scientific) spectrophotometer. Approximately 1 μg of template DNA was used as template for the T7 RiboMAX Express RNAi System (Promega). dsRNA was annealed by heating to 75 degrees and slow cooling to room temperature. dsRNA concentration was determined and each dsRNA was diluted to 1μg/μl. Gonads of *ky957 kyIs501* hermaphrodites were injected with each dsRNA and progeny of injected animals were scored for ASH-to-AVA GRASP phenotypes 72 hours later.

HDAC inhibitors

HDAC inhibitor experiments were performed as described (Grishok and Sharp, 2005). N-butyrate and Trichostatin A (TSA) (Sigma-Aldrich) were diluted in DMSO and added to *E. coli* OP50 food that was used to seed growth plates. 24-48 hours later, adult *ky957 kyIs501* and *kyIs501* animals were picked to plates containing n-butyrate, TSA, or DMSO. ASH-to-AVA GRASP labeling was scored in L4 progeny 72 hours later.

References

Abremski, K., and Hoess, R. (1984). Bacteriophage P1 site-specific recombination. Purification and properties of the Cre recombinase protein. J Biol Chem *259*, 1509-1514.

Ackley, B. D., Harrington, R. J., Hudson, M. L., Williams, L., Kenyon, C. J., Chisholm, A. D., and Jin, Y. (2005). The two isoforms of the Caenorhabditis elegans leukocyte-common antigen related receptor tyrosine phosphatase PTP-3 function independently in axon guidance and synapse formation. J Neurosci *25*, 7517-7528.

Ahmari, S. E., and Smith, S. J. (2002). Knowing a nascent synapse when you see it. Neuron *34*, 333-336.

Allen, M. J., Godenschwege, T. A., Tanouye, M. A., and Phelan, P. (2006). Making an escape: development and function of the Drosophila giant fibre system. Semin Cell Dev Biol *17*, 31-41.

Andrews, G. L., Tanglao, S., Farmer, W. T., Morin, S., Brotman, S., Berberoglu, M. A., Price, H., Fernandez, G. C., Mastick, G. S., Charron, F., and Kidd, T. (2008). Dscam guides embryonic axons by Netrin-dependent and -independent functions. Development *135*, 3839-3848.

Ango, F., di Cristo, G., Higashiyama, H., Bennett, V., Wu, P., and Huang, Z. J. (2004). Ankyrin-based subcellular gradient of neurofascin, an immunoglobulin family protein, directs GABAergic innervation at purkinje axon initial segment. Cell *119*, 257-272.

Arakawa, H., Lodygin, D., and Buerstedde, J. M. (2001). Mutant loxP vectors for selectable marker recycle and conditional knock-outs. BMC Biotechnol *1*, 7.

Arber, S., Ladle, D. R., Lin, J. H., Frank, E., and Jessell, T. M. (2000). ETS gene Er81 controls the formation of functional connections between group Ia sensory afferents and motor neurons. Cell *101*, 485-498.

Armstrong, J. D., Kaiser, K., Muller, A., Fischbach, K. F., Merchant, N., and Strausfeld, N. J. (1995). Flybrain, an on-line atlas and database of the Drosophila nervous system. Neuron *15*, 17-20.

Baran, R., Aronoff, R., and Garriga, G. (1999). The C. elegans homeodomain gene unc-42 regulates chemosensory and glutamate receptor expression. Development *126*, 2241-2251.

Barnea, G., Strapps, W., Herrada, G., Berman, Y., Ong, J., Kloss, B., Axel, R., and Lee, K. J.

(2008). The genetic design of signaling cascades to record receptor activation. Proc Natl Acad Sci U S A *105*, 64-69.

Betley, J. N., Wright, C. V., Kawaguchi, Y., Erdelyi, F., Szabo, G., Jessell, T. M., and Kaltschmidt, J. A. (2009). Stringent specificity in the construction of a GABAergic presynaptic inhibitory circuit. Cell *139*, 161-174.

Biederer, T., Sara, Y., Mozhayeva, M., Atasoy, D., Liu, X., Kavalali, E. T., and Sudhof, T. C. (2002). SynCAM, a synaptic adhesion molecule that drives synapse assembly. Science *297*, 1525-1531.

Binzegger, T., Douglas, R. J., and Martin, K. A. (2004). A quantitative map of the circuit of cat primary visual cortex. J Neurosci *24*, 8441-8453.

Briggman, K. L., and Denk, W. (2006). Towards neural circuit reconstruction with volume electron microscopy techniques. Curr Opin Neurobiol *16*, 562-570.

Brockie, P. J., Madsen, D. M., Zheng, Y., Mellem, J., and Maricq, A. V. (2001). Differential expression of glutamate receptor subunits in the nervous system of Caenorhabditis elegans and their regulation by the homeodomain protein UNC-42. J Neurosci *21*, 1510-1522.

Cabantous, S., Terwilliger, T. C., and Waldo, G. S. (2005). Protein tagging and detection with engineered self-assembling fragments of green fluorescent protein. Nat Biotechnol *23*, 102-107.

Cabot, J. B., Mennone, A., Bogan, N., Carroll, J., Evinger, C., and Erichsen, J. T. (1991). Retrograde, trans-synaptic and transneuronal transport of fragment C of tetanus toxin by sympathetic preganglionic neurons. Neuroscience *40*, 805-823.

Card, J. P., Rinaman, L., Schwaber, J. S., Miselis, R. R., Whealy, M. E., Robbins, A. K., and Enquist, L. W. (1990). Neurotropic properties of pseudorabies virus: uptake and transneuronal passage in the rat central nervous system. J Neurosci *10*, 1974-1994.

Carvelli, L., McDonald, P. W., Blakely, R. D., and Defelice, L. J. (2004). Dopamine transporters depolarize neurons by a channel mechanism. Proc Natl Acad Sci U S A *101*, 16046-16051.

Chan, S. S., Zheng, H., Su, M. W., Wilk, R., Killeen, M. T., Hedgecock, E. M., and Culotti, J. G. (1996). UNC-40, a C. elegans homolog of DCC (Deleted in Colorectal Cancer), is required in motile cells responding to UNC-6 netrin cues. Cell *87*, 187-195.

Christensen, M., Estevez, A., Yin, X., Fox, R., Morrison, R., McDonnell, M., Gleason, C., Miller, D. M., 3rd, and Strange, K. (2002). A primary culture system for functional analysis of C. elegans neurons and muscle cells. Neuron *33*, 503-514.

Christopherson, K. S., Ullian, E. M., Stokes, C. C., Mullowney, C. E., Hell, J. W., Agah, A., Lawler, J., Mosher, D. F., Bornstein, P., and Barres, B. A. (2005). Thrombospondins are astrocyte-secreted proteins that promote CNS synaptogenesis. Cell *120*, 421-433.

Clandinin, T. R., and Zipursky, S. L. (2000). Afferent growth cone interactions control synaptic specificity in the Drosophila visual system. Neuron *28*, 427-436.

Colon-Ramos, D. A., Margeta, M. A., and Shen, K. (2007). Glia promote local synaptogenesis through UNC-6 (netrin) signaling in C. elegans. Science *318*, 103-106.

Combes, D., Fedon, Y., Toutant, J. P., and Arpagaus, M. (2003). Multiple ace genes encoding acetylcholinesterases of Caenorhabditis elegans have distinct tissue expression. Eur J Neurosci *18*, 497-512.

Couteau, F., Guerry, F., Muller, F., and Palladino, F. (2002). A heterochromatin protein 1 homologue in Caenorhabditis elegans acts in germline and vulval development. EMBO Rep *3*, 235-241.

Craig, A. M., and Kang, Y. (2007). Neurexin-neuroligin signaling in synapse development. Curr Opin Neurobiol *17*, 43-52.

Crane, M. M., Chung, K., and Lu, H. (2009). Computer-enhanced high-throughput genetic screens of C. elegans in a microfluidic system. Lab Chip *9*, 38-40.

Crump, J. G., Zhen, M., Jin, Y., and Bargmann, C. I. (2001). The SAD-1 kinase regulates presynaptic vesicle clustering and axon termination. Neuron *29*, 115-129.

Cui, M., Kim, E. B., and Han, M. (2006). Diverse chromatin remodeling genes antagonize the Rb-involved SynMuv pathways in C. elegans. PLoS Genet *2*, e74.

Dalva, M. B., Takasu, M. A., Lin, M. Z., Shamah, S. M., Hu, L., Gale, N. W., and Greenberg, M. E. (2000). EphB receptors interact with NMDA receptors and regulate excitatory synapse formation. Cell *103*, 945-956.

Dalva, M. B., and Katz, L. C. (1994). Rearrangements of synaptic connections in visual cortex revealed by laser photostimulation. Science *265*, 255-258.

Dasen, J. S., Tice, B. C., Brenner-Morton, S., and Jessell, T. M. (2005). A Hox regulatory network establishes motor neuron pool identity and target-muscle connectivity. Cell *123*, 477-491.

Davis, M. W., Morton, J. J., Carroll, D., and Jorgensen, E. M. (2008). Gene activation using FLP recombinase in C. elegans. PLoS Genet *4*, e1000028.

Davis, M. W., Hammarlund, M., Harrach, T., Hullett, P., Olsen, S., and Jorgensen, E. M. (2005). Rapid single nucleotide polymorphism mapping in C. elegans. BMC Genomics *6*, 118.

Del Rio, J. A., Heimrich, B., Borrell, V., Forster, E., Drakew, A., Alcantara, S., Nakajima, K., Miyata, T., Ogawa, M., Mikoshiba, K.*, et al.* (1997). A role for Cajal-Retzius cells and reelin in

the development of hippocampal connections. Nature *385*, 70-74.

Ding, M., Chao, D., Wang, G., and Shen, K. (2007). Spatial regulation of an E3 ubiquitin ligase directs selective synapse elimination. Science *317*, 947-951.

Dul, J. L., Aviel, S., Melnick, J., and Argon, Y. (1996). Ig light chains are secreted predominantly as monomers. J Immunol *157*, 2969-2975.

Dunah, A. W., Hueske, E., Wyszynski, M., Hoogenraad, C. C., Jaworski, J., Pak, D. T., Simonetta, A., Liu, G., and Sheng, M. (2005). LAR receptor protein tyrosine phosphatases in the development and maintenance of excitatory synapses. Nat Neurosci *8*, 458-467.

Durbin, R.M. Ph.D. thesis, University of Cambridge, 1987.

Feinberg, E. H., Vanhoven, M. K., Bendesky, A., Wang, G., Fetter, R. D., Shen, K., and Bargmann, C. I. (2008). GFP Reconstitution Across Synaptic Partners (GRASP) defines cell contacts and synapses in living nervous systems. Neuron *57*, 353-363.

Frokjaer-Jensen, C., Davis, M. W., Hopkins, C. E., Newman, B. J., Thummel, J. M., Olesen, S. P., Grunnet, M., and Jorgensen, E. M. (2008). Single-copy insertion of transgenes in Caenorhabditis elegans. Nat Genet *40*, 1375-1383.

Fuerst, P. G., Bruce, F., Tian, M., Wei, W., Elstrott, J., Feller, M. B., Erskine, L., Singer, J. H., and Burgess, R. W. (2009). DSCAM and DSCAML1 function in self-avoidance in multiple cell types in the developing mouse retina. Neuron *64*, 484-497.

Fuerst, P. G., Koizumi, A., Masland, R. H., and Burgess, R. W. (2008). Neurite arborization and mosaic spacing in the mouse retina require DSCAM. Nature *451*, 470-474.

Ghosh, A., Antonini, A., McConnell, S. K., and Shatz, C. J. (1990). Requirement for subplate neurons in the formation of thalamocortical connections. Nature *347*, 179-181.

Ghosh, I., Hamilton, A.D., and Regan, L. (2000) Antiparallel leucine zipper-directed protein reassembly: application to the green fluorescent protein. J. Am. Chem. Soc. *122*, 5658–5659.

Godenschwege, T. A., Hu, H., Shan-Crofts, X., Goodman, C. S., and Murphey, R. K. (2002). Bi-directional signaling by Semaphorin 1a during central synapse formation in Drosophila. Nat Neurosci *5*, 1294-1301.

Gonzalez, D., van der Burg, M., Garcia-Sanz, R., Fenton, J. A., Langerak, A. W., Gonzalez, M., van Dongen, J. J., San Miguel, J. F., and Morgan, G. J. (2007). Immunoglobulin gene rearrangements and the pathogenesis of multiple myeloma. Blood *110*, 3112-3121.

Gordon, M. D., and Scott, K. (2009). Motor control in a Drosophila taste circuit. Neuron *61*, 373-384.

Graf, E. R., Zhang, X., Jin, S. X., Linhoff, M. W., and Craig, A. M. (2004). Neurexins induce differentiation of GABA and glutamate postsynaptic specializations via neuroligins. Cell *119*, 1013-1026.

Grewal, S. I., Bonaduce, M. J., and Klar, A. J. (1998). Histone deacetylase homologs regulate epigenetic inheritance of transcriptional silencing and chromosome segregation in fission yeast. Genetics *150*, 563-576.

Grishok, A., Sinskey, J. L., and Sharp, P. A. (2005). Transcriptional silencing of a transgene by RNAi in the soma of C. elegans. Genes Dev *19*, 683-696.

Gu, H., Marth, J. D., Orban, P. C., Mossmann, H., and Rajewsky, K. (1994). Deletion of a DNA polymerase beta gene segment in T cells using cell type-specific gene targeting. Science *265*, 103-106.

Hall, A. C., Lucas, F. R., and Salinas, P. C. (2000). Axonal remodeling and synaptic differentiation in the cerebellum is regulated by WNT-7a signaling. Cell *100*, 525-535.

Hall, I. M., Shankaranarayana, G. D., Noma, K., Ayoub, N., Cohen, A., and Grewal, S. I. (2002). Establishment and maintenance of a heterochromatin domain. Science *297*, 2232-2237.

Hallam, S. J., Goncharov, A., McEwen, J., Baran, R., and Jin, Y. (2002). SYD-1, a presynaptic protein with PDZ, C2 and rhoGAP-like domains, specifies axon identity in C. elegans. Nat Neurosci *5*, 1137-1146.

Hamelin, M., Zhou, Y., Su, M. W., Scott, I. M., and Culotti, J. G. (1993). Expression of the UNC-5 guidance receptor in the touch neurons of C. elegans steers their axons dorsally. Nature *364*, 327-330.

Hammarlund, M., Watanabe, S., Schuske, K., and Jorgensen, E. M. (2008). CAPS and syntaxin dock dense core vesicles to the plasma membrane in neurons. J Cell Biol *180*, 483-491.

Hammarlund, M., Davis, M. W., Nguyen, H., Dayton, D., and Jorgensen, E. M. (2005). Heterozygous insertions alter crossover distribution but allow crossover interference in Caenorhabditis elegans. Genetics *171*, 1047-1056.

Harris, W. A. (1980). The effects of eliminating impulse activity on the development of the retinotectal projection in salamanders. J Comp Neurol *194*, 303-317.

Hata, Y., Butz, S., and Sudhof, T. C. (1996). CASK: a novel dlg/PSD95 homolog with an N-terminal calmodulin-dependent protein kinase domain identified by interaction with neurexins. J Neurosci *16*, 2488-2494.

Hedgecock, E. M., Culotti, J. G., and Hall, D. H. (1990). The unc-5, unc-6, and unc-40 genes guide circumferential migrations of pioneer axons and mesodermal cells on the epidermis in C. elegans. Neuron *4*, 61-85.

Herman, R. K., Albertson, D. G., and Brenner, S. (1976). Chromosome rearrangements in Caenorhabditis elegans. Genetics *83*, 91-105.

Hiesinger, P. R., Zhai, R. G., Zhou, Y., Koh, T. W., Mehta, S. Q., Schulze, K. L., Cao, Y., Verstreken, P., Clandinin, T. R., Fischbach, K. F.*, et al.* (2006). Activity-independent prespecification of synaptic partners in the visual map of Drosophila. Curr Biol *16*, 1835-1843.

Hilliard, M. A., and Bargmann, C. I. (2006). Wnt signals and frizzled activity orient anterior-posterior axon outgrowth in C. elegans. Dev Cell *10*, 379-390.

Hortsch, M., Nagaraj, K., and Godenschwege, T. A. (2009). The interaction between L1-type proteins and ankyrins--a master switch for L1-type CAM function. Cell Mol Biol Lett *14*, 57-69.

Hsieh, J., Liu, J., Kostas, S. A., Chang, C., Sternberg, P. W., and Fire, A. (1999). The RING finger/B-box factor TAM-1 and a retinoblastoma-like protein LIN-35 modulate context-dependent gene silencing in Caenorhabditis elegans. Genes Dev *13*, 2958-2970.

Hu, C. D., and Kerppola, T. K. (2003). Simultaneous visualization of multiple protein interactions in living cells using multicolor fluorescence complementation analysis. Nat Biotechnol *21*, 539-545.

Huberman, A. D., Wei, W., Elstrott, J., Stafford, B. K., Feller, M. B., and Barres, B. A. (2009). Genetic identification of an On-Off direction-selective retinal ganglion cell subtype reveals a layer-specific subcortical map of posterior motion. Neuron *62*, 327-334.

Ichtchenko, K., Hata, Y., Nguyen, T., Ullrich, B., Missler, M., Moomaw, C., and Sudhof, T. C. (1995). Neuroligin 1: a splice site-specific ligand for beta-neurexins. Cell *81*, 435-443.

Imai, T., Yamazaki, T., Kobayakawa, R., Kobayakawa, K., Abe, T., Suzuki, M., and Sakano, H. (2009). Pre-target axon sorting establishes the neural map topography. Science *325*, 585-590.

Inaki, M., Yoshikawa, S., Thomas, J. B., Aburatani, H., and Nose, A. (2007). Wnt4 is a local repulsive cue that determines synaptic target specificity. Curr Biol *17*, 1574-1579.

Irie, M., Hata, Y., Takeuchi, M., Ichtchenko, K., Toyoda, A., Hirao, K., Takai, Y., Rosahl, T. W., and Sudhof, T. C. (1997). Binding of neuroligins to PSD-95. Science *277*, 1511-1515.

Jacobson, K., Derzko, Z., Wu, E. S., Hou, Y., and Poste, G. (1976). Measurement of the lateral mobility of cell surface components in single, living cells by fluorescence recovery after photobleaching. J Supramol Struct *5*, 565(417)-576(428).

Jorgensen, E. M., and Mango, S. E. (2002). The art and design of genetic screens: caenorhabditis elegans. Nat Rev Genet *3*, 356-369.

Kahn-Kirby, A. H., Dantzker, J. L., Apicella, A. J., Schafer, W. R., Browse, J., Bargmann, C. I.,

and Watts, J. L. (2004). Specific polyunsaturated fatty acids drive TRPV-dependent sensory signaling in vivo. Cell *119*, 889-900.

Kania, A., and Jessell, T. M. (2003). Topographic motor projections in the limb imposed by LIM homeodomain protein regulation of ephrin-A:EphA interactions. Neuron *38*, 581-596.

Kaufmann, N., DeProto, J., Ranjan, R., Wan, H., and Van Vactor, D. (2002). Drosophila liprin-alpha and the receptor phosphatase Dlar control synapse morphogenesis. Neuron *34*, 27-38.

Keino-Masu, K., Masu, M., Hinck, L., Leonardo, E. D., Chan, S. S., Culotti, J. G., and Tessier-Lavigne, M. (1996). Deleted in Colorectal Cancer (DCC) encodes a netrin receptor. Cell *87*, 175-185.

Kerppola, T. K. (2006). Visualization of molecular interactions by fluorescence complementation. Nat Rev Mol Cell Biol *7*, 449-456.

Klassen, M. P., and Shen, K. (2007). Wnt signaling positions neuromuscular connectivity by inhibiting synapse formation in C. elegans. Cell *130*, 704-716.

Komiyama, T., Sweeney, L. B., Schuldiner, O., Garcia, K. C., and Luo, L. (2007). Graded expression of semaphorin-1a cell-autonomously directs dendritic targeting of olfactory projection neurons. Cell *128*, 399-410.

Komiyama, T., Johnson, W. A., Luo, L., and Jefferis, G. S. (2003). From lineage to wiring specificity. POU domain transcription factors control precise connections of Drosophila olfactory projection neurons. Cell *112*, 157-167.

Kuersten, S., Lea, K., MacMorris, M., Spieth, J., and Blumenthal, T. (1997). Relationship between 3' end formation and SL2-specific trans-splicing in polycistronic Caenorhabditis elegans pre-mRNA processing. Rna *3*, 269-278.

Kurusu, M., Cording, A., Taniguchi, M., Menon, K., Suzuki, E., and Zinn, K. (2008). A screen of cell-surface molecules identifies leucine-rich repeat proteins as key mediators of synaptic target selection. Neuron *59*, 972-985.

Lang, B., and Vincent, A. (2009). Autoimmune disorders of the neuromuscular junction. Curr Opin Pharmacol *9*, 336-340.

Lee, C. H., Herman, T., Clandinin, T. R., Lee, R., and Zipursky, S. L. (2001). N-cadherin regulates target specificity in the Drosophila visual system. Neuron *30*, 437-450.

Lein, E. S., Hawrylycz, M. J., Ao, N., Ayres, M., Bensinger, A., Bernard, A., Boe, A. F., Boguski, M. S., Brockway, K. S., Byrnes, E. J.*, et al.* (2007). Genome-wide atlas of gene expression in the adult mouse brain. Nature *445*, 168-176.

Lemke, G., and Reber, M. (2005). Retinotectal mapping: new insights from molecular genetics.

Annu Rev Cell Dev Biol *21*, 551-580.

Leonardo, E. D., Hinck, L., Masu, M., Keino-Masu, K., Ackerman, S. L., and Tessier-Lavigne, M. (1997). Vertebrate homologues of C. elegans UNC-5 are candidate netrin receptors. Nature *386*, 833-838.

Li, H., Ruan, J., and Durbin, R. (2008). Mapping short DNA sequencing reads and calling variants using mapping quality scores. Genome Res *18*, 1851-1858.

Lickteig, K. M., Duerr, J. S., Frisby, D. L., Hall, D. H., Rand, J. B., and Miller, D. M., 3rd (2001). Regulation of neurotransmitter vesicles by the homeodomain protein UNC-4 and its transcriptional corepressor UNC-37/groucho in Caenorhabditis elegans cholinergic motor neurons. J Neurosci *21*, 2001-2014.

Linhoff, M. W., Lauren, J., Cassidy, R. M., Dobie, F. A., Takahashi, H., Nygaard, H. B., Airaksinen, M. S., Strittmatter, S. M., and Craig, A. M. (2009). An unbiased expression screen for synaptogenic proteins identifies the LRRTM protein family as synaptic organizers. Neuron *61*, 734-749.

Livet, J., Sigrist, M., Stroebel, S., De Paola, V., Price, S. R., Henderson, C. E., Jessell, T. M., and Arber, S. (2002). ETS gene Pea3 controls the central position and terminal arborization of specific motor neuron pools. Neuron *35*, 877-892.

Ly, A., Nikolaev, A., Suresh, G., Zheng, Y., Tessier-Lavigne, M., and Stein, E. (2008). DSCAM is a netrin receptor that collaborates with DCC in mediating turning responses to netrin-1. Cell *133*, 1241-1254.

Lyuksyutova, A. I., Lu, C. C., Milanesio, N., King, L. A., Guo, N., Wang, Y., Nathans, J., Tessier-Lavigne, M., and Zou, Y. (2003). Anterior-posterior guidance of commissural axons by Wnt-frizzled signaling. Science *302*, 1984-1988.

Lohr, R., Godenschwege, T., Buchner, E., and Prokop, A. (2002). Compartmentalization of central neurons in Drosophila: a new strategy of mosaic analysis reveals localization of presynaptic sites to specific segments of neurites. J Neurosci *22*, 10357-10367.

Macosko, E. Z., Pokala, N., Feinberg, E. H., Chalasani, S. H., Butcher, R. A., Clardy, J., and Bargmann, C. I. (2009). A hub-and-spoke circuit drives pheromone attraction and social behaviour in C. elegans. Nature *458*, 1171-1175.

Maskos, U., Kissa, K., St Cloment, C., and Brulet, P. (2002). Retrograde trans-synaptic transfer of green fluorescent protein allows the genetic mapping of neuronal circuits in transgenic mice. Proc Natl Acad Sci U S A *99*, 10120-10125.

Maydan, J. S., Flibotte, S., Edgley, M. L., Lau, J., Selzer, R. R., Richmond, T. A., Pofahl, N. J., Thomas, J. H., and Moerman, D. G. (2007). Efficient high-resolution deletion discovery in Caenorhabditis elegans by array comparative genomic hybridization. Genome Res *17*, 337-347.

McCabe, B. D., Marques, G., Haghighi, A. P., Fetter, R. D., Crotty, M. L., Haerry, T. E., Goodman, C. S., and O'Connor, M. B. (2003). The BMP homolog Gbb provides a retrograde signal that regulates synaptic growth at the Drosophila neuromuscular junction. Neuron *39*, 241-254.

Mellem, J. E., Brockie, P. J., Zheng, Y., Madsen, D. M., and Maricq, A. V. (2002). Decoding of polymodal sensory stimuli by postsynaptic glutamate receptors in C. elegans. Neuron *36*, 933-944.

Mello, C., and Fire, A. (1995). DNA transformation. Methods Cell Biol *48*, 451-482.
Millard, S. S., Flanagan, J. J., Pappu, K. S., Wu, W., and Zipursky, S. L. (2007). Dscam2 mediates axonal tiling in the Drosophila visual system. Nature *447*, 720-724.

Miller, D. M., Shen, M. M., Shamu, C. E., Burglin, T. R., Ruvkun, G., Dubois, M. L., Ghee, M., and Wilson, L. (1992). C. elegans unc-4 gene encodes a homeodomain protein that determines the pattern of synaptic input to specific motor neurons. Nature *355*, 841-845.

Mombaerts, P., Wang, F., Dulac, C., Chao, S. K., Nemes, A., Mendelsohn, M., Edmondson, J., and Axel, R. (1996). Visualizing an olfactory sensory map. Cell *87*, 675-686.

Morey, M., Yee, S. K., Herman, T., Nern, A., Blanco, E., and Zipursky, S. L. (2008). Coordinate control of synaptic-layer specificity and rhodopsins in photoreceptor neurons. Nature *456*, 795-799.

Murphey, R. K., Froggett, S. J., Caruccio, P., Shan-Crofts, X., Kitamoto, T., and Godenschwege, T. A. (2003). Targeted expression of shibire ts and semaphorin 1a reveals critical periods for synapse formation in the giant fiber of Drosophila. Development *130*, 3671-3682.

Murphey, R. K., and Godenschwege, T. A. (2002). New roles for ubiquitin in the assembly and function of neuronal circuits. Neuron *36*, 5-8.

Nagiel, A., Patel, S. H., Andor-Ardo, D., and Hudspeth, A. J. (2009). Activity-independent specification of synaptic targets in the posterior lateral line of the larval zebrafish. Proc Natl Acad Sci U S A.

Nonet, M. L. (1999). Visualization of synaptic specializations in live C. elegans with synaptic vesicle protein-GFP fusions. J Neurosci Methods *89*, 33-40.

Packard, M., Koo, E. S., Gorczyca, M., Sharpe, J., Cumberledge, S., and Budnik, V. (2002). The Drosophila Wnt, wingless, provides an essential signal for pre- and postsynaptic differentiation. Cell *111*, 319-330.

Patel, M. R., Lehrman, E. K., Poon, V. Y., Crump, J. G., Zhen, M., Bargmann, C. I., and Shen, K. (2006). Hierarchical assembly of presynaptic components in defined C. elegans synapses. Nat Neurosci *9*, 1488-1498.

Peschanski, M., and Ralston, H. J., 3rd (1985). Light and electron microscopic evidence of transneuronal labeling with WGA-HRP to trace somatosensory pathways to the thalamus. J Comp Neurol *236*, 29-41.

Petrovic, M., and Hummel, T. (2008). Temporal identity in axonal target layer recognition. Nature *456*, 800-803.

Pflugrad, A., Meir, J. Y., Barnes, T. M., and Miller, D. M., 3rd (1997). The Groucho-like transcription factor UNC-37 functions with the neural specificity gene unc-4 to govern motor neuron identity in C. elegans. Development *124*, 1699-1709.

Pohar, N., Godenschwege, T. A., and Buchner, E. (1999). Invertebrate tissue inhibitor of metalloproteinase: structure and nested gene organization within the synapsin locus is conserved from Drosophila to human. Genomics *57*, 293-296.

Poon, V. Y., Klassen, M. P., and Shen, K. (2008). UNC-6/netrin and its receptor UNC-5 locally exclude presynaptic components from dendrites. Nature *455*, 669-673.

Poulopoulos, A., Aramuni, G., Meyer, G., Soykan, T., Hoon, M., Papadopoulos, T., Zhang, M., Paarmann, I., Fuchs, C., Harvey, K.*, et al.* (2009). Neuroligin 2 drives postsynaptic assembly at perisomatic inhibitory synapses through gephyrin and collybistin. Neuron *63*, 628-642.

Priess, J.R., Schnabel, H., Schnabel, R. (1987). The glp-1 locus and cellular interactions in early C. elegans embryos. Cell *51*, 601-611.

Pulak, R. (2006). Techniques for analysis, sorting, and dispensing of C. elegans on the COPAS flow-sorting system. Methods Mol Biol *351*, 275-286.

Pedelacq, J. D., Cabantous, S., Tran, T., Terwilliger, T. C., and Waldo, G. S. (2006). Engineering and characterization of a superfolder green fluorescent protein. Nat Biotechnol *24*, 79-88.

Reid, R. C., and Alonso, J. M. (1995). Specificity of monosynaptic connections from thalamus to visual cortex. Nature *378*, 281-284.

Richardson, S. M., Wheelan, S. J., Yarrington, R. M., and Boeke, J. D. (2006). GeneDesign: rapid, automated design of multikilobase synthetic genes. Genome Res *16*, 550-556.

Robert, V., and Bessereau, J. L. (2007). Targeted engineering of the Caenorhabditis elegans genome following Mos1-triggered chromosomal breaks. Embo J *26*, 170-183.

Rogers, C., Reale, V., Kim, K., Chatwin, H., Li, C., Evans, P., and de Bono, M. (2003). Inhibition of Caenorhabditis elegans social feeding by FMRFamide-related peptide activation of NPR-1. Nat Neurosci *6*, 1178-1185.

Ryu, S. E., Kwong, P. D., Truneh, A., Porter, T. G., Arthos, J., Rosenberg, M., Dai, X., Xuong,

N. H., Axel, R., Sweet, R. W., and Hendrickson, W. A. (1990). Crystal structure of an HIV-binding recombinant fragment of human CD4. Nature *348*, 419-426.

Sano, K., Tanihara, H., Heimark, R. L., Obata, S., Davidson, M., St John, T., Taketani, S., and Suzuki, S. (1993). Protocadherins: a large family of cadherin-related molecules in central nervous system. Embo J *12*, 2249-2256.

Sato, M., Yasuoka, Y., Kodama, H., Watanabe, T., Miyazaki, J. I., and Kimura, M. (2000). New approach to cell lineage analysis in mammals using the Cre-loxP system. Mol Reprod Dev *56*, 34-44.

Schaefer, A. M., Hadwiger, G. D., and Nonet, M. L. (2000). rpm-1, a conserved neuronal gene that regulates targeting and synaptogenesis in C. elegans. Neuron *26*, 345-356.

Scheiffele, P., Fan, J., Choih, J., Fetter, R., and Serafini, T. (2000). Neuroligin expressed in nonneuronal cells triggers presynaptic development in contacting axons. Cell *101*, 657-669.

Schmucker, D., Clemens, J. C., Shu, H., Worby, C. A., Xiao, J., Muda, M., Dixon, J. E., and Zipursky, S. L. (2000). Drosophila Dscam is an axon guidance receptor exhibiting extraordinary molecular diversity. Cell *101*, 671-684.

Schwab, M. E., and Thoenen, H. (1976). Electron microscopic evidence for a transsynaptic migration of tetanus toxin in spinal cord motoneurons: an autoradiographic and morphometric study. Brain Res *105*, 213-227.

Serafini, T., Kennedy, T. E., Galko, M. J., Mirzayan, C., Jessell, T. M., and Tessier-Lavigne, M. (1994). The netrins define a family of axon outgrowth-promoting proteins homologous to C. elegans UNC-6. Cell *78*, 409-424.

Shatz, C. J., and Stryker, M. P. (1988). Prenatal tetrodotoxin infusion blocks segregation of retinogeniculate afferents. Science *242*, 87-89.

Shen, K., Fetter, R. D., and Bargmann, C. I. (2004). Synaptic specificity is generated by the synaptic guidepost protein SYG-2 and its receptor, SYG-1. Cell *116*, 869-881.

Shen, K. (2004). Molecular mechanisms of target specificity during synapse formation. Curr Opin Neurobiol *14*, 83-88.

Shen, K., and Bargmann, C. I. (2003). The immunoglobulin superfamily protein SYG-1 determines the location of specific synapses in C. elegans. Cell *112*, 619-630.

Shinza-Kameda, M., Takasu, E., Sakurai, K., Hayashi, S., and Nose, A. (2006). Regulation of layer-specific targeting by reciprocal expression of a cell adhesion molecule, capricious. Neuron *49*, 205-213.

Shishido, E., Takeichi, M., and Nose, A. (1998). Drosophila synapse formation: regulation by

transmembrane protein with Leu-rich repeats, CAPRICIOUS. Science *280*, 2118-2121.

Smith, M. A., Yao, Y. M., Reist, N. E., Magill, C., Wallace, B. G., and McMahan, U. J. (1987). Identification of agrin in electric organ extracts and localization of agrin-like molecules in muscle and central nervous system. J Exp Biol *132*, 223-230.

Spieth, J., Brooke, G., Kuersten, S., Lea, K., and Blumenthal, T. (1993). Operons in C. elegans: polycistronic mRNA precursors are processed by trans-splicing of SL2 to downstream coding regions. Cell *73*, 521-532.

Sretavan, D. W., Shatz, C. J., and Stryker, M. P. (1988). Modification of retinal ganglion cell axon morphology by prenatal infusion of tetrodotoxin. Nature *336*, 468-471.

Srinivas, S., Watanabe, T., Lin, C. S., William, C. M., Tanabe, Y., Jessell, T. M., and Costantini, F. (2001). Cre reporter strains produced by targeted insertion of EYFP and ECFP into the ROSA26 locus. BMC Dev Biol *1*, 4.

Stevens, B., Allen, N. J., Vazquez, L. E., Howell, G. R., Christopherson, K. S., Nouri, N., Micheva, K. D., Mehalow, A. K., Huberman, A. D., Stafford, B.*, et al.* (2007). The classical complement cascade mediates CNS synapse elimination. Cell *131*, 1164-1178.

Suter, C. M., and Martin, D. I. (2009). Paramutation: the tip of an epigenetic iceberg? Trends Genet.

Tabara, H., Sarkissian, M., Kelly, W. G., Fleenor, J., Grishok, A., Timmons, L., Fire, A., and Mello, C. C. (1999). The rde-1 gene, RNA interference, and transposon silencing in C. elegans. Cell *99*, 123-132.

Terskikh, A., Fradkov, A., Ermakova, G., Zaraisky, A., Tan, P., Kajava, A. V., Zhao, X., Lukyanov, S., Matz, M., Kim, S.*, et al.* (2000). "Fluorescent timer": protein that changes color with time. Science *290*, 1585-1588.

Tessier-Lavigne, M., and Goodman, C. S. (1996). The molecular biology of axon guidance. Science *274*, 1123-1133.

Torres, R., Firestein, B. L., Dong, H., Staudinger, J., Olson, E. N., Huganir, R. L., Bredt, D. S., Gale, N. W., and Yancopoulos, G. D. (1998). PDZ proteins bind, cluster, and synaptically colocalize with Eph receptors and their ephrin ligands. Neuron *21*, 1453-1463.

Umemori, H., Linhoff, M. W., Ornitz, D. M., and Sanes, J. R. (2004). FGF22 and its close relatives are presynaptic organizing molecules in the mammalian brain. Cell *118*, 257-270.

Ushkaryov, Y. A., Petrenko, A. G., Geppert, M., and Sudhof, T. C. (1992). Neurexins: synaptic cell surface proteins related to the alpha-latrotoxin receptor and laminin. Science *257*, 50-56.

Vaney, D. I., and Taylor, W. R. (2002). Direction selectivity in the retina. Curr Opin Neurobiol

12, 405-410.

Varoqueaux, F., Aramuni, G., Rawson, R. L., Mohrmann, R., Missler, M., Gottmann, K., Zhang, W., Sudhof, T. C., and Brose, N. (2006). Neuroligins determine synapse maturation and function. Neuron *51*, 741-754.

Vastenhouw, N. L., Brunschwig, K., Okihara, K. L., Muller, F., Tijsterman, M., and Plasterk, R. H. (2006). Gene expression: long-term gene silencing by RNAi. Nature *442*, 882.

Verhage, M., Maia, A. S., Plomp, J. J., Brussaard, A. B., Heeroma, J. H., Vermeer, H., Toonen, R. F., Hammer, R. E., van den Berg, T. K., Missler, M*., et al.* (2000). Synaptic assembly of the brain in the absence of neurotransmitter secretion. Science *287*, 864-869.

Vogel, B. E., and Hedgecock, E. M. (2001). Hemicentin, a conserved extracellular member of the immunoglobulin superfamily, organizes epithelial and other cell attachments into oriented line-shaped junctions. Development *128*, 883-894.

Volpe, T. A., Kidner, C., Hall, I. M., Teng, G., Grewal, S. I., and Martienssen, R. A. (2002). Regulation of heterochromatic silencing and histone H3 lysine-9 methylation by RNAi. Science *297*, 1833-1837.

Von Stetina, S. E., Fox, R. M., Watkins, K. L., Starich, T. A., Shaw, J. E., and Miller, D. M., 3rd (2007). UNC-4 represses CEH-12/HB9 to specify synaptic inputs to VA motor neurons in C. elegans. Genes Dev *21*, 332-346.

Wang, D., Kennedy, S., Conte, D., Jr., Kim, J. K., Gabel, H. W., Kamath, R. S., Mello, C. C., and Ruvkun, G. (2005). Somatic misexpression of germline P granules and enhanced RNA interference in retinoblastoma pathway mutants. Nature *436*, 593-597.

Wang, J., Zugates, C. T., Liang, I. H., Lee, C. H., and Lee, T. (2002). Drosophila Dscam is required for divergent segregation of sister branches and suppresses ectopic bifurcation of axons. Neuron *33*, 559-571.

Wang, X., Weiner, J. A., Levi, S., Craig, A. M., Bradley, A., and Sanes, J. R. (2002). Gamma protocadherins are required for survival of spinal interneurons. Neuron *36*, 843-854.

White, J. G., Albertson, D. G., and Anness, M. A. (1978). Connectivity changes in a class of motoneurone during the development of a nematode. Nature *271*, 764-766.

White, J. G., Southgate, E., Thomson, J. N., and Brenner, S. (1976). The structure of the ventral nerve cord of Caenorhabditis elegans. Philos Trans R Soc Lond B Biol Sci *275*, 327-348.

White, J. G., Southgate, E., Thomson, J. N., and Brenner, S. (1986a). The structure of the nervous system of *Caenorhabditis elegans*. Philos Trans R Soc Lond B Biol Sci *314*, 1-340.

Wickersham, I. R., Lyon, D. C., Barnard, R. J., Mori, T., Finke, S., Conzelmann, K. K., Young,

J. A., and Callaway, E. M. (2007). Monosynaptic restriction of transsynaptic tracing from single, genetically targeted neurons. Neuron *53*, 639-647.

Wilhelm, B. T., and Landry, J. R. (2009). RNA-Seq-quantitative measurement of expression through massively parallel RNA-sequencing. Methods *48*, 249-257.

Winberg, M. L., Mitchell, K. J., and Goodman, C. S. (1998). Genetic analysis of the mechanisms controlling target selection: complementary and combinatorial functions of netrins, semaphorins, and IgCAMs. Cell *93*, 581-591.

Wojtowicz, W. M., Flanagan, J. J., Millard, S. S., Zipursky, S. L., and Clemens, J. C. (2004). Alternative splicing of Drosophila Dscam generates axon guidance receptors that exhibit isoform-specific homophilic binding. Cell *118*, 619-633.

Wu, Q., and Maniatis, T. (1999). A striking organization of a large family of human neural cadherin-like cell adhesion genes. Cell *97*, 779-790.

Wassle, H., and Boycott, B. B. (1991). Functional architecture of the mammalian retina. Physiol Rev *71*, 447-480.

Yamagata, M., and Sanes, J. R. (2008). Dscam and Sidekick proteins direct lamina-specific synaptic connections in vertebrate retina. Nature *451*, 465-469.

Yamagata, M., Weiner, J. A., and Sanes, J. R. (2002). Sidekicks: synaptic adhesion molecules that promote lamina-specific connectivity in the retina. Cell *110*, 649-660.

Yamagata, M., Herman, J. P., and Sanes, J. R. (1995). Lamina-specific expression of adhesion molecules in developing chick optic tectum. J Neurosci *15*, 4556-4571.

Yamagata, M., and Sanes, J. R. (1995). Lamina-specific cues guide outgrowth and arborization of retinal axons in the optic tectum. Development *121*, 189-200.

Yandell, M. D., Edgar, L. G., and Wood, W. B. (1994). Trimethylpsoralen induces small deletion mutations in Caenorhabditis elegans. Proc Natl Acad Sci U S A *91*, 1381-1385.

Yoshihara, Y., Mizuno, T., Nakahira, M., Kawasaki, M., Watanabe, Y., Kagamiyama, H., Jishage, K., Ueda, O., Suzuki, H., Tabuchi, K.*, et al.* (1999). A genetic approach to visualization of multisynaptic neural pathways using plant lectin transgene. Neuron *22*, 33-41.

Yoshikawa, S., McKinnon, R. D., Kokel, M., and Thomas, J. B. (2003). Wnt-mediated axon guidance via the Drosophila Derailed receptor. Nature *422*, 583-588.

Yoshimura, Y., and Callaway, E. M. (2005). Fine-scale specificity of cortical networks depends on inhibitory cell type and connectivity. Nat Neurosci *8*, 1552-1559.

Zahn, T. R., Angleson, J. K., MacMorris, M. A., Domke, E., Hutton, J. F., Schwartz, C., and

Hutton, J. C. (2004). Dense core vesicle dynamics in Caenorhabditis elegans neurons and the role of kinesin UNC-104. Traffic *5*, 544-559.

Zallen, J. A., Yi, B. A., and Bargmann, C. I. (1998). The conserved immunoglobulin superfamily member SAX-3/Robo directs multiple aspects of axon guidance in C. elegans. Cell *92*, 217-227.

Zhang, B., Luo, S., Wang, Q., Suzuki, T., Xiong, W. C., and Mei, L. (2008). LRP4 serves as a coreceptor of agrin. Neuron *60*, 285-297.

Zhang, S., Ma, C., and Chalfie, M. (2004). Combinatorial marking of cells and organelles with reconstituted fluorescent proteins. Cell *119*, 137-144.

Zhao, H., and Nonet, M. L. (2000). A retrograde signal is involved in activity-dependent remodeling at a C. elegans neuromuscular junction. Development *127*, 1253-1266.

Zhen, M., Huang, X., Bamber, B., and Jin, Y. (2000). Regulation of presynaptic terminal organization by C. elegans RPM-1, a putative guanine nucleotide exchanger with a RING-H2 finger domain. Neuron *26*, 331-343.

Zhen, M., and Jin, Y. (1999). The liprin protein SYD-2 regulates the differentiation of presynaptic termini in C. elegans. Nature *401*, 371-375.

Zhu, H., Hummel, T., Clemens, J. C., Berdnik, D., Zipursky, S. L., and Luo, L. (2006). Dendritic patterning by Dscam and synaptic partner matching in the Drosophila antennal lobe. Nat Neurosci *9*, 349-355.

Zhu, H., and Luo, L. (2004). Diverse functions of N-cadherin in dendritic and axonal terminal arborization of olfactory projection neurons. Neuron *42*, 63-75.

Zhu, S., Lin, S., Kao, C. F., Awasaki, T., Chiang, A. S., and Lee, T. (2006). Gradients of the Drosophila Chinmo BTB-zinc finger protein govern neuronal temporal identity. Cell *127*, 409-422.

Zhu, Y., and Stevens, C. F. (2008). Probing synaptic vesicle fusion by altering mechanical properties of the neuronal surface membrane. Proc Natl Acad Sci U S A *105*, 18018-18022.